EXPERIMENTAL INVESTIGATION OF FLOW BOILING AND SPRAY COOLING ON ENHANCED SURFACES IN FC-72

by

GILBERTO MORENO, JR.

Presented to the Faculty of the Graduate School of
The University of Texas at Arlington in Partial Fulfillment
of the Requirements
for the Degree of

DOCTOR OF PHILOSOPHY

THE UNIVERSITY OF TEXAS AT ARLINGTON
August 2009

ACKNOWLEDGEMENTS

Credit for all my academic accomplishments belongs to my parents, Raquel Moreno (mother) and Gilberto Moreno (father). Their hard work, guidance and support allowed me to be the first in my family to graduate from college. I am truly grateful. I would also like to thank my beloved sisters, Mari and Judi, for all their encouragement and support.

Finally, I would like to thank my advising professor, Dr. Seung Mun You for allowing me to study under his guidance and to participate in his research activities.

July 30, 2009

ABSTRACT

EXPERIMENTAL INVESTIGATION OF FLOW BOILING AND

SPRAY COOLING ON ENHANCED SURFACES

IN FC-72

Gilberto Moreno, PhD

The University of Texas at Arlington, 2009

Supervising Professor: Supervising Professor Seung Mun You

In this study the effect of a recently developed, thermally conductive microporous coating on flow boiling and spray cooling performance was studied using FC-72 as the working fluid. The overall goal is to further increase heat transfer in forced convection systems and in doing so, provide a viable option for future cooling applications. In flow boiling, the coating increased heat transfer coefficients by as much as 400% and produced values exceeding 40,000 $W\text{-}m^{-2}\ K^{-1}$. This enhancement is believed to be a result of both an increase in active nucleation sites and a decrease of the superheated liquid layer. It is believed that the thinner superheated layer combined with the highly conductive coating produces high liquid temperature gradients and is the reason for the slightly negative wall superheats recorded in subcooled tests. Additionally, the coatings ability to wick fluid delays the onset of CHF and results in dual temperature excursions at high heat fluxes.

The application of the coating to spray cooling was found to increase heat transfer coefficients by ~45% throughout the entire boiling curve. Even though this enhancement is less than that achieved with flow boiling; it is still significant considering the already high heat transfer coefficients of spray cooling. In addition to enhancing nucleate boiling, the coating is

also believed to facilitate evaporation in spray cooling. Evaporation efficiency is increased as a result of the wicking effect of microporous coating which pulls the liquid toward the surface and thus decreases film thickness and increases the three-phase contact line length. The unique flow characteristic of spray cooling allows it to outperform flow boiling by producing higher CHF and *h*-values (especially at low heat fluxes). However, this is at the expense of pumping power which can be three orders of magnitude higher than those of flow boiling. Finally, in both flow boiling and spray cooling, the new coating was found to outperform a previously developed aluminum based (ABM) coating.

TABLE OF CONTENTS

LIST OF ILLUSTRATIONS

LIST OF TABLES

NOMENCLATURE

CHF	critical heat flux, [kW/m^2]
$C_{p,l}$	specific heat, [J/kg-K]
D_h	hydraulic diameter, [m^2]
d_o	nozzle orifice diameter
H	nozzle-to-heater distance
h	heat transfer coefficient, [W-m^{-2}-K^{-1}]
h_{lv}	latent heat, [kJ/kg]
k	thermal conductivity, [W-m^{-1} K^{-1}]
L	heater length, [m]
Nu_L	Nusselt Number, [$h\ L/\ k$]
$\dot{m}$	mass flow rate, [kg/s]
Pr	Prandtl Number, [$C_{p,}$ μ / k]
ΔP	pressure drop, [N/m^2]
q''	heat flux, [kW/m^2]
q_m^{**}	non-dimensional CHF defined in eq. 3.1
$Re_{,d}$	Reynolds Number, [$\rho_l U D_h$ / μ]
$Re_{,L}$	Reynolds Number, [$\rho_l U L$ / μ]
SMD	Sauter Mean Diameter, [μm]
t	liquid film thickness
ΔT_{bulk}	difference between wall & liquid temperature, $T_w - T_L$
ΔT_{sat}	wall superheat, $T_w - T_{sat}(P_{sys})$
ΔT_{sub}	liquid subcooling, $T_{sat}(P_{sys}) - T_L$

U velocity, [m/s]

We Weber number, [$\rho_l U^2 L / \sigma$]

GREEK SYMBOLS

μ absolute viscosity, [kg/m-s]

ν kinematic viscosity, [m^2/s]

θ spray cone angle

ρ density, [kg/m^3]

σ surface tension, [N/m]

ω variable uncertainty

SUBSCRIPTS

a air

b heat spreader base

l liquid

sat saturated

sp spreading (associated with spreading resistance)

sub subcooling

v vapor

w wall, heater surface

CHAPTER 1

INTRODUCTION

1.1 Background

Forced convective cooling in conjunction with phase change heat transfer is regarded as one of the most effective means of high heat flux dissipation. The forced convection aspect can be implemented in several methods including flow boiling, jet impingement and spray cooling. However, the high heat dissipation potential of these types of cooling schemes is mostly a result of the high heat transfer rates and near isothermal characteristics associated with phase change (boiling & evaporation) heat transfer. Therefore, any attempt to further increase the already high heat dissipation potential of these cooling schemes must be aimed at enhancing the phase change mechanisms and this is what this investigation will attempt. This study will investigate the effect of a recently developed thermally conductive microporous coating on both flow boiling and spray cooling performance.

One of the most commonly investigated forms of phase change enhancement is achieved through surface roughening. Throughout the years, the UTA Microscale Heat Transfer Lab has developed several microporous coatings [1-3] which can be applied to heated surfaces and are a form of surface roughening. When tested in pool boiling these microporous coatings have demonstrated significant enhancement to the heat transfer coefficients, critical heat flux (CHF) and boiling incipience. However, when these coatings were applied to flow boiling they have shown mixed results; enhancement at lower velocities but degradation at higher velocities [4, 5]. The heat transfer degradation observed is due to the low-thermally conductive nature of bonding epoxies used in these microporous coatings. This “flaw” in past microporous coatings lead to the development of a new thermally conductive microporous coating (TCMC) which is

composed entirely of thermally (metallic) conductive components [6]. Pool boiling tests (water) using this coating have produced drastic enhancements of about 300% to the heat transfer coefficient and 100% to the CHF. In this study, the effect of this thermally conductive microporous coating on both flow boiling and spray cooling performance will be investigated.

1.2 Project Motivation

Increasing power densities, in high power electronics, have rendered traditional air cooling system inadequate in many applications. In many instances the advancement of electronics technology is dependent on the development of new and innovative cooling solutions. It is therefore, critical to conduct research into emerging thermal technologies to determine their capabilities as well as their limitations and this is what this study aims to accomplish. The main beneficiary of the current study is the electronics industry however; this technology can also be applied to other industries including power generation (nuclear, solar, etc...), military electronics and electric car technology (power electronics).

1.3 Project Objectives

The overall purpose of this study is to enhance heat dissipation in forced convective boiling systems and in doing so, provide a viable option for future cooling applications. With this in mind, two goals are proposed for this project with each goal having several objectives. The goals and objectives are listed below.

1. Investigate flow boiling and spray cooling enhancement using a thermally conductive microporous coating (TCMC).

1.1. Quantify enhancement to the heat transfer coefficients and critical heat flux (CHF) (if possible)

1.2. Indentify the mechanisms believed to be responsible for microporous coating enhancement

1.3. Maximize the effect of the microporous coating by increasing its effective area

2. Compare the heat transfer performance of flow boiling and spray cooling.

2.1. Compare performance of flow and spray using identical heaters while considering the pumping power requirements of each (non-coated & coated)

2.2. Determine effect of nozzle type (spray), flow rate/velocity and subcooling on performance (coated & non-coated)

With regard to the first goal, experiments were conducted using both TCMC and non-coated heaters and results were then compared to quantify any performance enhancements. Experiments were conducted at various flow rates/velocities, degrees of subcooling (non-degassed), nozzle-to-heater distances (spray) and channel heights (flow). Results from these experiments are discussed in Chapters 4 and 5 for flow boiling and spray cooling, respectively. With regard to the second goal, the flow boiling and spray cooling results are compared in Chapter 6. However, the issue of comparing these cooling schemes is complicate by the fact that spray cooling requires significantly higher inlet pressures but lower flow rates as compared to flow boiling. Therefore, both the pressure drop and the flow rate requirements are considered by calculating the pumping power and this is then considered when comparing flow boiling and spray cooling performance.

3M Fluorinert® FC-72 was the working fluid used in this study. Dielectric refrigerants such as FC-72 are ideal for electronics cooling applications due to their high dielectric strength, low saturation temperature, low freezing temperature, and good chemical compatibility with many materials.

1.4 Phase Change Enhancement using Enhanced Surfaces (Literature Review)

Two-phase (nucleation and evaporation) enhancement has been the topic of many studies and there are many ways to achieve enhancement. One of the most effective means to augment phase change (boiling) heat transfer is through an increase in the number of active nucleation sites on the heated surface. This can be achieved through either surface roughening and/or the creation of artificial micro cavities on the heated surface [7]. In addition to enhancing nucleate boiling heat transfer, the capillary wicking of some enhanced surfaces have also been found to enhance evaporation [8-10]. Thus it seems that enhanced/structured surfaces can increase heat transfer by facilitation phase change in both nucleation and evaporation. The following is a summary of some of the research into surface enhancement techniques applied to pool boiling, flow boiling and spray cooling.

1.4.1 Pool Boiling on Enhanced Surfaces

The majority of all studies into the effect of enhanced surfaces on boiling enhancement have been carried out under pool boiling conditions. This is due to the fact that pool boiling is the more fundamental and least complex means of boiling heat transfer. Therefore, in order to understand the effects of porous coatings on flow boiling or spray cooling, it is important to first understand how these porous coatings affect a more fundamental phase change phenomenon, such as pool boiling.

Marto & Lepere [11] conducted pool boiling tests with FC-72 and Freon-113 using three different commercially available copper enhanced surfaces. They reported that all three enhanced surfaces enhance boiling heat transfer coefficients and reduce boiling incipience superheats. Of the three surfaces tested, only one was found to enhance CHF (with FC-72) and is due to, according to the author, the relatively larger spacing between pores which reduces coalescence of the vapor columns and thus extend CHF. An investigation by Bergles & Chyu

[12] studied enhancing pool boiling by also using commercially available porous surface which consisted of copper particles brazed onto a heated surface. Tests revealed that the coating significantly increases the heat transfer coefficients by as much as 800% and 250% for R-113 and water, respectively. This study [12] goes on to present a possible scenario of boiling on coated surfaces by hypothesizing that nucleation on porous coatings occurs internally within cavities, which are not flooded with liquid. The resulting vapor then exits through preferred escape channels and rewetting liquid is then supplied through other connected channels within the coating. Compared to the previous studies of [11, 12], Nakayama et al. [13] used more structured porous surfaces composed of rectangular channels (250 (wide) × 400 (deep) μm) imbedded into the heated surface with only small holes (50-150 μm) penetrating to the surface. It is reported that an increase in the number of active nucleation sites does not always result in an increase in heat transfer. Murthy et al. [14] later used this data to develop a semi-analytical correlation for pool boiling on structured surfaces.

Several studies have been carried out in an attempt to try to understand the physics involved in pool boiling on porous surfaces and to investigate how these surfaces enhance boiling heat transfer. One such study was done by Kim et al. [15] using low-thermally conductive porous coatings composed of diamond particles bonded to the surface with epoxy. Their tests revealed enhancement to both the heat transfer coefficients and CHF. The increase in heat transfer coefficient was attributed to the higher number of active nucleation sites of the coating. Additionally, measurements of the bubble departure diameters and frequencies of both coated and non-coated surfaces revealed that the porous coated surfaces produce smaller bubble departure diameters and higher bubble departure frequencies as compared to the non-coated heaters. Therefore, concluding that at higher heat fluxes, the porous coated surfaces enhance micro-convection and reduce vapor generation which results in higher CHF. Li & Peterson [16, 17] conducted a parametric study with thermally conductive coatings created by sintering layers of copper wire screens to produce porous coatings with various thicknesses, porosities and

pore sizes. They report that there is a distinct difference in performance between thin and thick coatings with thin coatings resulting in higher heat transfer coefficients while thick coatings produce higher CHF. Moreover, [16] agreed with [15] by attributing the pool boiling enhancement of the coatings to higher active nucleation sites but also included the effects of capillary pumping action and more wetting area.

A review of existing microstructure enhancement techniques was conducted by Honda & Wei [18]. Their study reviewed all forms of microstructure enhancement including micro-fins, porous coatings, sputtered surfaces, laser drilled cavities, etc... They concluded that in general, micro-fins are more effective at increasing CHF while microporous structures are more effective at increasing nucleate boiling heat transfer.

1.4.2 Flow Boiling on Enhanced Surfaces

Finned structures on heater surfaces have been used as a means of flow boiling enhancement by [4, 19, 20]. Maddox & Mudawar [19] conducted flow boiling tests with square fins with sizes ranging from 0.25 to 1.02 mm using water, FC-72 and FC-77. Rainey [4] used larger fins (4 & 8 mm in height) and conducted flow boiling tests using FC-72. The relatively large fins used by Rainey [4] resulted large temperature gradients throughout the fins which resulted in large portions of the fins undergoing single phase heat transfer even at high heat fluxes. Because of this, his finned structures demonstrated dependence to both velocity and subcooling. This velocity dependence was not observed by Lie et al. [20] using smaller, micro finned structures (70 μm in height). This same study reported that the micro fin structures decrease bubble departure diameters but increase their departure frequency. All investigations [4, 19, 20] found that the finned structures increase heat transfer (single and two phase) and increase CHF (CHF results not reported in [20]). It is important to note that enhancements reported from the larger finned structures of [4, 19] are more a result of an increase in effective heat transfer area and not from an enhancement in the phase change mechanisms.

As opposed to the previous studies, several investigators have used more random surface structures as a means to enhance flow boiling. One of the more fundamental studies was conducted by Kandlikar & Spiesman [21] who studied the effect of sand paper roughened surfaces on flow boiling performance. Their results found no clear trend in performance. For example, at the highest flow rate tested the roughest surface and the “mirror” like surface had about the same performance. These results indicate that roughening surfaces with different grit sand paper does not significantly affect the cavity size distributions and therefore is not an optimal means of enhancing flow (nucleate) boiling heat transfer.

The use of microporous surface coatings on flow boiling performance using FC-72 was studied by Rainey et al. [22]. This study used a microporous coating developed by [1] which could be applied to most any surface and was composed of three components; aluminum particles (1-20 μm), ceramic epoxy and methyl ethyl-keytone (M.E.K.). The M.E.K. acted as a carrier for the particles, epoxy mixture and evaporated after application. Results showed that the microporous coating provided heat transfer enhancement at lower velocities. However, at higher velocities and subcooling the added thermally resistance of the epoxy resulted in a degradation of performance. Increasing velocity was also found to decrease the magnitude of the CHF enhancement produced by the coating. Similar results were reported in flow boiling tests by Ammerman & You [5] using small, square channels and FC-87. Sarwar et al. [23] investigated the effect of microporous coatings on flow boiling CHF using water as the coolant. The microporous coatings used in this study were similar in composition to that used by [5, 22] with the exception that alumina, and not aluminum, particle were used. They report that the alumina microporous coating provided the most CHF enhancement (~25%) while alumina nanoporous coating provided negligible enhancement. Yet another study by Yildiz [24] only focused on the pressure drop associated with two-phase flow through microporous coated tubes and not the heat transfer performance of the coatings.

Kuo & Peles [25] created micro-sized (7.5 μm) re-entrant cavities onto microchannels to determine their effect on flow boiling performance. The enhanced microchannels were found to increased CHF and reduce in boiling incipience superheats. A later study by, again by Kuo & Peles [26] reported that re-entrant cavities can be used to suppress flow oscillations intrinsic to microchannels. This suppression of flow instabilities is then believed to delay/extend CHF. More recently the effect of nano-sized structures on flow boiling performance has been investigated. Khanikar et al. [27] deposited carbon nanotubes (CNT) on microchannels and compared their performance to a plain, reference surface. The CNT coated microchannels are found produce enhancement to both single and two phase heat transfer as well as CHF at low velocities. The enhancements however, are found to diminish or disappear with increasing velocity.

1.4.3 Spray Cooling on Enhanced Surfaces

The use of enhanced surfaces on spray cooling has received much less attention as compared to their application to both pool and flow boiling. However, a review of available literature into this topic shows an increasing interest in this field.

The effect of surface roughness on spray cooling was studied by Pais et al. [28] who reported heat flux as high as 1,200 W/cm^2 at low wall superheats using water on roughened surfaces. In this study, surfaces were roughened using sand paper of varying grit textures. The claim is made that higher roughened surfaces create larger liquid films on the heated surfaces whereas lesser-roughened surfaces create thinner liquid films. This in turn results in evaporation being the dominant heat transfer mode for the lesser roughened surfaces and it is these surfaces which outperform the more roughened surfaces. Unlike [28], Kim et al. [9] experimented using porous coatings to evaluated their effect on spray cooling performance. Experiments were conducted using air atomized water sprays at relatively low flow rates (≤3 ml/min) and low-thermally conductive microporous coatings. Their results show enhancement to

both heat transfer rates (at higher heat fluxes) and CHF for the coated surface as compared to the uncoated one. They associate this enhancement to the liquid wicking effect of the coating.

Other investigators have used more highly structure surfaces, as compared to those of [9, 28], as a means to enhance spray cooling. Silk et al. [29] used various embedded (dimples & porous tunnels) and extended surface (straight, cubic, radial, etc.. fins) structures on spray cooling using PF-5060. It is reported that of all tested surfaces, the straight fins and porous tunnels provided the highest CHF. Inspired by these results, Silk [30] investigated the effect of the pore size (0.25, 0.5 & 1 mm) on porous tunnel spray cooling performance. Results showed that the largest pore size produced the highest CHF while the smallest pore produced the lowest. The size of the structures tested in both [29, 30] were on the order of a millimeter and therefore most of enhancement from these surfaces is likely due to the fin effect.

The use of smaller, micron sized fins has been recently investigated. Hsieh & Yao [10] fabricated micro-sized square fins (grove width 120-360 μm and depth 333-455 μm) structures onto silicon surfaces reported heat transfer enhancement. A comparison of the contact angle, using water, revealed that the capillary force of the structured surface spreads liquid and thus creates lower contact angles as compared to a plain surface. This effect reduces the liquid film thickness and facilitates evaporation which in turn enhances cooling performance.

Horacek et al. [31] showed that the dissipated heat flux can be correlated to the three-phase contact line length or the boundary where liquid, vapor and solid (heater surface) meet. An increase in contact line length was found to increase heat dissipation due high evaporation at this boundary. With this in mind, Sodtke & Stephan [32] created micron-sized pyramidal structures and used them increase the contact line length and thus increase heat transfer. The increase in the contact line length was due to the capillary pumping effect of the micro-structures. More recently, Bostanci et al. [8] experimented using surfaces with what are described as indentations and protrusions. Spray cooling tests using ammonia as the working fluid, revealed enhancement with these structured surfaces and heat transfer coefficients as

high as 470,000 W $m^{-2}K^{-1}$. From the surface description, it is unclear whether this surface has a porous structure.

1.5 Parametric Effects (Literature Review)

This section provides a summary on the effect of parameters including flow rate/velocity, subcooling, dissolved air content, etc… on flow boiling and spray cooling performance. The focus is on those parameters which are applicable to the current study.

1.5.1 Flow Boiling Parametric Effects

Heater geometries in flow boiling can vary considerably however, the heater geometries of most interest for this project are internal flows with flow over flat (square) heated surfaces. Studies, using flush mounted 1 cm^2 heater, have shown that heat transfer coefficients within the fully developed nucleate boiling regime demonstrate little dependence to fluid velocity and subcooling [22, 33]. Similar results were reported by Gersey & Mudawar [34] using an array of protruded, 1 cm^2 chips. This insensitivity to both fluid velocity and subcooling clearly demonstrates nucleate boiling heat transfer as the dominant mode of heat transfer. However, both fluid velocity and subcooling has been shown to affect CHF and single phase heat transfer coefficients [22, 33, 34]. An increase in either velocity or subcooling will increase CHF and single phase heat transfer rates. These aforementioned studies performed experiments using FC-72 as the working fluid however the same results can be expected with most any working fluid [7].

It is known that dielectric fluids, such as FC-72, can absorb significant amounts of air and thus the effect of dissolved air content on boiling performance has been widely studied. Pool boiling studies investigating the effect of dissolved air content on boiling heat transfer generally agree that the effect of dissolved air is to decrease boiling incipience superheats and provided higher heat transfer within the partial boiling regime (low heat fluxes) [35, 36]. At

higher heat fluxes, within the fully developed nucleate boiling regime, the effect of dissolved gas on nucleate boiling is much less apparent as the liquid near the heated surface is believed become nearly de-gassed [35-37]. Additionally, the work of O'Connor et al. [36] found that dissolved gas has less effect on microporous coated surfaces as compared to smooth surfaces. Watwe & Bar-Cohen [37] reported no discernable difference in CHF between degassed and non-degassed cases.

The effect of dissolved gas on flow boiling using FC-72 was studied by Wu & Simon [38]. In general, the effect of dissolved gas in flow boiling was similar to its effect in pool boiling. They also report that dissolved air slightly decreases CHF for straight flow tests but has no noticeable effect in the curved flow case. Chen & Garimella [39] investigated the effect of dissolved gas in flow boiling within microchannels using FC-77 where it is determined that dissolved gas increases both pressure drop and flow instabilities as compared to the degassed case.

The effect of channel height in FC-72 flow boiling tests was studied by Willingham & Mudawar [40] for a linear array of discrete heater. Channel heights of 2, 5 and 10 mm were tested at various flow rates and degrees of subcooling. It is found that changing the channel height has no effect on fully developed nucleate boiling but the 2 mm channel did have higher incipience superheats. In addition, it is found that the 5 mm channel height consistently produced the highest CHF. The effect of gap size on flow boiling within narrow annular channels was studied by Su & Wang [41] using water and by Lie & Lin [42] using R-134a. Both report that decreasing the channel gap size increases nucleate boiling heat transfer.

A reduction in channel size is known to increase single phase heat transfer rates [7]. This was demonstrated by Bowers & Mudawar [43] when comparing the performance of mini and micro diameter channel heat sinks. However, within the nucleate boiling regime, the boiling curves for the mini and micro channels were found to collapse to one line, indicating no difference in heat transfer coefficients within this regime. This same study reports slightly higher

CHF for the micro as compared to the mini channel but, prefers the use of the mini channel due to its significantly lower pressure drop.

1.5.2 Spray Cooling Parametric Effects

Spray cooling is a highly efficient means of dissipation high heat fluxes and hence its applications to metal casting fabrication, laser cooling and electronics cooling. The finely atomized droplets of the sprays in addition to the thin liquid films promote evaporation. In addition to evaporation, higher heat fluxes can produce nucleation which further increases heat dissipation. The cooling effectiveness of these two phase change methods combined with single phase forced convection heat transfer allows spray cooling to produce critical heat flux (CHF) values which can be about one order of magnitude higher than that possible with pool boiling [44]. However, spray cooling does have its drawbacks including high pressure drop and the possibility of nozzle clogging. Thus, a successful implementation of spray cooling requires both an understanding the spray cooling performance as well as an awareness of its disadvantages.

Characterizing sprays is more complicated as compared to characterizing other forced convective cooling methods. Parameters including the mean droplet velocity, size and flux are generally used to characterize sprays and quantifying these parameters generally requires expensive equipment. The influence of the various parameters on spray cooling performance was studied by Chen et al. [44]. This was done by varying one parameter while the other two were maintained nearly constant. In doing so, they report that of all three parameters, the mean droplet velocity has the most effect on spray cooling performance. An increase in this parameter resulted in the highest increase in both CHF and heat transfer. It is further reported that increasing the spray mass flux does not increase CHF if the droplet velocity is maintained constant. Finally, the claim is made that a change in the Sauter Mean Diameter (SMD) has little affect either CHF or heat transfer. This claim differs from the previous findings of Estes & Mudawar [45] who report that nozzles with small droplet sizes produce higher CHF. In this

investigation, a CHF correlation was developed for full cone spray nozzles which was a function of spray volumetric flux and the SMD. This same CHF correlation was later used by Rybicki & Mudawar [46] to predict CHF for upward-facing sprays indicating that heater orientation has little, if any, effect CHF. Moreover, separate correlations were also developed to predict single phase and nucleate boiling heat transfer for both upward and downward facing sprays. Additional spray cooling correlations have been developed including those of [47, 48].

The droplets that make up sprays can contain or entrain air/vapor within them. Upon striking the heater surface the air/vapor nuclei are released within the thin liquid film on the heater surface and make up what are called “secondary” nuclei. The significance of these secondary nuclei, to spray cooling performance, was reported by Rini et al. [49]. In this study it was reported that secondary nuclei make up the majority of all the nuclei on the heated surface and constitute a significant amount of the total heat flux dissipated (as much as 40 % according to the author). In addition, increasing the droplet flux increases the nucleation site density which in turn increases the heat transfer coefficient.

In the present study, tests were conducted with both single and multi-jet spray nozzles. While there is currently a significant amount of spray cooling research using single nozzles [44-50]; the same cannot be said for spray cooling using multi-nozzle sprays. Lin & Ponnappan [51, 52] conducted spray cooling tests FC-72, FC-87 and methanol using miniature multi-nozzle sprays. In their study it is reported that increasing volumetric flux increases both heat transfer coefficients and CHF. Pautsch & Shedd [53] tested both single and multi-nozzle sprays and compared their performance. Results showed that nozzles which make less use of phase change generally produce higher CHF values. Also, tests comparing the single and multi-nozzle spray demonstrated that single spray nozzles produced the lowest heat transfer coefficients at the heater perimeter while multi-nozzles sprays produced the lowest heat transfer coefficients at heater areas where spray cones intersect to create stagnation zones.

One of the parameter in the current study is the effect of nozzle-to-heater distance on both heat transfer and CHF for both hollow cone and multi-jet spray nozzles. A detailed study investigating the effect of nozzle-to-heater distance on CHF using single nozzle full cone sprays was performed by Mudawar & Estes [50]. It was reported that the optimal nozzle-to-heater distance is achieved when the spray cone just inscribes the perimeter of the heater. Low nozzle-to-heater distances resulted in lower CHF values due to poor spray coverage on the heater. While large nozzle-to-heater distances also decreased CHF because the spray cone extended beyond the periphery of the heater resulting in wasted spray.

CHAPTER 2

EXPERIMENTAL APPARATUS AND PROCEDURES

In this chapter, the various test sections and test heaters used, in this study, are described and the experimental procedures are explained. A total of three different test sections were designed and fabricated to carry out various experiments. The three test sections include a pool boiling, flow boiling and spray cooling test facility. In addition, an uncertainty analysis is provided.

2.1 Test Heaters

Two different test heaters were used in this investigation and schematics of each are shown in Fig. 2.1. All heaters were flush mounted and horizontally oriented (upward facing). The heaters used in pool, flow and spray tests were essentially the same and therefore only one heater description is provided. The only difference in heaters construction between flow boiling heaters and spray cooling heaters is in the design of the lexan substrate.

2.1.1 Heater Construction

The 10×10 mm heater consists of three components; a polycarbonate substrate, a copper block (10 × 10 × 3 mm) and a heating element. A 10 mm square 20 Ω resistor is utilized as the heating element and is soldered to the copper block. A T-type thermocouple imbedded in the copper block provides test heater temperature measurements. The thermocouple is located 1.5 mm below the heater surface and therefore, surface temperature is calculated assuming one-dimension steady state conduction. The copper block and heating element assembly are placed on a polycarbonate substrate, copper side up. 3M 1838 Scotch-Wedld Epoxy is then

applied around the perimeter of the copper block and heating element exposing only the top of the copper block. Both the epoxy and the substrate also functioned as insulators by preventing heat loss through the sides and bottom.

Tests were also conducted using heat spreaders of various sizes and thicknesses centered above the 10×10×3 mm block (Fig. 2.1). Both the heat spreader plate and the 10×10×3 mm block are one piece assembly machined from a single copper block. Aside from the attached heat spreader plate, the fabrication of these heaters is identical to that of the 10×10 mm heater describe above. Temperature measurements for heat spreader heaters were taken at the same location as the 10×10 mm heater. Surface temperatures given for these heat spreaders, are calculated at the interface between the 10×10 mm heater and the heat spreader plate assuming one-dimension heat transfer (see Fig. 2.1). Heat flux was calculated using the area of the 10×10 mm block (1 cm^2) and not the area of the heat spreader plate.

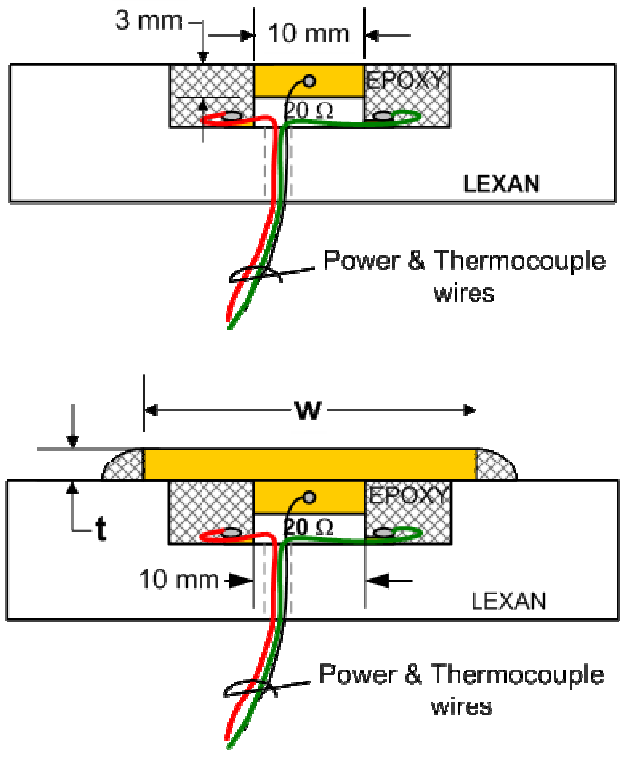

Figure 2.1. Schematic of test heaters. 10×10 heater (top) and heat spreader heater (bottom).

Heater surface conditions are very important in boiling heat transfer performance and are a key parameter of this study. Therefore, a plain/non-coated surface is used as a reference from which to compare results obtained from microporous coated surfaces. A plain/non-coated surface is defined as a copper surface which has been polished using 600 grit sand paper. Before each test, all plain/non-coated surfaces are swabbed with 2% HCL to remove surface oxidation then swabbed with isopropanol and finally rinsed with distilled water.

2.1.2 Microporous Coated Heaters

The coating method is generally a surface treatment technique used to increase vapor/gas entrapment volume and active nucleation site density by forming a porous structure with cavities. A thermally conducting microporous coating (TCMC) technique was developed by researchers at University of Texas at Arlington [6]. The coating consists of a mixture of copper particles (40-70 μm in size) and solder to produce an approximately 150 μm thick porous structure with numerous internal micron size cavities. Fabrication of the coating involves mixing the various coating components including particles, solder paste along with isopropyl alcohol. The mixture is then evenly spread onto a copper surface and heated; allowing the alcohol to evaporate and the solder to bond the particles to the surface. The resulting porous coating structure is estimated to have a porosity of about 40%. Fig. 2.2 shows a microscopic image of the TCMC microporous structure.

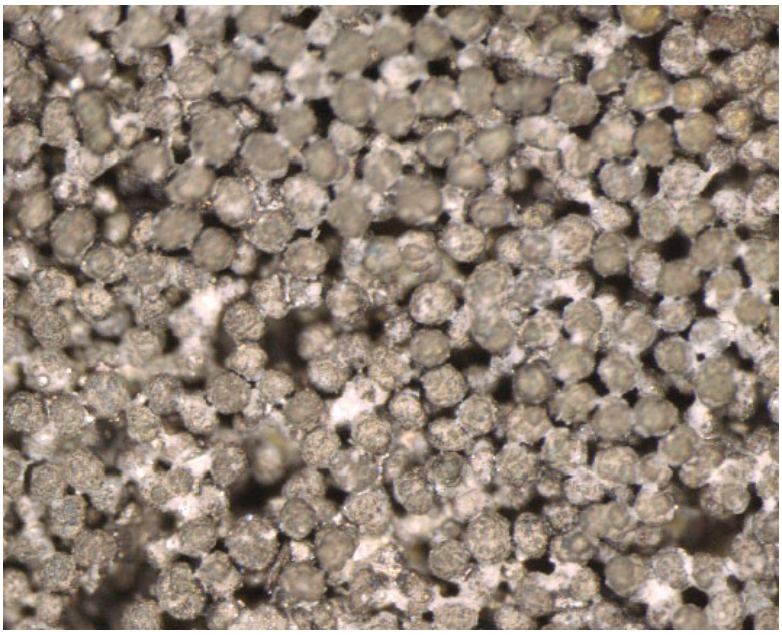

Figure 2.2. Microscope image of the TCMC microporous coating.

2.2 Pool Boiling Apparatus and Procedures

This section describes the pool boiling test loop and identifies its various components. It also discusses the procedures used to conduct pool boiling experiments.

2.2.1 Pool Boiling Apparatus

The pool boiling test section is a modified version of the test section used to conduct spray cooling experiments. The pool boiling test facility consists of a 4 inch I.D., ¼ inch thick Pyrex glass cylinder approximately 6 inches length and has a capacity of about 1¼ liters (Fig. 2.3). Two aluminum disks form the upper and lower enclosures and secure the glass cylinder. To prevent leakage, two ethylene-propylene diene M-class rubber (EPDM) gaskets are placed between the cylinder and the aluminum plates. EPDM was selected due to its compatibility with the various dielectric fluids used. A copper, concentric tube heat exchanger was located above

the test section and was used as a condenser during fluid degassing procedures. An exit port, with valve, was attached to the bottom plate and used to drain the test fluid.

A 500 watt, stainless steel cartridge heater inside the test section and two external band heaters provided heat during degassing procedures prior to testing. During tests, a temperature controller controlled the two band heaters to maintain fluid temperatures. Power to both the cartridge heater and the band heaters was adjusted using variable transformers (VARIACs). During pool boiling tests, the test heater was bolted onto an aluminum stand, within the test section. The temperatures of both the liquid and the vapor were measured using T-type thermocouples inside the test section. System pressure was measure using an Omegdyne PX35D1 (0-50 psia) absolute pressure transducer.

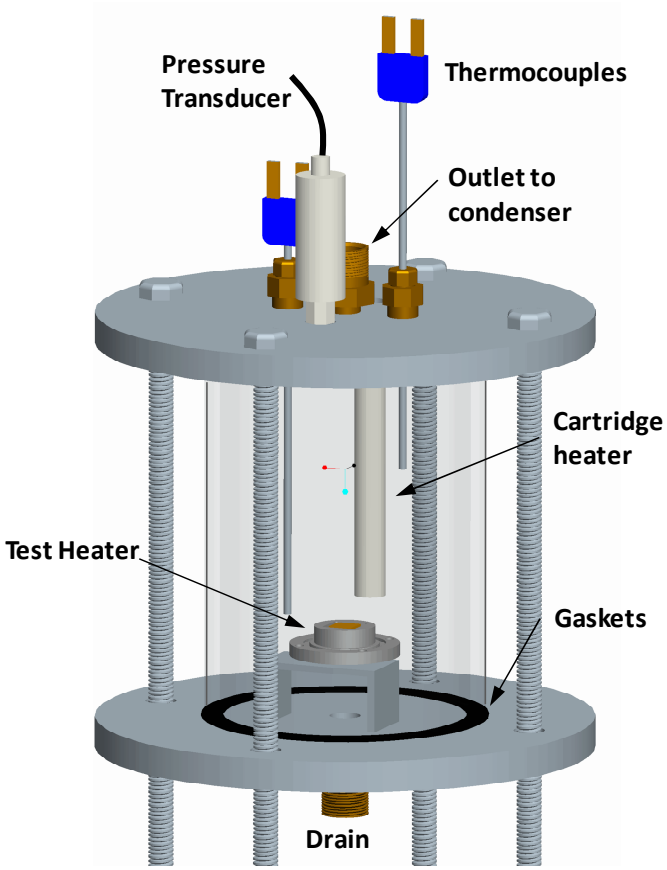

Figure 2.3. Schematic of the pool boiling test facility.

2.2.2 Pool Boiling Procedures

All pool boiling experiments were conducted under saturated conditions. The test heater was placed and secured to the test stand within the test section. About 0.8 liters of FC-72 were then deposited into the test section. The liquid was brought up to saturation temperature using the cartridge and band heaters. Upon reaching saturation temperatures, the liquid was allowed to boil for an additional hour to remove any non-condensable gasses (mostly air) from the system. The chilled water condenser, above the test section, allowed air to escape but condensed and returned any FC-72 vapor to the system. Once the system was degassed, the valve between the condenser and the test section was closed and the system was sealed. Pool boiling experiments were then controlled and monitored using a LabVIEW program which increments the heater heat flux up to CHF.

2.3 Flow Boiling Apparatus and Procedures

This section describes the flow boiling test loop and identifies its various components. It also discusses the procedures used to conduct flow boiling experiments.

2.3.1 Flow Boiling Apparatus

Of the three test facilities used, the flow loop facility is the most complex. A schematic of the flow boiling loop test apparatus is provided in Fig. 2.4. This flow loop is a modified variant of the spray loop apparatus and thus both loops share some of the same components. A 5 gallon capacity, stainless steel reservoir tank contains the approximately 4 liters of working fluid used during tests. Heat to the fluid is supplied using a 1 kW stainless steel cartridge heater located within the reservoir tank and a 180 W exterior band heater. Power to both heaters is manually controlled through VARIACs. To increase flow rate capacity, two pumps connected in a parallel arrangement were used. Both pumps are variable speed, magnetic drive gear pumps

manufactured by the Micropump Co. Pump 1 has a flow has a flow rate capacity of 0 to 1.7 lpm (~80 psi. max diff pressure). Pump 2 has a flow has a flow rate capacity of 0 to 2.1 lpm (~80 psi. max diff pressure). The suction end of both pumps were connected and pulled liquid through (draw-through design) the test section.

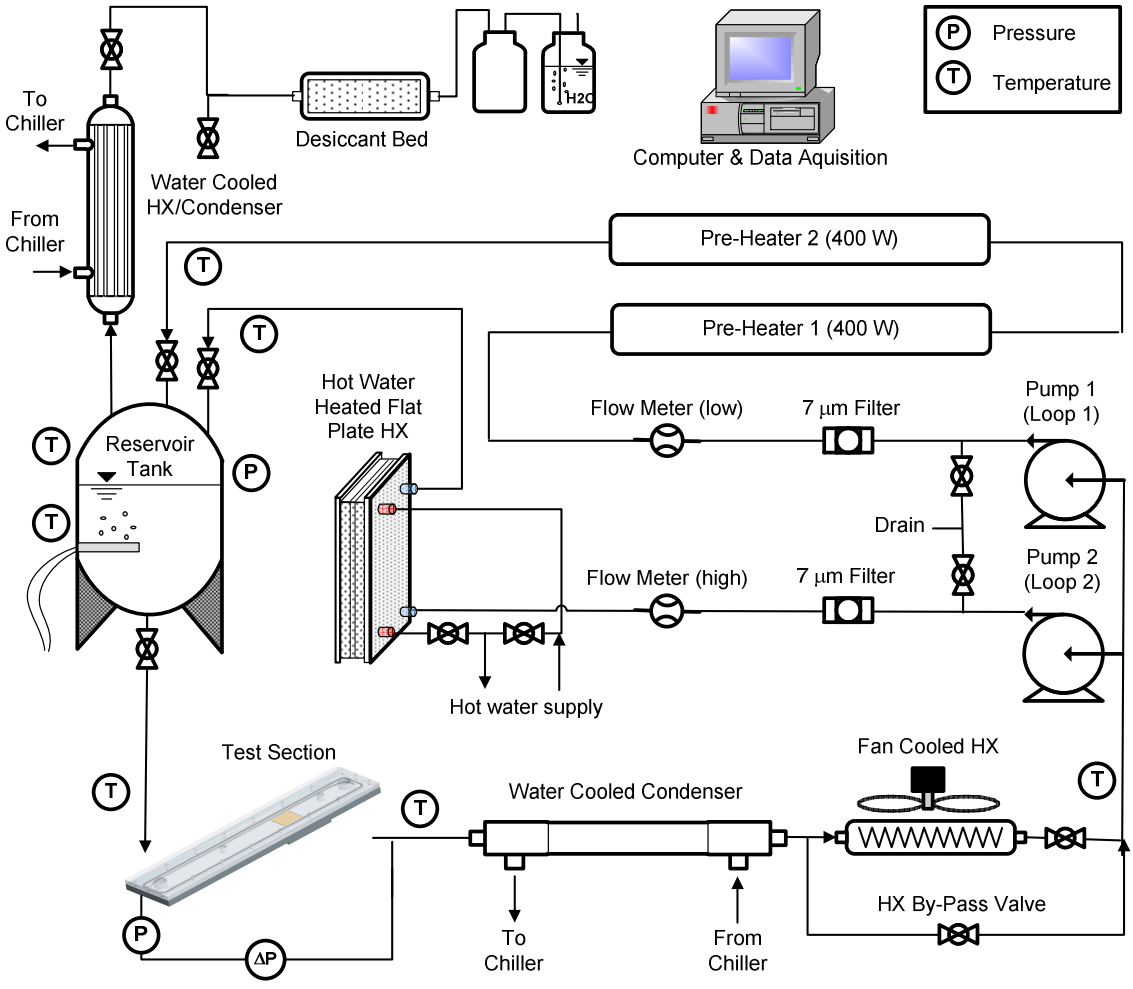

Figure 2.4. Flow loop schematic.

In order to maintain constant inlet conditions during flow boiling tests, the test section was located upstream of the pumps utilizing a draw-through design. This design ensured that any pressure drop associated from vapor generation on the heated surface would only affect

pressures downstream of the test heater; inlet pressures would be unaffected. A schematic of the test sections is provided in Fig. 2.5. Various test sections were used depending on the type of heater tested (with or without heat spreader) and the channel height. Relevant test section data is provided in table 2.1. The test sections consisted of two components (top and bottom) each machined entirely from transparent ½ inch thick polycarbonate. An o-ring channel was machined into the bottom component and an EPDM o-ring (-177 size) was placed within this channel. Inlet and outlet ports as well as two 1/16 inch dia. pressure ports (on either side of the test heater) were machined into the top components. The two components were bolted together to form the test section.

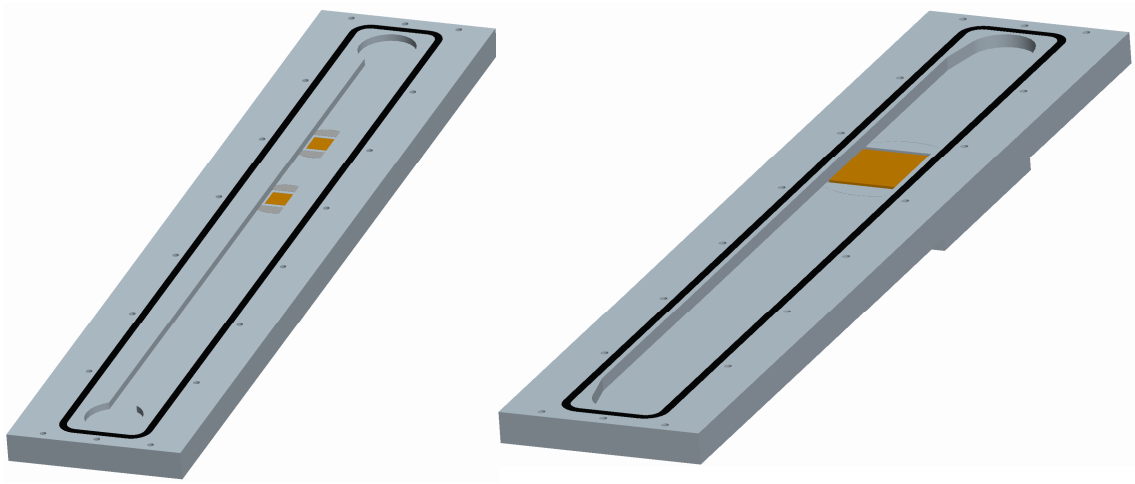

Figure 2.5. CAD models of the 10×10 mm heater (left) and heat spreader (right) test sections. For clarity, the top lexan plate is not shown.

Table 2.1. Test section channel dimensions and entrance length.

Heater design	channel height (mm)	channel width (mm)	D_h (mm)	Entrance length (mm)
10×10 mm	1	12	1.85	258 mm ($140\times D_h$)
10×10 mm	3	12	4.80	258 mm ($54\times D_h$)
Heat spreader	1	30	1.94	213 mm ($110\times D_h$)
Heat spreader	3	30	5.45	213 mm ($39\times D_h$)

Pressure at the inlet of the test section was measured using an Omegdyne PX35D1 (0-50 psia) absolute pressure transducer. Pressure drop across the test heater was measured using a Validyne DP15-44 differential pressure transducer. Test section inlet and outlet temperatures as well as additional system temperatures were measured using T-type probe thermocouples.

Two heat exchangers located immediately downstream of the test section were used to cool and condense the liquid/vapor prior to entering the pumps. The first heat exchanger is a chilled water cooled, concentric tube heat exchanger approximately 3.5 feet in length. The working fluid (FC-72) passed through inner tube constructed of ¾ inch O.D. copper tubing while chilled water circulated through the outer PVC shell (1 inch sch. 40). This heat exchanger was used to condense vapor exiting the test section. The second heat exchanger is fan cooled heat exchanger and was used to further reduce fluid temperatures to avoid pump cavitation issues. The outlets of each pump were connected to two independent loops. The flow loop connected to Pump 1 is designated as Loop 1 (low flow rate) and the other loop connected to Pump 2 was designated as the Loop 2 (high flow rate). Each loop contained the same components including a filter, flow meter and a heat exchanger. The filter was an inline 7 μm filter used to remove fluid particulates prior to entering the flow meters. Turbine flow meters purchased from Omega (Loop 1: FTB-601 with a 0.1 to 2 lpm range and Loop 2: FTB-603 with a 0.5 to 15 lpm range) were used to measure flow rates.

Two inline 3/8 inch I.D. copper tube heat exchangers, each approximately 4 ft in length, were installed in Loop 1 providing a total heat capacity of 800 watts. Heat to each heater was provided using 400 W rope heaters (Omega: FGR-080) wrapped around the copper tube and the entire assembly was insulated using 2 in thick, high temperature insulation. Power to these heaters was computer controlled, through relays, to maintain a constant fluid temperature. A flat plate heat exchanger (Flatplate FP5X12-8) was used in Loop 2. Hot water provided the heat source for this heat exchanger. Hot water, set to the desired temperature set point, was

generated using immersion heaters (2 kW total) and circulated from the hot water tank to the heat exchanger using a pump. Control of the hot water set point as well as a hot water fluid by-pass valve system was used to control FC-72 fluid temperatures leaving the flat plate heat exchanger. The heat exchangers were used to increase liquid temperatures prior to entering the reservoir tank. In this manner, the liquid was returned to the reservoir tank at a constant temperature throughout the duration of the flow boiling tests, which prevented any system temperature fluctuations.

2.3.2 Flow Boiling Test Procedures

SATURATED FLOW BOILING. First, both pumps were activated to each circulate about 400 ml/min of fluid. All system heaters were then activated including the two inline heaters, flat plate HX, reservoir cartridge heater and reservoir band heater to increase the liquid temperatures to saturated conditions. During this time, only the chilled water condenser, above the reservoir/degassing tank, was provided with chilled water; no other system cooling was provided (chilled water and air cooled heat exchangers were off). Once the liquid reached saturated conditions, the liquid was allowed to continue circulating for an additional hour to degass the system. Degassing took place within the reservoir tank where the cartridge and band heaters boiled the fluid. Vapor and non-condensable generated were forced up through the chilled water condenser above. The condenser allowed non-condensables to escape but condensed FC-72 back into the system.

After an hour of degassing, the valve above the condenser was closed; sealing the system and leaving only FC-72 liquid and vapor. Power to both the cartridge and band heaters were then reduced and system temperatures were maintained constant by controlling the liquid temperatures entering the reservoir tank. Pump speed(s) were then adjusted to achieve the desired flow rate. For lower flow rates, only Pump 1 was used and for higher flow rates, both pumps were used. To prevent pump cavitation issues, the fan and chilled water cooled heat

exchangers upstream of the pump were activated. Testing then begins once steady state conditions were reached. For all tests, the inlet pressure was maintained at about 1 atm. Being that this pressure can vary based on flow rate, its magnitude was controlled by controlling the system pressure, at the reservoir tank, and/or by throttling the valve just upstream of the test section. In this manner, fluid temperatures at the test section inlet were maintained to near saturated conditions ($\Delta T_{sub} \leq 1K$).

SUBCOOLED FLOW BOILING. Both pumps were activated to each circulate about 400 ml/min of fluid. All system heaters were then activated including the two inline heaters, flat plate HX, reservoir cartridge heater and reservoir band heater to increase the liquid temperatures to 25℃ (ΔT_{sub}=32K). During this time, the valve above the condenser (heat exchanger above the reservoir tank) is left open to allow outside air to freely enter/exit the system. Upon reaching this condition, the fluid is allowed to continue circulating for approximately 15 minutes before a test is run. After 15 minutes, the valve above the chilled water condenser is closed. This procedure ensured constant dissolved air content in the liquid for the duration of the tests. Once these preliminary procedures are completed, flow boiling experiments can begin.

Flow boiling tests were controlled and monitored using a program created in LabVIEW. The program controls a data acquisition system and power supply to generate heat flux controlled boiling curves. This is accomplished by incrementing the heater heat flux up until the heater reaches the temperature limit (~120℃). The program measures and records system temperatures and pressures at every heat flux. Upon reaching the heater temperature limit, the program shuts down power to the heater and saves all the data to a file.

2.4 Spray Cooling Apparatus and Procedures

This section describes the spray cooling test loop and identifies its various components. It also discusses the procedures used to conduct spray cooling experiments.

2.4.1 Spray Cooling Apparatus

A schematic of the spray loop used in this study is shown in Fig. 2.6. A stainless steel reservoir holds the approximately 2-3 liters of working fluid. The working fluid was circulated through the loop with a magnetically coupled gear pump (~80 psi. max.) and the speed of the pump was manually controlled though a variable D.C. power supply. A 5 μm filter installed after the pump filtered out particulates and prevented nozzle clogging issues. Fluid volumetric flow rate was measured using an Omega Turbine Flowmeter which has a range of 0.1-2 lpm. In order to maintain desired nozzle inlet fluid temperatures, two inline pre-heaters were constructed of ¾ inch O.D. aluminum tubing wrapped in coils of nichrome resistance wire and the entire assembly was then externally insulated. Power to the pre-heaters was computer controlled through relays and in this manner, nozzle inlet temperatures were maintained to with $\pm 0.5^{o}$C. The fluid exits the pre-heaters and enters the test section within which the spray nozzle and test heater were located.

The test section consists of a 4 inch I.D. Pyrex glass cylinder, approximately 6 inch in length, held in place with two aluminum plates (Fig. 2.6). EPDM gaskets (80 durameter) were placed at the joints (top and bottom) between the glass cylinder and aluminum plates to maintain an air tight seal. A fan cooled heat exchanger, downstream of the test section, removes heat from the fluid which then drains back in to the reservoir tank and completes the fluid cycle. Temperature measurements are taken at various locations on the spray loop using T-type thermocouples. Pressure drop across the nozzle and the pressure of the reservoir tank were measured using Omega PX603 (0-60 psi) pressure transducers.

2.4.2 Spray Cooling Test Procedures

Before an experiment was performed a series of procedures were first conducted. First, the valve located between the reservoir tank and the chilled water condenser was opened

allowing air to freely enter or leave the system. Any vapor would condense on the condenser and be returned to the system. The pump speed is manually adjusted to obtain the desired flow rate and the pre-heaters are then activated increasing the nozzle inlet fluid temperature to 25℃. Upon reaching this condition, the fluid is allowed to continue circulating for approximately 15 minutes before a test is run. After 15 minutes, the valve between the reservoir tank and chilled water condenser is closed. This procedure ensured constant dissolved air content in the liquid for the duration of the test. Once these preliminary procedures are completed, spray cooling tests can begin.

A LabVIEW computer program controls and monitors the spray cooling experiments. The program controls a data acquisition system and power supply to generate heat flux controlled boiling curves. This is accomplished by increasing the heater heat flux at constant increments up to CHF. After each heat flux increment, the program evaluates for heater temperature equilibrium before the next heat flux increment is made. When heater temperature exceeds the temperature limit, power to the heater is shut down and all data then saved to a text file.

2.5 High Speed Video

High speed video was obtained using a Vision Research Phantom V4.3 High Speed Video Camera. The camera is capable of 1,000 fps at the maximum resolution of 800×600 pixels and a minimum shutter speed of 10 μs. Higher frame speeds (max. 90,000 fps) are possible at lower resolutions.

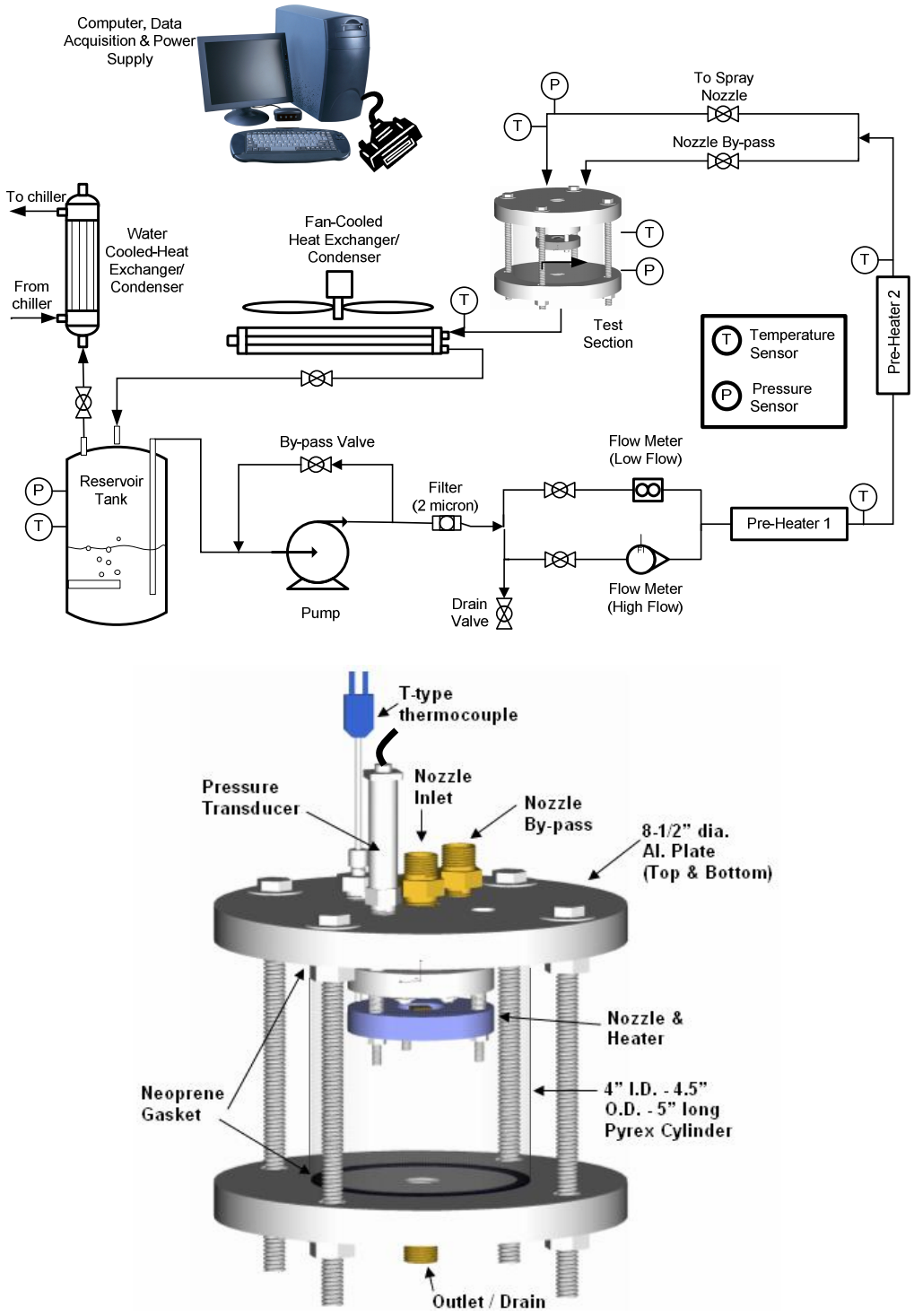

Figure 2.6. Spray loop schematic (top) and spray test section model (bottom).

2.6 Uncertainty Analysis

An uncertainty analysis was conducted to estimate the uncertainties in the various measurements and calculations in this study. To calculate the total uncertainty of a measurement first, the uncertainties of all components (DAQ, transducers, instruments, etc…) used in obtaining that measurement were identified and characterized as either bias or precision errors per procedures outlined in [54, 55]. Total bias (B) and precision (P) errors were then each separately totaled using the propagation of error equation (eq. 2.1).

$$\omega = \left[\sum_{i=1}^{n} \left(\frac{\partial f}{\partial x_i}\omega_{x_i}\right)^2\right]^{1/2} \tag{2.1}$$

Where the x_i's represent the different variables used to calculate the parameter (i.e. heat flux, velocity, flow rate) and ω_{xi}'s represent the variable uncertainties. The total error was then calculated by taking the root sum squared (RSS) of the bias and precision errors (eq. 2.2).

$$\omega_{total} = (B^2 + P^2)^{1/2} \tag{2.2}$$

This section summarizes results obtained from this analysis. Details of this uncertainty analysis procedure are provided in Appendix A.

2.6.1 Heat flux Uncertainty Analysis

For all experiments, the heat flux was calculated using the 4-wire method. This method required for the voltage drop across a shunt resistor to be measured and used to calculate the current (*I*) flowing through the heater. The current was then multiplied by the voltage drop (*V*) across the heater to calculate the power. The power was then divided by the heater surface area (A_{heater}) to calculate the heat flux (eq. 2.3).

$$q'' = \frac{V \cdot I}{A_{heater}} \tag{2.3}$$

The heat flux uncertainty was calculated to be ~5.1% at 100 W/cm^2. The majority of which is due to the uncertainty in the shunt resistor.

Design of the test heaters included using finite element analysis to estimate the heat loss through the sides and bottom of the heaters. A detailed 3-D model of each heater (with and without a heat spreader) were created using Pro/E. The models included components such as the copper block, epoxy, polycarbonate, power wires, solder, etc… The models were then imported to ANSYS 11 where they were meshed and thermal loads were imposed on the model. Conservative estimates to the heat transfer coefficients were imposed on the external insulation surfaces to assume worst case scenarios.

The FEM simulation for the 10×10 mm heater outputting 20 watts revealed that heat loss through the insulation is about 0.3 watts or 1.5%. An FEM simulation of a 30×30×3 mm heat spreader outputting 80 watts found about 4 watts (5%) of the heat is loss through the insulation. It should be noted, that these FEM calculated heat loss estimates were not deducted from any experimental data obtained. A detailed description on this FEM analysis procedure is provided in Appendix B.

2.6.2 Flow Rate/Velocity Uncertainty Analysis

The uncertainties of both the liquid flow rates and velocities were estimated. Liquid flow rate and velocity were the indicators used to quantify fluid movement in spray cooling and flow boiling experiments, respectively. The error/uncertainty in each was therefore obtained. Equation 2.4 was used to calculate the flow rate for both spray cooling and flow boiling experiments. In this equation, *f* (pulses per second) is the frequency output from the turbine flow meters and *k* is a calibration constant with units of pulses per liter. The estimated uncertainty in

the flow rate measurements is about 1.6%. The calibration factor, *k*, was found to be the largest contributor to this uncertainty.

$$Q = \frac{f}{k} \tag{2.4}$$

Fluid velocities, in flow loop experiments, were calculated by diving eq. 2.4 with the test section channel cross sectional area (width × height). The added error in the area inevitably introduced more uncertainty into velocity measurements as compared to flow rate measurements. The uncertainty in velocity was estimated to be about 2%. The calibration factor, *k*, was found to be the largest contributor to this uncertainty followed by the uncertainty in area.

2.6.3 Temperature and Pressure Uncertainty Analysis

Uncertainty in temperature measurements is estimate to be ±0.5℃. The uncertainties for the pressure were determined using uncertainties in both the transducers and the data acquisition system and were estimated to be less than 2.5%.

CHAPTER 3

FLOW BOILING

The flow boiling results on the effect of the TCMC coating is reported in this section. Tests were conducted using flush mounted, horizontally oriented (upward facing) 10×10 mm heaters both with and without attached heat spreader plates (30×30×3 mm). The effect of flow boiling parameters including fluid velocity, subcooling and test section channel height (1 & 3 mm) on TCMC coated heater performance is investigated. All experiments were conducted while maintaining constant inlet (upstream of heater) pressure (atmospheric) and temperature conditions.

3.1 Flow Boiling on Non-coated Surfaces: Flow Loop Qualification

Experiments were first conducted using non-coated heaters. The results were then compared to existing and accepted correlations and data sets to qualify the flow loop. In Fig. 3.1, the saturated flow boiling curves for the non-coated heaters at flow rates of 0.1, 0.5 and 1 m/s are shown. The arrows shown at the end of the boiling curves, in this figure and all future figures, indicate the onset of CHF. The test section channel dimensions, for these tests, were 12 mm wide by 3 mm high. For reference, an FC-72 pool boiling curve from Rainey [4] is also provided. This figure clearly demonstrates that increasing velocity has minimal effect on nucleate boiling performance as indicated by the convergence of all three flow boiling curves which is consistent with that previously reported by [22, 34]. In addition, the nucleate boiling segments of the flow boiling curves, nearly match those of the pool boiling curve. The slight differences between the current flow boiling curves and the Rainey [4] pool boiling curve are likely a result of slight differences in surface roughness between the heaters.

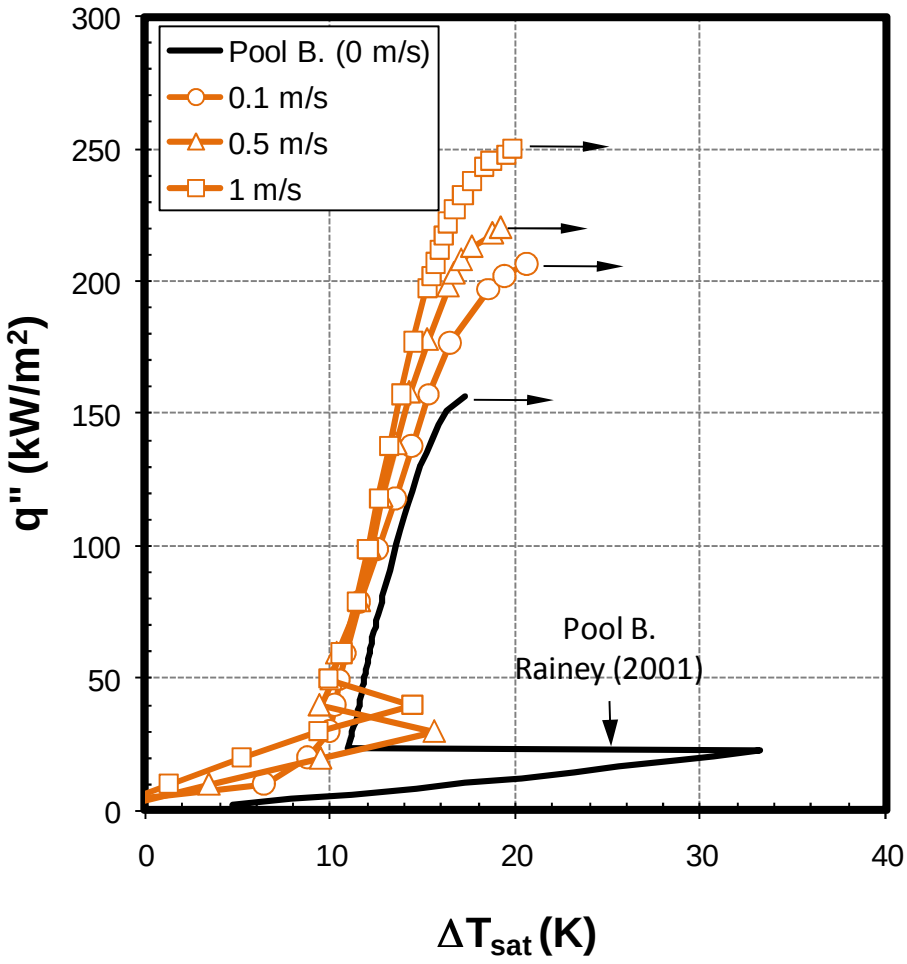

Figure 3.1. Saturated flow boiling curves for a non-coated heater at 0.1, 0.5 and 1 m/s. Channel height is 3 mm.

Fig. 3.2 plots the single phase Nusselt numbers for the non-coated heaters and compares them to the single-phase FC-72 correlation developed by Gersey & Mudawar [34] (eq. 3.1). The characteristic length in both the Nusselt and Reynolds numbers is the length of the heater in the direction of flow. The forced convection heat transfer coefficient values for non-coated heaters are in agreement with those predicted by eq. 3.1 and are not significantly affected by a change in channel height (1 & 3 mm).

$$\overline{Nu_L} = 0.362\, Re_L^{0.614}\, Pr_f^{1/3} \tag{3.1}$$

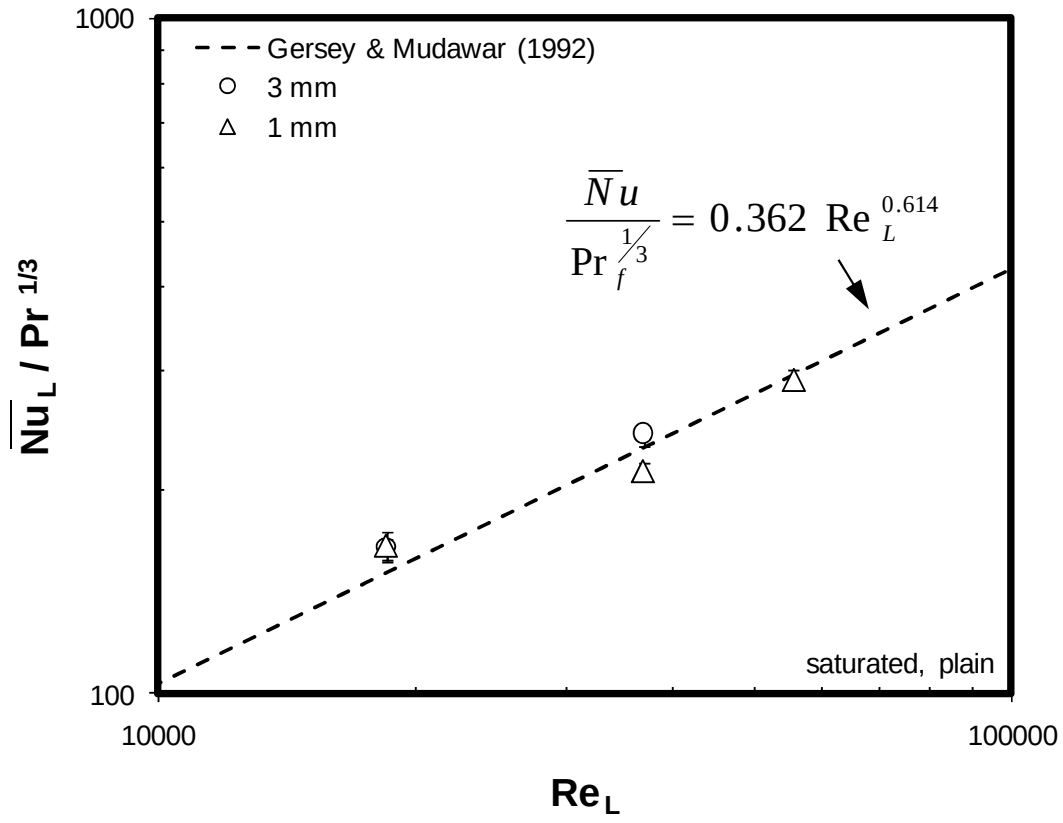

Figure 3.2. Single phase Nusselt numbers plotted versus the Reynolds numbers for non-coated heaters.

In Fig. 3.3, the CHF for all non-coated heater tests, including saturated and subcooled (non-degassed) at both 1 and 3 mm channel heights are provided. The CHF values were compared to those predicted by the Mudawar & Maddox [56] CHF correlation (eq. 3.2) which considers flow rate, subcooling and channel geometry. In order to compare the current CHF values to those predicted by the CHF correlation it was necessary to normalize the CHF values into a non-dimensional form according to eq. 3.2. The non-dimensional CHF (q_m") is then plotted as a function of the inverse of the Weber number (Fig. 3.3). In general, the correlation

over predicts saturated cases and under predicts subcooled cases. However, considering the correlation uncertainty, the current data sets match fairly well with the correlation predictions.

$$q_m^{**} = \frac{\frac{q"_m}{\rho_v U h_{lv}}}{\left(\frac{\rho_l}{\rho_v}\right)^{15/23}\left(\frac{L}{D_h}\right)^{15/23}\left(1+\frac{C_{p,l}\Delta T_{sub}}{h_{lv}}\right)^{7/23}\left(1+0.021\left(\frac{\rho_l}{\rho_v}\right)\frac{C_{p,l}\Delta T_{sub}}{h_{lv}}\right)^{16/23}}$$

$$= 0.161(We)^{-8/23}$$

(3.2)

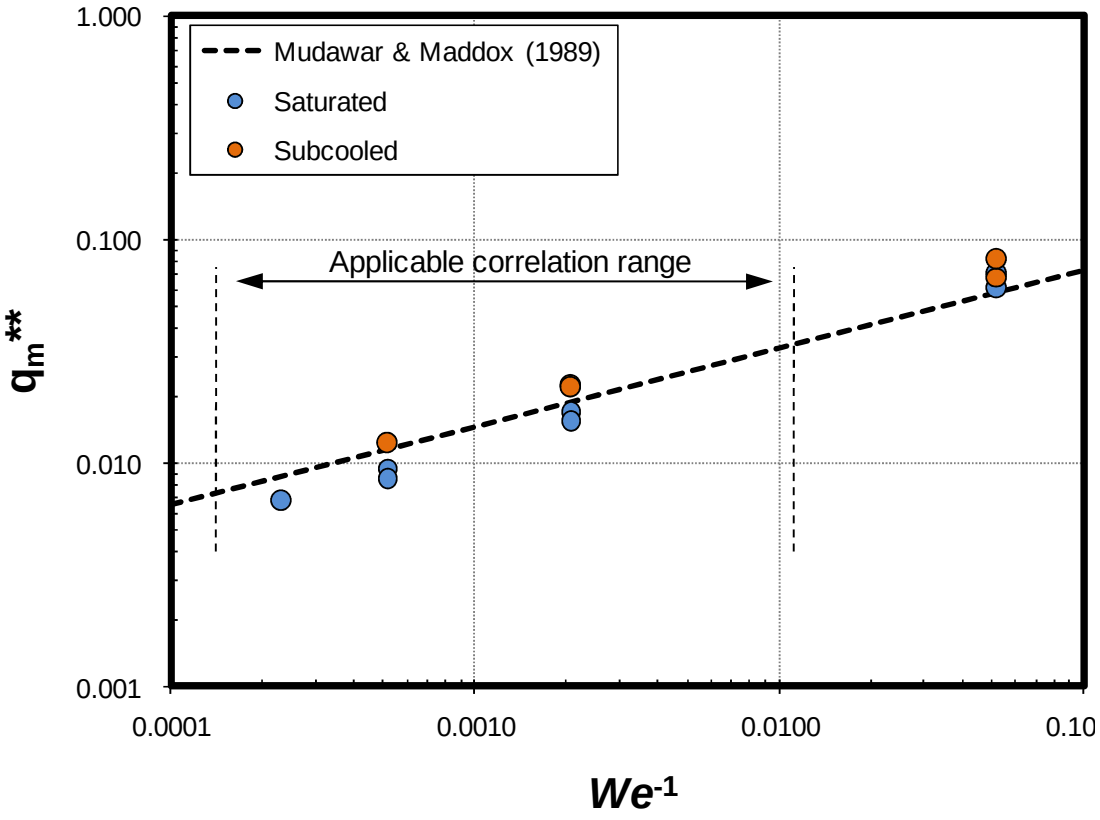

Figure 3.3. Non-dimensional CHF values for non-coated heater. Saturated and subcooled (non-degassed) results at both 1 & 3 mm channel heights shown.

Agreement between the current results and those of existing and accepted correlations validate the data (single-phase, nucleate boiling & CHF) produced from the flow boiling test loop. Having qualified the flow loop for a non-coated/plain heater, experiments were then conducted using the TCMC coated heaters.

3.2 Flow Boiling on TCMC Coated Heaters

Flow boiling experiments were then conducted using TCMC coated 10×10 mm heaters at flow rates ranging from 0.1 to 1.5 m/s. The results revealed that the single-phase forced convection heat transfer coefficients (*h*-values), of the TCMC boiling curves, were higher than those of the non-coated heaters. There are two possible reasons for this occurrence; one is associated with the slight protrusion of the TCMC heater and the other is from nucleation within the coating. The former of the two, nucleation within the coating, is believed to be the dominating contributor. Although no surface boiling is observed, the high *h*-values indicate that there could be some, minimal boiling occurring within the coating. This would likely occur at the downstream end of the heater where temperatures are expected to be higher. In this case, any bubbles/vapor generated would be swept away from the heater and thus would not seed additional nucleation sites which could then result in full surface boiling.

The second likely reason is associated with the manner in which the epoxy surrounding the TCMC coated heater is applied. Being that the porous nature of the TCMC coating can wick pre-hardened epoxy into the coating, and thus degrade performance, much care is taken not contact the coating as the epoxy is being applied. This in turn leaves a slight downward curvature in the hardened epoxy which surrounds the TCMC coated heaters. This depression surrounding the coating in combination with the slightly protruding thickness of the coating (~150 μm) is believed to disrupt or “trip” the flow and induce turbulence thus increasing single phase *h*-values. A flow boiling study comparing flush mounted and protruding heaters by Gersey & Mudawar [34] report similar results. Their study reported that the protruding heaters (1

mm protrusion) had higher single phase heat transfer coefficients but about the same nucleate boiling heat transfer performance as compared to flush mounted heaters. Therefore, since the higher “single”-phase heat transfer coefficients of the TCMC coated heaters are believed to be affected, in part, by the slight protrusion of the TCMC coated heater, only the nucleate boiling portions of the TCMC boiling curves will be shown.

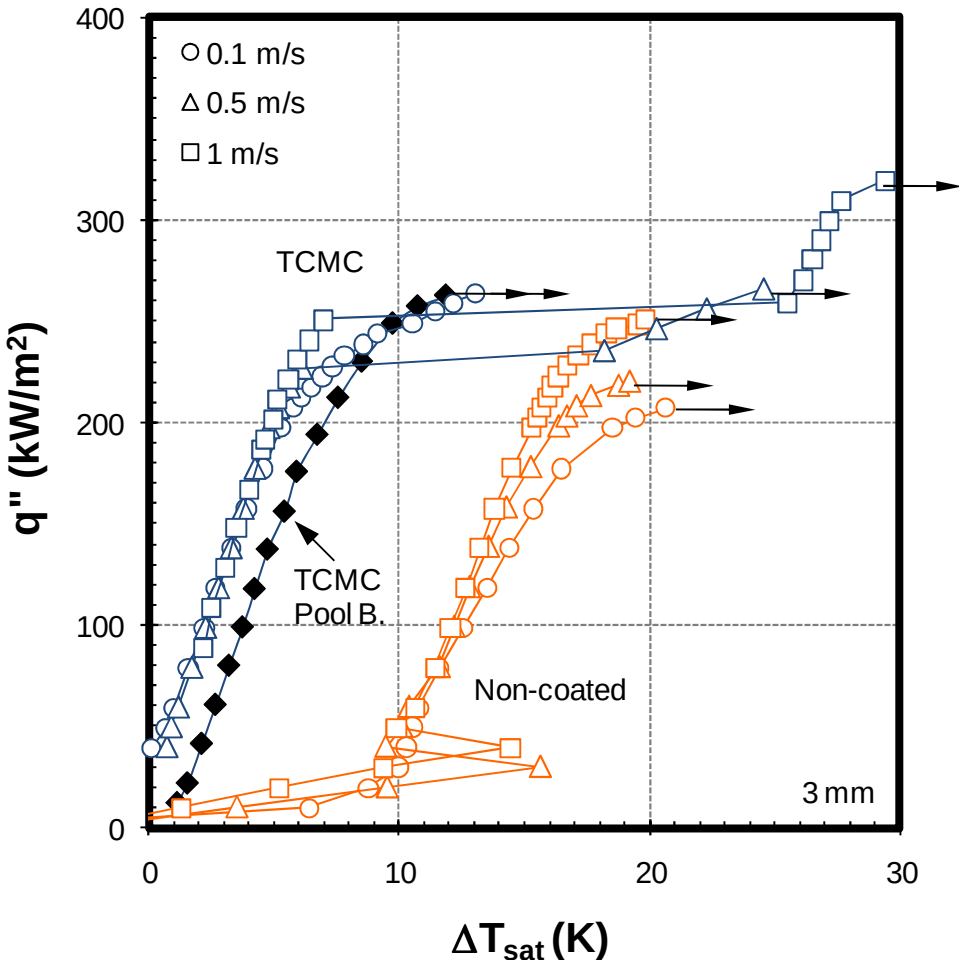

Figure 3.4. Saturated flow boiling curves for TCMC coated and non-coated heaters tested at a channel height of 3 mm.

Flow boiling curves for TCMC coated and non-coated heaters are shown in Fig. 3.4. These tests were done under saturated conditions using a channel height of 3 mm at flow velocities of 0.1, 0.5 and 1 m/s. As was the case with the non-coated heaters, velocity has minimal effect on nucleate boiling heat transfer with the TCMC coated heaters as indicated by the convergence of the flow boiling curves at the three velocities tested. The pool boiling curve for the TCMC heater is also shown (Fig. 3.4) and is slightly shifted to the right as compared to the flow boiling curves. This slight increase in performance, for the flow boiling tests as compared to the pool boiling test, might be attributed to the effect of fluid motion (velocity) pushing vapor within the coating and thus activating additional nucleation sites.

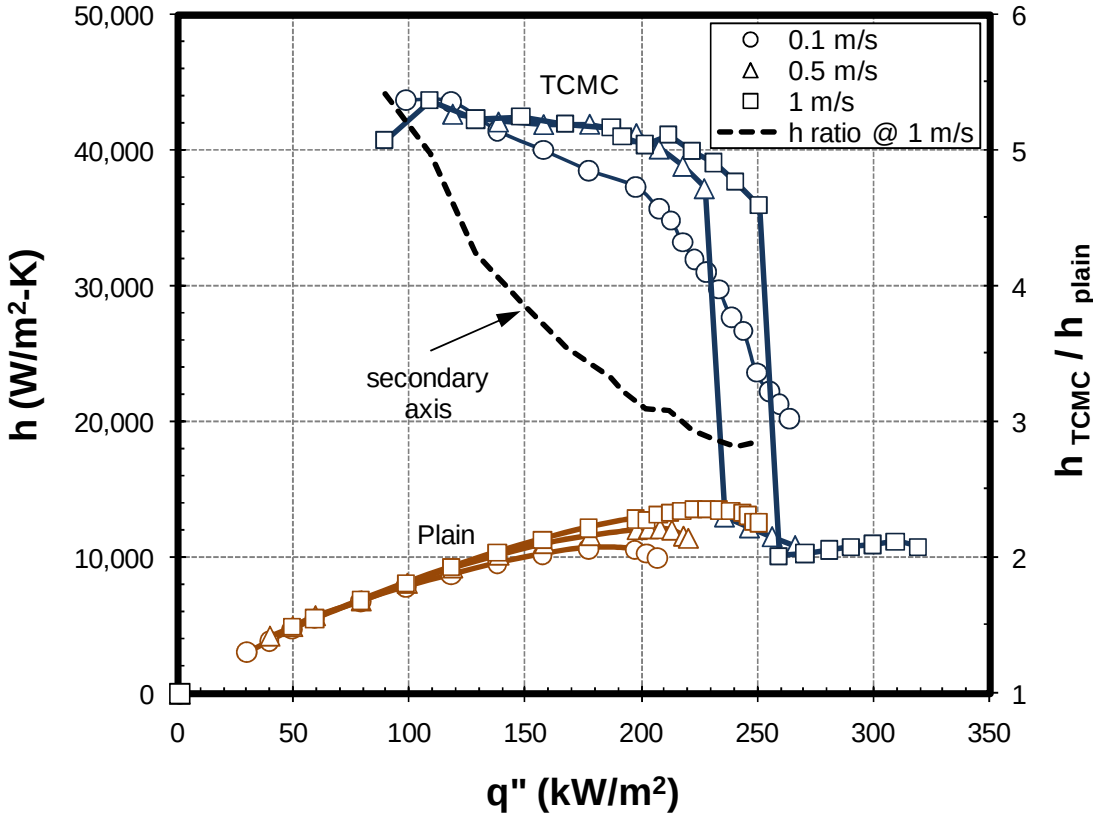

Figure 3.5. Nucleate boiling heat transfer coefficients for both coated and non-coated heaters.

Comparing the performance of the TCMC coated heaters to the non-coated heaters, it is clear that the coating provides significant nucleate boiling heat transfer enhancement. The coating can increase the heat transfer coefficient by as much as about 400% and produce values as high as ~42,000 W m^{-2} K^{-1} (Fig. 3.5). These *h*-values produced by the coating are significantly high considering that they were achieved using a dielectric fluid. Dielectric fluids are typically considered to produce lower *h*-values due to their poor thermal properties (as compared to water). Another trend that can be observed from Fig. 3.5 is that *h*-values for TCMC coated heaters are nearly constant (≥ 0.5 m/s) whereas *h*-values of non-coated heaters are found to increase with increasing heat flux.

The TCMC coating is also found to affect surface dry out behavior. This is evident in the manner in which the TCMC flow boiling curves demonstrate two distinct temperature spikes at high heat fluxes (Fig. 3.4). The initial temperature excursion is observed to be a gradual increase in temperature the duration (just before temperature jump to temp. equilibrium afterwards) of which taking about 10-15 min. It is believed that during this process, vapor patches blanket a significant portion of downstream half of the heater and this is what creates an increase in temperature. However, this phenomenon is countered by the wicking action of the microporous coating which is believed to retain and passively transport fluid and thus delays complete dryout, CHF. Following the initial temperature spike, the heater once again reaches temperature equilibrium and the experiment continues on to higher heat fluxes. The second temperature excursion is a quick process where the temperature quickly increases and exceeds heater temperature limits prompting an experiment shut down by the computer.

It should be noted that the initial temperature spike, for TCMC coated heaters at higher flow rates (≥ 0.5 m/s), occurs at heat fluxes lower than the CHF at 0.1 m/s (274 kW/m^2) and even pool boiling (266 kWm^2) (Fig. 3.6). Thus it seems that one of the effects of increasing velocity on TCMC coated heaters is to suppress vapor near the heater and thus cause the initial temperature spike behavior, as this phenomenon is not observed at the lowest velocity or pool

boiling. But as previously stated, wicking of fluid from the front and sides of the heater, from the coating, is believed to prevent complete surface dryout.

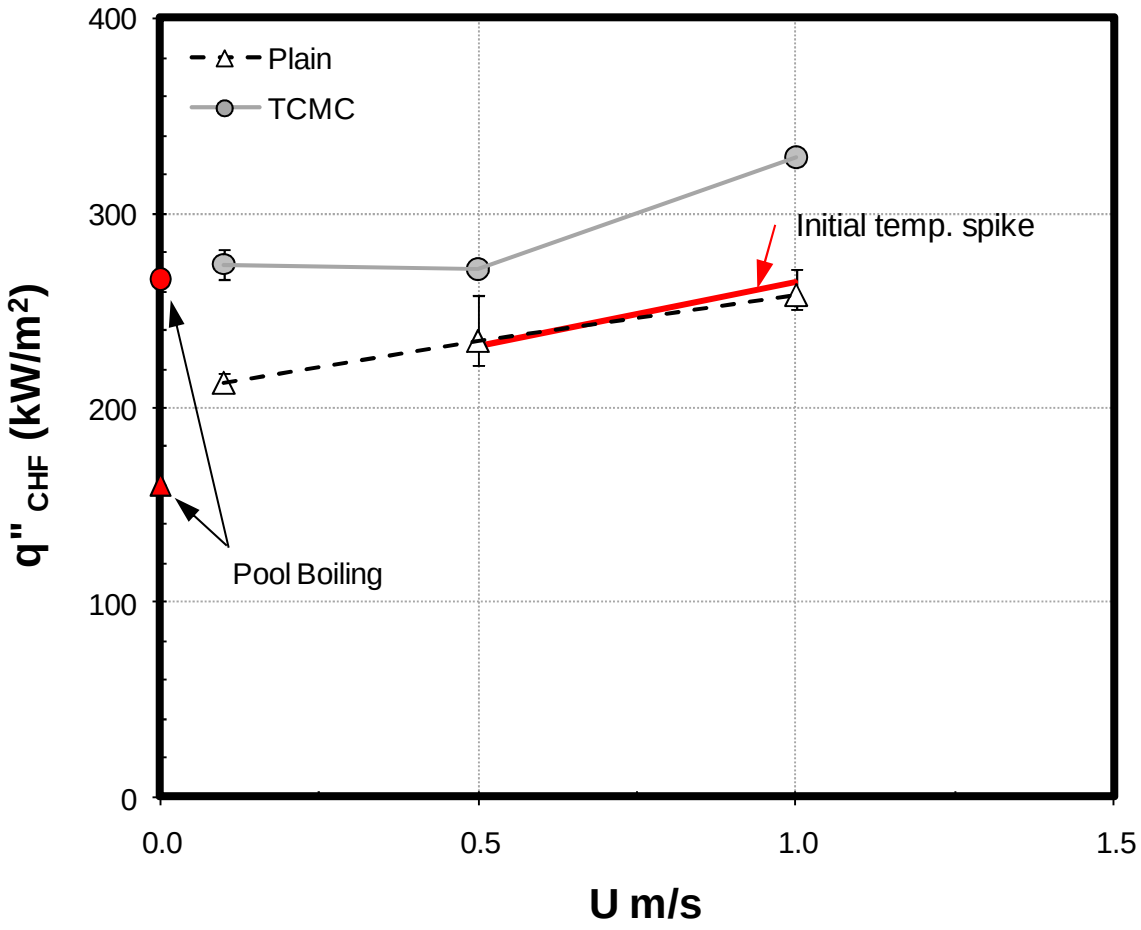

Figure 3.6. CHF values for all flow velocities for both coated and non-coated heaters.

High speed video of flow boiling tests shows that at heat fluxes after the initial temperature excursion but before the second, liquid to surface contact still occurs. Prior to this point (before initial temperature spike) there was no boiling at the leading edge of the heater (Fig. 3.7a). However, after the initial temperature excursion, boiling is only observed to occur at the front (~1 mm thick strip at the leading edge) and the sides the heater. Random boiling is also likely to occur at other parts of the heater, however, a vapor blanket likely covers a

significant portion of the downstream half of the heater as indicated by the decrease in heat transfer coefficients (Fig. 3.7b). At still higher heat fluxes, upstream fluid initially contacting the leading edge of the heater instantly vaporizes and coalesces creating sort of vapor boundary layer. This vapor boundary layer forces most of the incoming liquid to flow over it, thus restricting fluid-to-surface contact to the leading edge of the heater. Hydrodynamic instabilities as well as vigorous boiling at the leading edge then create waves at the vapor-fluid interface. Intermittent fluid to surface contact then also occurs as the trough of the waves ripple across the heater. Soon after, vapor generation from the heater surface is strong enough to prevent any further liquid to surface contact. This in turn leads to the second temperature excursion which is observed to be followed by a complete surface dryout (Fig. 3.7c). CHF is then said to have occurred.

This transient vapor to liquid wave behavior is consisted with that reported by [57-59]. All of whom also observed that at higher heat fluxes, near CHF, fluid to surface contact only occurred at the leading edge and at “wetting” fronts which swept over the surface. In their study using smooth heaters, Galloway & Mudawar [57, 58] make the claim that CHF in flow boiling is triggered when vapor pressure at the surface in conjunction with the momentum of the rising vapor from boiling at the wetting fronts overcomes and pushes away the wetting fronts.

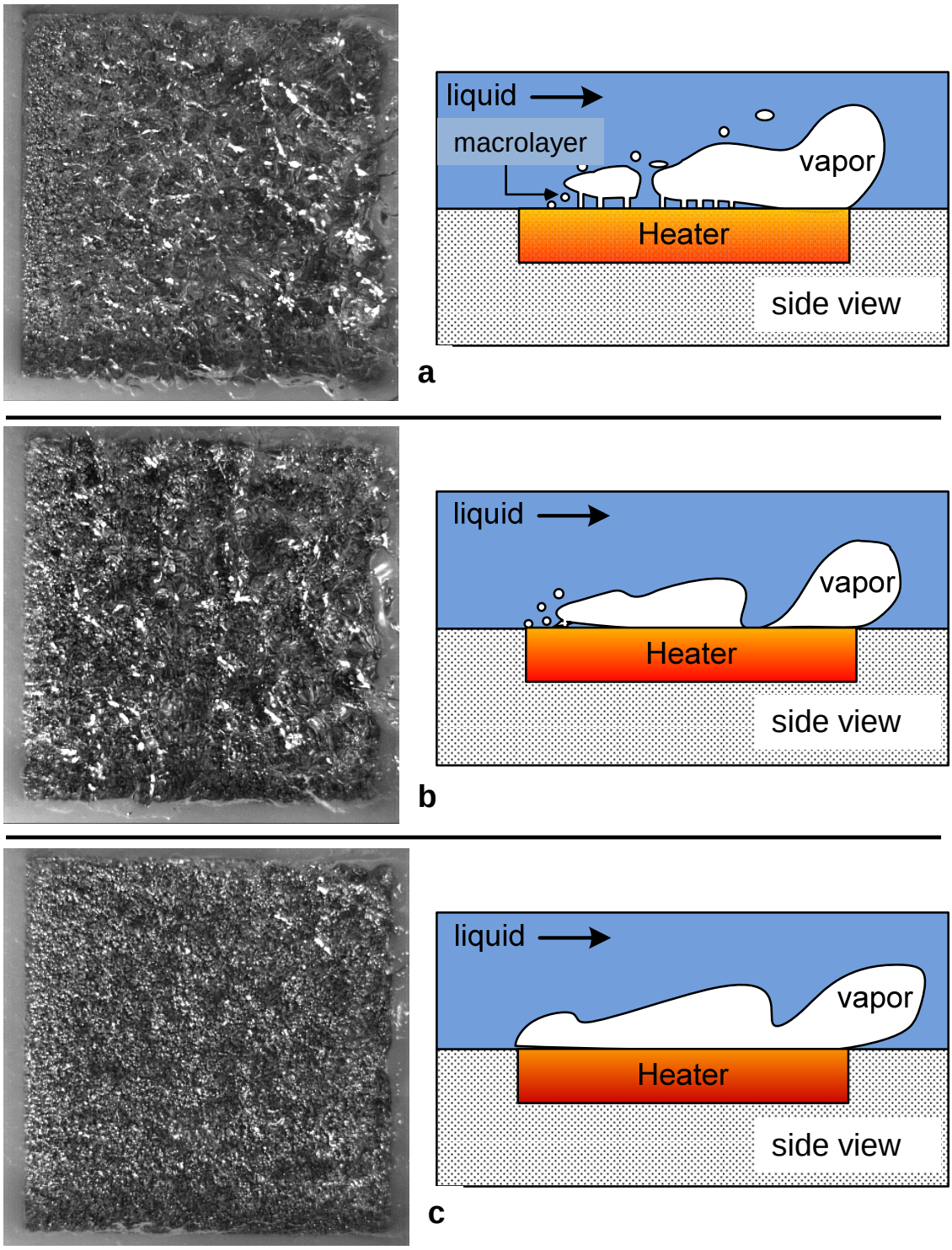

Figure 3.7. High speed video images (left) and drawing representations (right) of flow boiling over a TCMC heater at 1 m/s. At 250 kW/m^2 prior to temperature excursion (a), at 300 kW/m^2 after first temperature excursion (b) and at 320 kW/m^2 CHF (c).

3.2.1 Effect of Channel Height

Experiments were conducted using test channel with channel heights of 1 and 3 mm using both non-coated and TCMC coated heaters. Experiments were conducted under saturated conditions and results are shown in Fig. 3.8. It is clear from the figure that changing the channel height (from 3 to 1 mm) has minimal effect on nucleate boiling heat transfer performance, but does influence CHF. These results are consistent with those of Willingham & Mudawar [40] who conducted test with smooth/non-coated heaters with channel heights of 2, 5 and 10 mm. The current tests also show that the TCMC coated heater also produces the dual temperature excursions at 1 mm channel height.

The trend for both TCMC coated and non-coated heaters was the same; in general, at higher velocities (≥ 0.5 m/s) the lower channel height of 1 mm produced higher CHF. In the larger channel (3 mm) the vapor production at the heated surface forms a sort of vapor barrier above the heater which forces the incoming liquid to flow above it. However, the confined space of the smaller channel (1 mm) forces the upstream liquid closer to the heater surface which then effectively “sweeps” vapor off the heater and extends CHF. Higher CHF in the smaller channel comes at the expense of a higher pressure drop (~4× higher). At the lowest flow rate however, a combination of the confined 1 mm channel and low velocity stagnates vapor above the heater and results in lower CHF as compared to the 3 mm channel. This observed effect of channel height on CHF differs from that of [40] who reported that the 5 mm channel produced the highest CHF as compare to smaller 2 mm channel. However, their tests were done using a linear array of heaters and heater interaction might have affected their results.

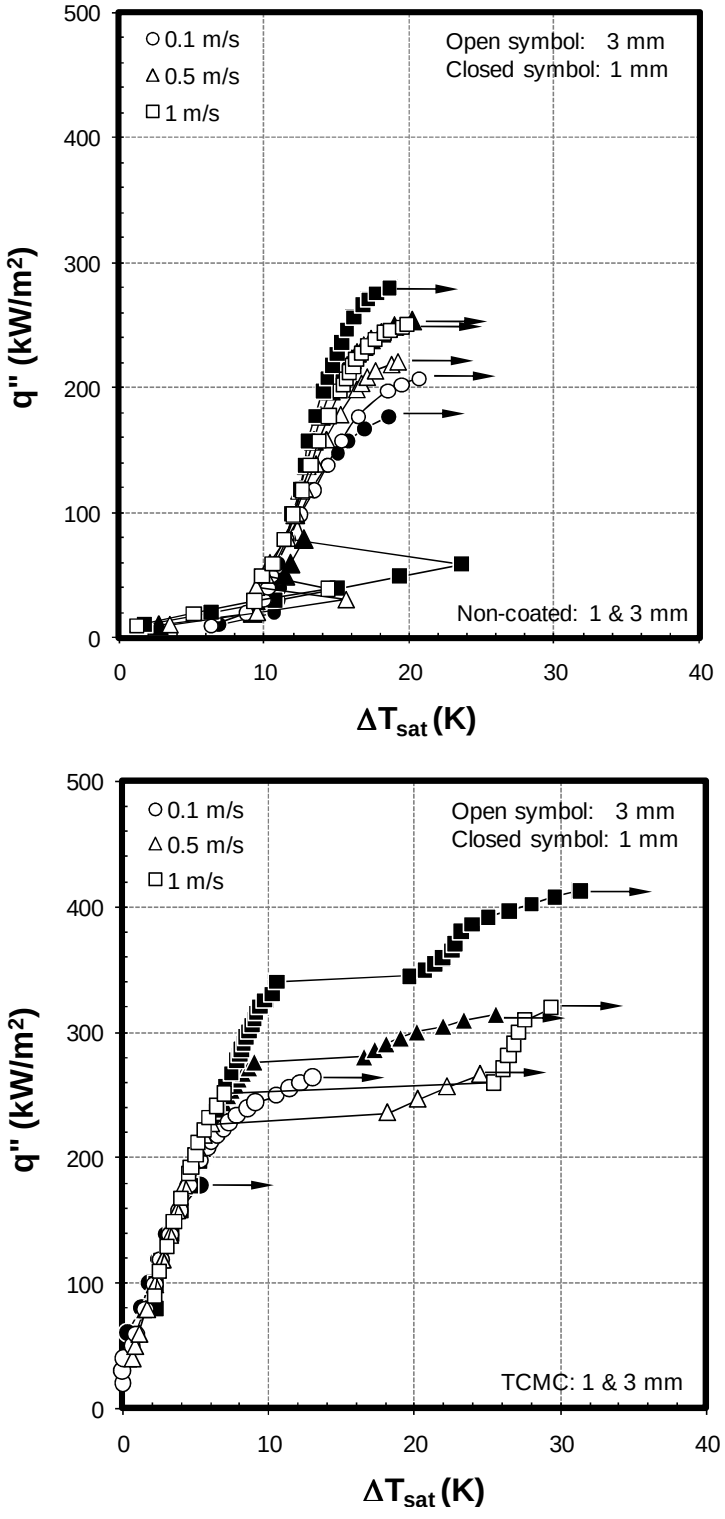

Figure 3.8. Effect of channel height on flow boiling performance; non-coated (top) and TCMC coated (bottom).

Reducing the channel height is expected to have more of an effect on flow boiling performance for long rectangular heaters where small channel heights can confine and thus coalesce vapor which then blankets the downstream end of the heater. In this scenario, the benefits of the coating could be even more pronounced as wicking through the coating could transport liquid to localized dryout spots at the downstream side of the heater.

3.2.2 Effect of Subcooling

"Gassy" subcooled FC-72 ($\Delta T_{sub} \approx 32K$) tests at near atmospheric conditions were conducted using both coated and non-coated heaters. Gassy or non-degassed refers to the dissolved air content within the subcooled FC-72. It is well known that air is highly soluble in FC-72. Air's solubility in FC-72 has been estimated to be as high as ~48% by volume at atmospheric pressure [36]. The amount of dissolved air can be estimated using Henry's Law (eq. 3.3).

$$C_g = H(T_{bulk})P_g \tag{3.3}$$

In this equation, the C_g is the ratio of moles of dissolved air/gas to moles of liquid and H is Henry's proportionality constant the value of which is taken as 5.5×10^{-5} moles/moles-kPa and is obtained from O'Connor et al. [36]. The partial gas pressure is calculated as the difference between the total pressure (at the reservoir tank) and the saturation pressure corresponding to the bulk liquid temperature (25℃). The dissolved gas concentration is then estimated to be 0.0037 $moles_v/moles_l$. The degree of subcooling is quantified as the difference between the liquid inlet temperature and the saturation temperature corresponding to the inlet pressure.

In the case of the non-coated heater, the effect of subcooling is to shift the boiling curve to the left (enhance heat transfer) and to increase CHF (Fig. 3.9). The added partial pressure of the dissolved gas adds to the vapor pressure within embryonic bubbles which then is believed

to facilitate nucleation [36, 38, 60]. This in combination with the convection effects of the departing bubbles as they promote mixing of the superheated liquid layer with the much cooler bulk liquid results in significant heat transfer enhancement at lower heat fluxes, as compared to saturated case. At higher heat fluxes however, the liquid near the heater becomes depleted of air/gas at which point the subcooled and saturated flow boiling curves approach one another, but never completely merge. Further merging between the subcooled and saturated boiling curves might occur at higher velocities (i.e. higher heat fluxes).

In the case of the TCMC coated heaters, the effect of gassy subcooling is more pronounced as compared to the non-coated case (Fig.3.9). Previous flow boiling tests by Rainey [4] using an aluminum based ABM microporous coating and pool boiling tests by O'Connor et al. [36] using a diamond based microporous coating both report better performance, at lower heat fluxes, for the subcooled case. However, at higher heat fluxes their coated surfaces showed little sensitivity to subcooling and/or dissolved air content. This is not the case for the TCMC coating, where the gassy subcooling case is observed to provide significant nucleate boiling heat transfer enhancement (when referenced to the inlet saturation temperature) throughout the entire flow boiling curve.

A recent study by Kim et al. [15] investigated the boiling mechanisms on microporous surfaces. They report that microporous surfaces increase bubble departure frequencies which in turn increases micro-convection. They then hypothesize that this increased micro-convection could then decrease the superheated liquid layer thickness. If so, the effect of a thinner superheated layer could be more effective for the thicker (~150 μm) and thermally conductive TCMC coating. The high temperature gradients associated with a thinner superheated liquid layer in combination with thicker and more thermally conductive TCMC coating could be the reason for the enhancement observed for gassy-subcooled tests. This in addition to the partial gas pressure of the dissolved air, in the gassy-subcooled case, which adds to the vapor pressure within embryonic bubbles (trapped air in within coating micro-cavities) further

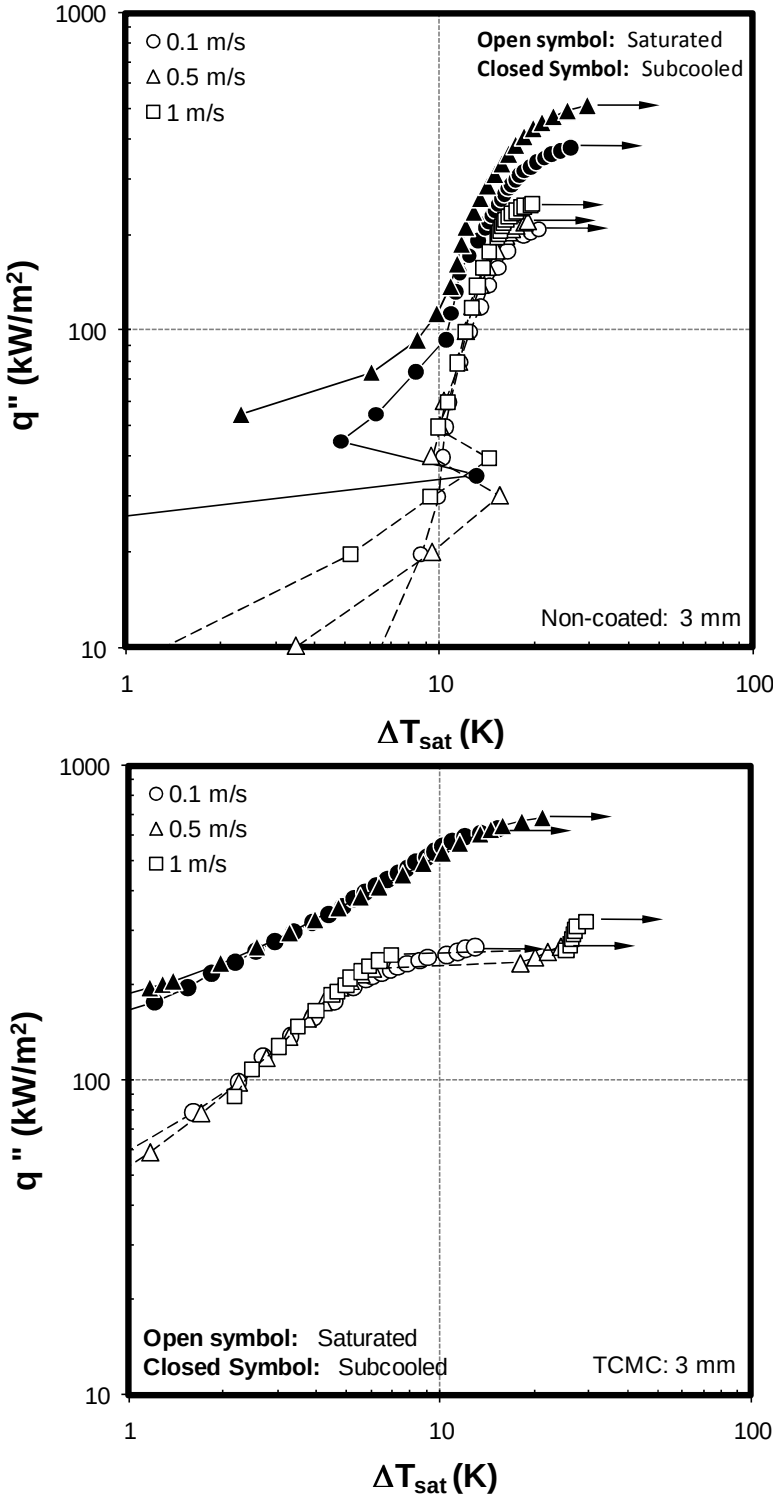

Figure 3.9. Flow boiling curves for saturated and non-degassed, subcooled (ΔT_{sub}~32K) heaters: non-coated (top) and TCMC coated (bottom).

facilitates nucleation. The subcooled enhancements were strong enough to produce slightly negative superheat values at low heat fluxes following boiling incipience. Negative superheats have been previous reported by [36] for highly subcooled (non-degassed) cases at higher pressures (3 atm). For comparison, the microporous coatings of [36, 61] were stated to have a thickness of ~40-50 μm and an effective thermal conductivities of ~0.95-1 W m^{-1} K^{-1}.

In Fig. 3.10 all previously reported data is plotted in the same figure including saturated and subcooled for both coated and non-coated heaters. For clarity, all single phase results are omitted from this figure. The non-coated heater boiling curves (grouped on the right) demonstrate less sensitivity between pool and flow boiling and between saturated and gassy-subcooled flow boiling. This is depicted in the manner in which the non-coated boiling curves seem to converge. On the other hand, the TCMC coated heaters clearly are more sensitive to the effects of the addition of fluid velocity (comparison between pool and flow) as well as to the effect of subcooling (non-degassed).

The flow boiling performance of the TCMC microporous coating is compared to the flow boiling performance of a previously developed coating, ABM microporous coating. ABM flow boiling results were obtained from an equation provided by Rainey et al. [22] and depicted as a dashed line in Fig. 3.10. According to [22], all ABM coated results correlated well to this line regardless of fluid velocity and/or subcooling. Comparing the performance of the two coatings clearly shows the superior performance of the current TCMC coating as compared to the ABM coating. Although the ABM coating is reported to enhance nucleate boiling heat transfer, this enhancement is only observed at lower velocities. Increasing fluid velocity and degrees of subcooling are reported to diminish the enhancement until eventually, at high velocities, the ABM coating is found to degrade nucleate boiling heat transfer *h*-values. Similar results were reported by Ammerman & You [5] using flow boiling within small channels. In both studies [5, 22], increasing velocity increased *h*-values for the non-coated heaters, a result of increasing forced convection. However, the added thermal resistance of the low-thermally conductive

bonding epoxy used in the ABM coatings (50 μm) placed on upper limit the *h*-values for the coated heaters. Thus, at higher velocities, the non-coated heaters outperformed the ABM coated heaters.

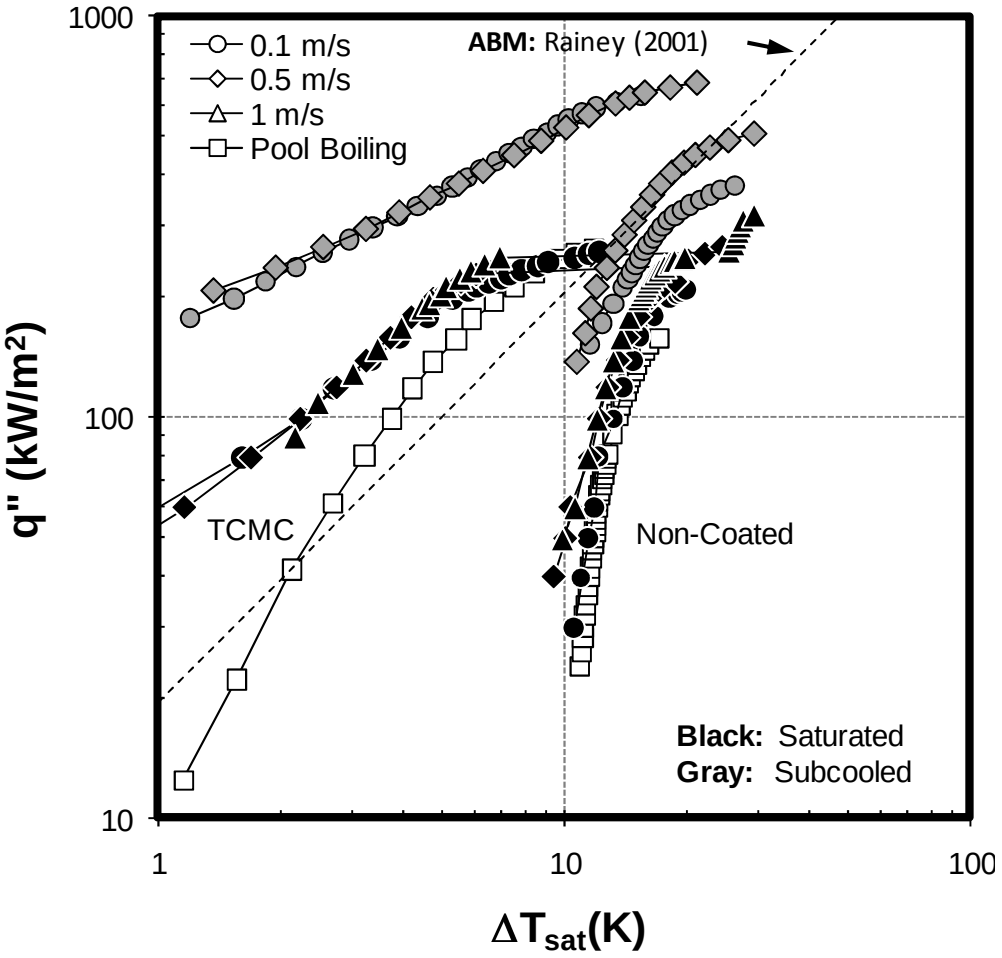

Figure 3.10. Boiling curves (flow and pool) for TCMC and non-coated surfaces. Saturated and subcooled tests shown. For clarity, the CHF arrows are not shown.

Since the TCMC coating is composed entirely of materials with relatively high thermal conductivities, the coatings is found to enhance boiling *h*-values at all velocities and degrees of subcoolings tested. Other factors including coating wicking speeds and micro-cavity sizes could also play a role in the superior performance of the TCMC coating as compared to the ABM

coating. However, due to the volatile nature (highly wetting, low saturation temperature, low latent heat of vaporization) of FC-72 it was not possible to quantify wicking speed for either coating. Attempts to do so, could incur errors associated with the loss of fluid through evaporation.

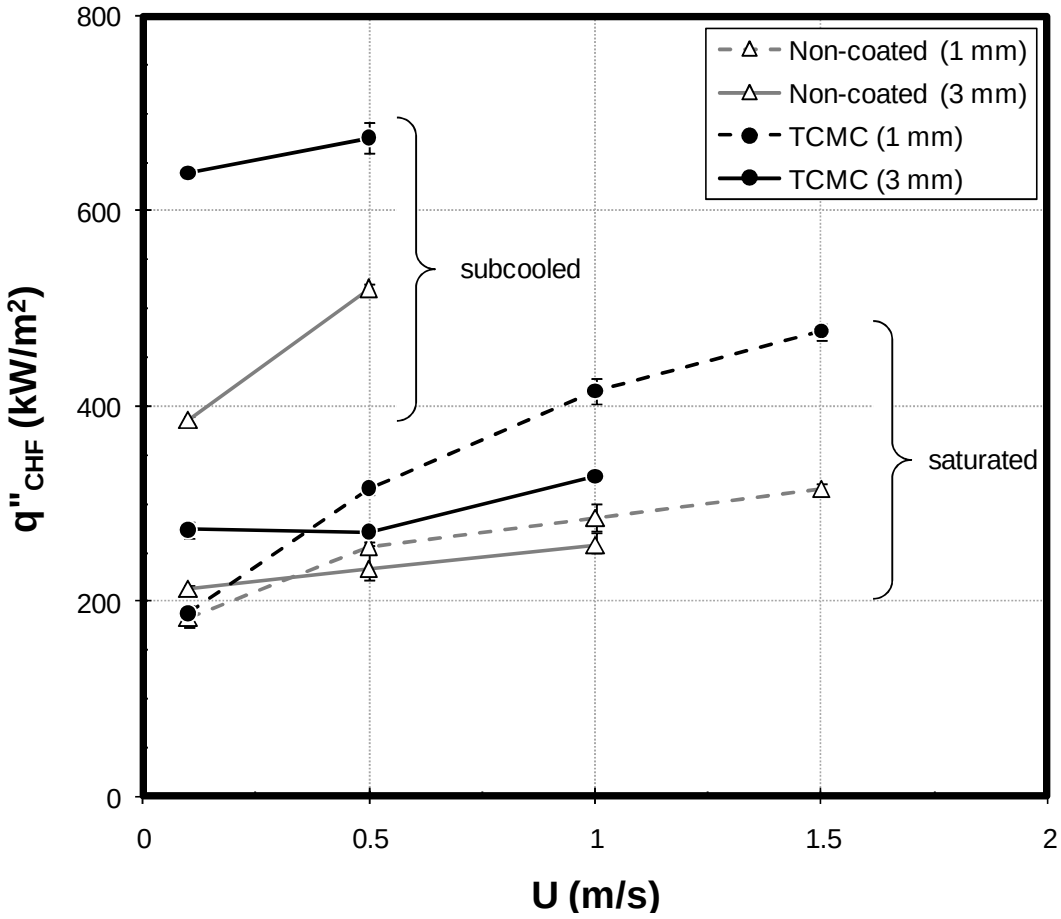

Figure 3.11. CHF versus velocity plot for both TCMC coated and non-coated heaters. CHF results for saturated and subcooled cases as well as 1 & 3 mm channels are provided.

A summary of the CHF values obtained for all tested cases (saturated & subcooled, 1 & 3 mm channel heights) is shown in Fig. 3.11. In every case, the TCMC coated heaters are found to produce higher CHF values as compared to their non-coated counterparts. In both

coated and non-coated cases, the smaller 1 mm channel produced higher CHF values by forcing liquid closer to the heater surface which then effectively removes vapor from the heater. By forcing the liquid closer to the heater surface, the TCMC coating then has relatively (compared to larger, 3 mm channel) more access to fluid which it can then passively transport, through wicking, and thus extend CHF. This effect is believed to be the reason that the TCMC coating produces more CHF enhancement (compared to the non-coated heater) in the 1 mm channel than in the 3 mm channel. A similar effect is believed to occur in the subcooled case with the exception that in this case, more liquid to surface access is provided through significantly less vapor crowding on the heater surface as a result of vapor condensation, as it comes in contact with the much cooler bulk liquid. With more liquid to surface contact, the coating can then wick fluid to areas experiencing localized dryout and enhance CHF by as much as ~65%.

3.3 Effect of Extended Surface, Heat Spreaders

In an attempt to maximize the cooling performance of the TCMC coating, the heater surface area was increased using heat spreaders (30×30×3 mm). TCMC coating was then applied to the heat spreader and in this manner; the potential of the coating could be maximized by increasing its effective area. The objective in this case is to both decrease chip (10×10 mm heater) junction temperatures and increase CHF.

3.3.1 Non-coated Heat Spreaders

As was the case for the 10×10 mm heaters, experiments were conducted under saturated and subcooled (non-degassed) conditions using channels with heights of 1 & 3 mm. The test channel width was 30 mm. The larger channel area and pumping limitations, limited the maximum flow velocities, for the larger 3 mm channel, to only 0.5 m/s. As stated in the Chapter 2, the provided wall temperatures for these heat spreader tests are those calculated at the

interface between the 10×10 mm heater and the heat spreader plate. Also, the heat flux is calculated using the area of the 10×10 mm heater (note the *b* subscript on heat flux labels) and not the larger heat spreader area. These referenced wall temperatures and heat fluxes are appropriate given that the 10 mm square heater represents a computer processor and thus the critical component.

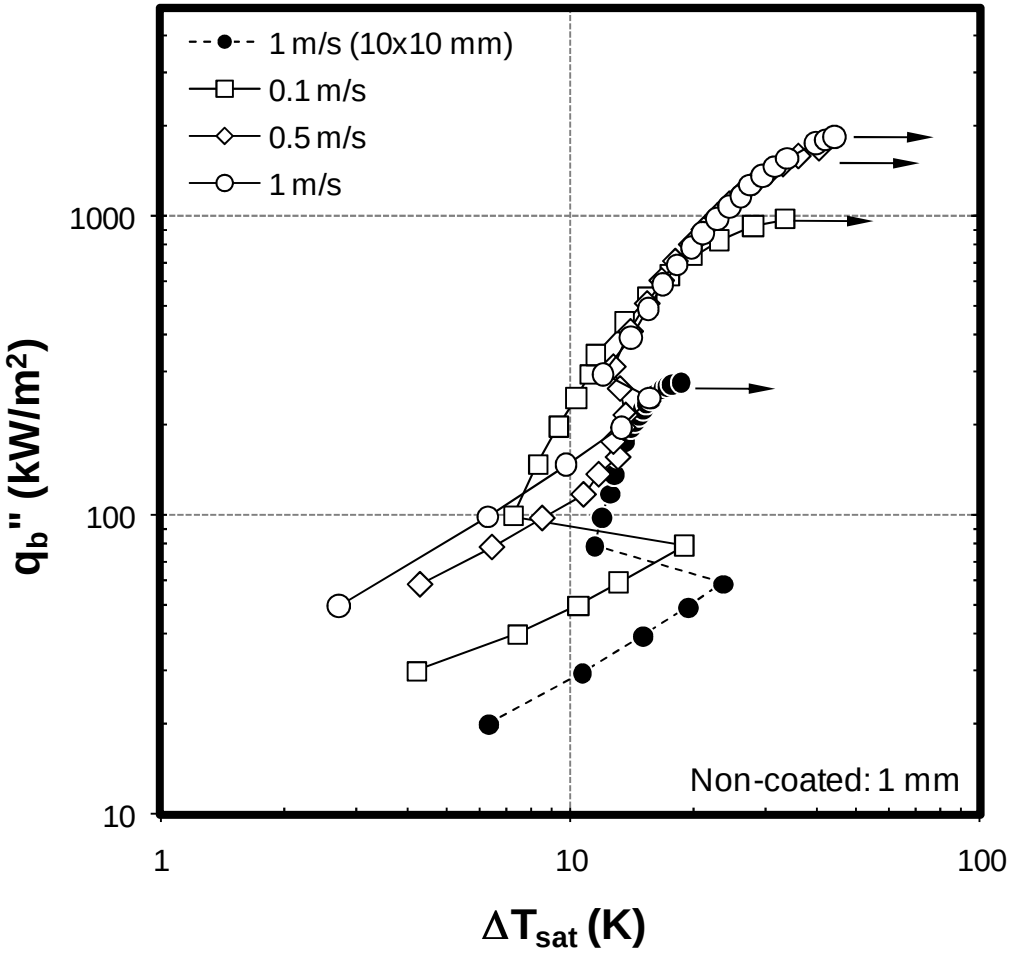

Figure 3.12. Heat spreader saturated flow boiling curves.

Experiments were first conducted using non-coated heaters to provide a baseline from which to compare the TCMC coated results. Fig. 3.12 displays the entire (single-phase and

nucleate boiling) saturated flow boiling curves for the non-coated spreaders. For reference, the flow boiling curve for the non-coated 10×10 mm heater at 1 m/s is also provided (shown as black circles). Results show that the increased area of the heat spreader decreases wall temperatures and significantly increases CHF (calculate using base area) as compared to the 10×10 mm heater. At the highest flow rate tested, an average CHF of 1,900 kW/m^2 was achieved which is about 6.6 times greater than of the 10×10 mm heater. Thus the use of heat spreaders provides a simple, yet effective means of increasing the typically low CHF values produced using dielectric fluids.

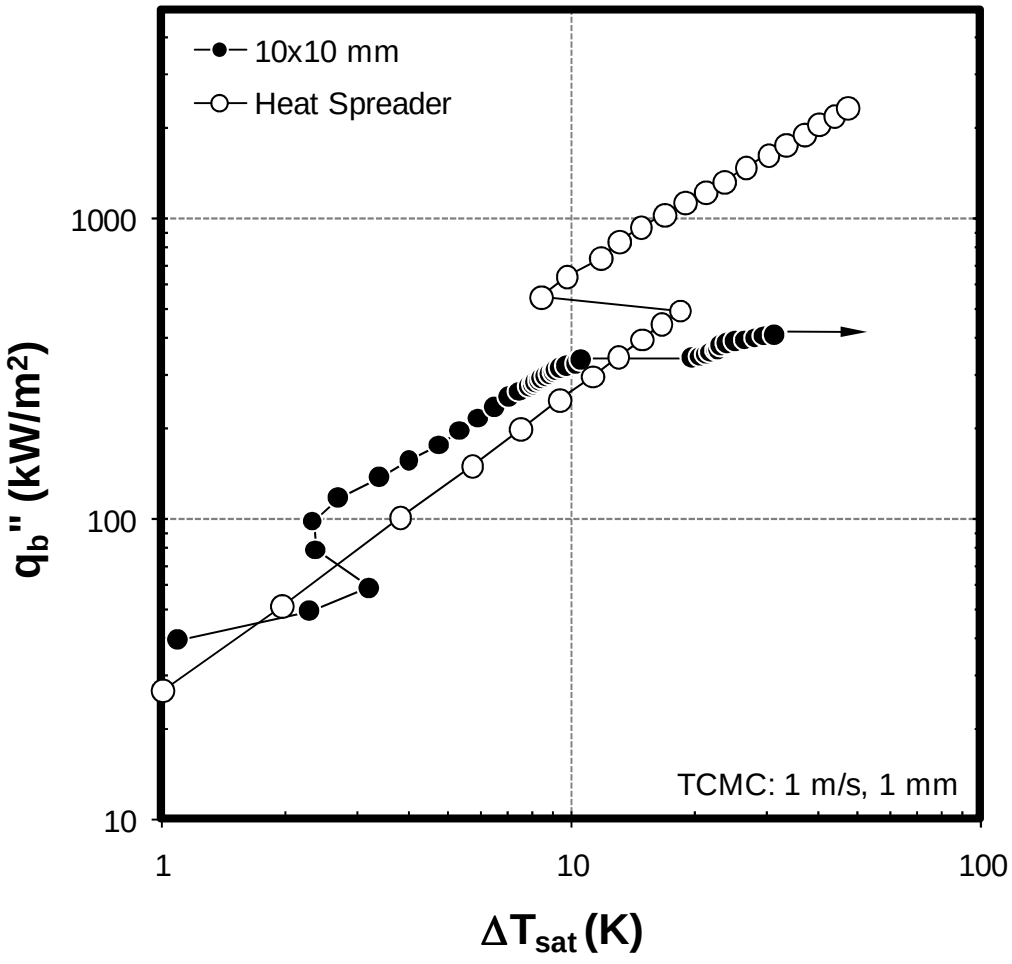

Figure 3.13. TCMC coated heat spreader and 10×10 mm heater at 1 m/s.

Table 3.1. Boiling incipience superheat values for non-coated and TCMC coated heat spreaders. Values provided for both 1 & 3 mm channel heights.

Boiling Incipience Superheat ($T_{b,w} - T_{sat}$)		
U m/s	**Non-coated: 1 mm (3 mm)**	**TCMC: 1 mm (3 mm)**
0.1	9.8-13.2 (9.7-10.4)	10.4-10.8 (9.8-9.9)
0.5	12.7-13.1 (14.1-15.3)	9.7-11.7 (14.8-15.1)
1	15.6-16.0	15.1-18.5

3.3.2 TCMC Coated Heat Spreaders

Figure 3.13 compares the cooling performance of the TCMC coated heat spreader with that of the smaller, 10×10 mm TCMC coated heater at 1 m/s. As was the case for the 10×10 mm heaters, the single-phase heat transfer coefficients of the TCMC coated spreaders were found to be higher than those of their non-coated counterparts. The reason for this increase is again believed to be a result of a minimal amount of nucleation occurring within the coating and "tripping" of the upstream fluid from the slight downward curvature of the epoxy surrounding the coating and the slight protrusion (150 μm) of the TCMC coating. This behavior is identical to that observed with the smaller 10×10 mm TCMC heater (Section 3.2).

The results also show that the application of TCMC coating, to the heat spreaders, does not significantly affect boiling incipience superheats as shown in table 3.1. It should be noted, that the superheat values provided are calculated using the temperature at the interface of the spreader and the 10 mm square heater. The actual incipience superheats, calculated using the spreader surface temperature, will be lower due to spreading resistance. Nevertheless, the higher incipience temperatures of the spreader, results in the transition from the inefficient single-phase convective heat transfer to the highly efficient nucleate boiling heat transfer to occur at relatively high powers. This means that at powers below incipience, the coated 10×10 mm heater actually outperforms the coated spreader (Fig 3.13). However, the eventual

incipience in the coated spreaders results in drastic reductions of wall superheat and higher CHF.

It should also be noted that the TCMC coating applied to the heat spreader proved to be an effective means of increasing heat dissipation. In many cases heater temperature limitations were exceeded before CHF was reached and thus the effect of the TCMC coating on heat spreader CHF could not be fully investigated. Any flow boiling curves, which are not labeled with the CHF arrow, are those pertaining to experiments where CHF was not reached.

3.3.3 Effect of velocity and Channel Height

The effect of channel height (1 & 3 mm) and fluid velocity on TCMC spreader performance is depicted in Fig. 3.14. As was the case with the 10×10 heaters, velocity and channel height have minimal effect on nucleate boiling performance for the coated spreaders. Evidence of this is shown in the near convergence of all the boiling curves. The exception to this is at 0.1 m/s using the 1 mm channel, where a combination of low velocity and low channel height trapped vapor above the heater leading to decreased performance and low CHF.

To compare the performance of TCMC coated spreaders to non-coated spreader, the flow boiling curve for the non-coated spreader (@ 1 m/s, 1 mm) is also shown in Fig. 3.14 (depicted as a solid black line). The effect of the coating is found to be more pronounced at lower heat fluxes where the numerous micro-cavities of the coating promote nucleation and thus enhance heat transfer. However, at higher heat fluxes, the effect of the coating diminishes and the non-coated boiling curve approaches the coated boiling curves. This behavior is different than that observed for 10×10 heaters where the coating was found to produce substantial boiling enhancement throughout the entire boiling curve. It is believed that the non-uniform heat flux distribution of the heat spreader, where most of the heat is dissipated in the central core, combined with the relatively large surface area of the spreaders is partially responsible for the observed behavior.

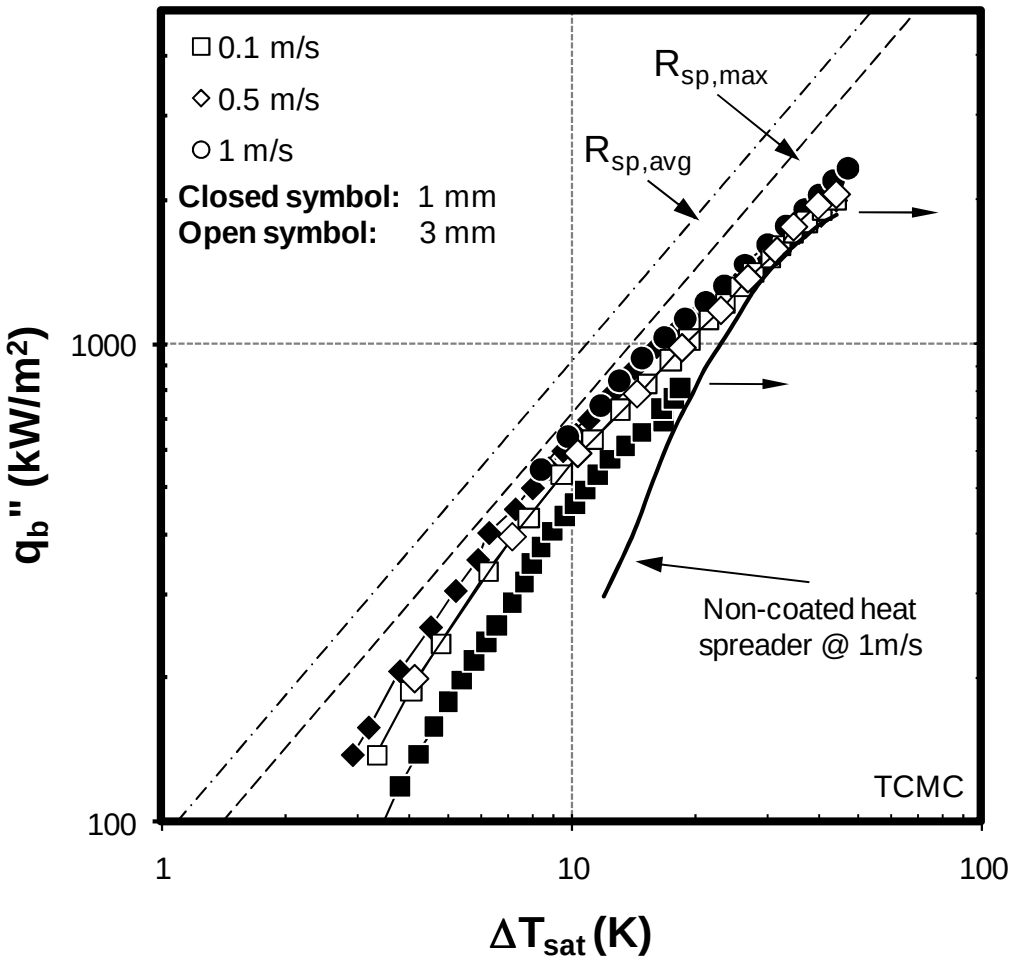

Figure 3.14. Saturated flow boiling curves for TCMC coated heat spreaders.

The larger area means that by the time the fluid reaches the heater core, much of the generated vapor produced upstream has coalesced leaving a high quality mixture (mostly vapor) to cool the hot central core which by this time is experiencing localized dryout. High speed video images seem to concur with this theory. Therefore, since both coated and non-coated spreaders are believed to experience this localized and transient dryout at the spreader core, just above the heat source (where the majority of the heat is concentrated), then the performance of both coated and non-coated spreaders suffers and their boiling curves are

observed to approach one another. However, the coated spreader still benefits from the wicking effects of the coating and produces slightly higher heat transfer rates and extends CHF.

In this study, CHF is said to occur when at a given heat flux, the temperature suddenly increments and that increment exceeds the previously recorded steady state value by more than 20°C. At higher flow rates (≥ 0.5 m/s) only the non-coated heat spreader was found to satisfy this CHF condition and hence only it is marked with a CHF arrow. At higher heat fluxes, temperature excursions of between 13-6°C were recorded, for the TCMC spreaders, as the heater temperature soared past the temperature limits before being automatically shut down by the computer. Since these recorded TCMC spreader temperature excursions did not meet the CHF condition it is unknown whether they are actually CHF. Nevertheless, TCMC is observed to increase CHF in heat spreaders however, due to the heater temperature limitations, the magnitude of the enhancement is unknown.

In an attempt to isolate the effects of the coating from the effects of the heat spreader; the temperature drop across the heat spreader (conduction resistance) is estimated using the procedures/equations outlined by Song et al. [62]. This procedure requires solving 8 equations to estimate the average *(avg)* (eq. 3.4) and maximum *(max)* spreading resistance (eq. 3.5).

$$R_{sp,avg} = \frac{\overline{T_b} - \overline{T_{sp}}}{P} \tag{3.4}$$

$$R_{sp,max} = \frac{T_{b,max} - \overline{T_{sp}}}{P} \tag{3.5}$$

The T_{sp} represents the average temperature at the top surface of the spreader. T_b and $T_{b,max}$ represent the average and maximum temperatures at the spreader base, (interface between 10×10 mm heater and spreader) respectively. The equations estimate the spreading resistance by assuming a uniform heat transfer coefficient on the top of the heat spreader and considers

factors such as geometry and material. A uniform heat transfer coefficient is an assumption (40,000 W m^{-2} K^{-1} in this case, from Fig.3.5) that is made being that the actual non-uniform *h*-value distribution is unknown and varies with increasing heat flux. The estimated spreading resistances are then calculated to be $R_{sp,avg}$=0.104 and $R_{sp,max}$=0.14℃/W which is in agreement with 2D finite element simulation results of 0.109°C/W and 0.12℃/W for the average and maximum resistance. These values are then used to estimate heater temperatures by only considering the spreading resistance while neglecting the resistance associated with forced convection or boiling (shown as dashed lines in Fig. 3.14). Therefore, theoretically these lines represent the temperature increase due only to spreading resistance and thus the difference in temperature between these lines and the boiling curves then represents the resistance associated with convective boiling.

These calculated spreader resistances are again plotted in Fig. 3.15 alongside the total thermal resistance for both the coated and non-coated spreaders. The total resistance is an experimentally obtained value defined as the difference between the temperature of the 10×10 heater (base of the spreader) and the temperature of the bulk fluid divided by the total power dissipated. The effect of the coating is then to reduce the thermal resistance of the spreaders by 16-50%. However, spreading resistance accounts for a significant amount of the total resistance and therefore a better representation, of the effect of the coating, is to subtract the spreading resistance from the total resistance to estimate the convection/boiling resistance. This then gives an indication of the effect of the coating on convective boiling resistance. The coating is then estimated to reduce convection/boiling resistance by 50 to 75% at 100 W (q_b"= 1,000 kW/m^2) using either $R_{sp,avg}$ or $R_{sp,max}$, respectively. Below 1,000 kW/m^2, the coating is found to produce the most heat transfer enhancement. However, at higher heat fluxes, the larger number of active nucleation site for the coated heater results in more vapor coalescence thus depriving the downstream half of the spreader of liquid. Consequently, the enhancement of the coating is negatively affected, as seen by the increase in its thermal resistance (Fig. 3.15).

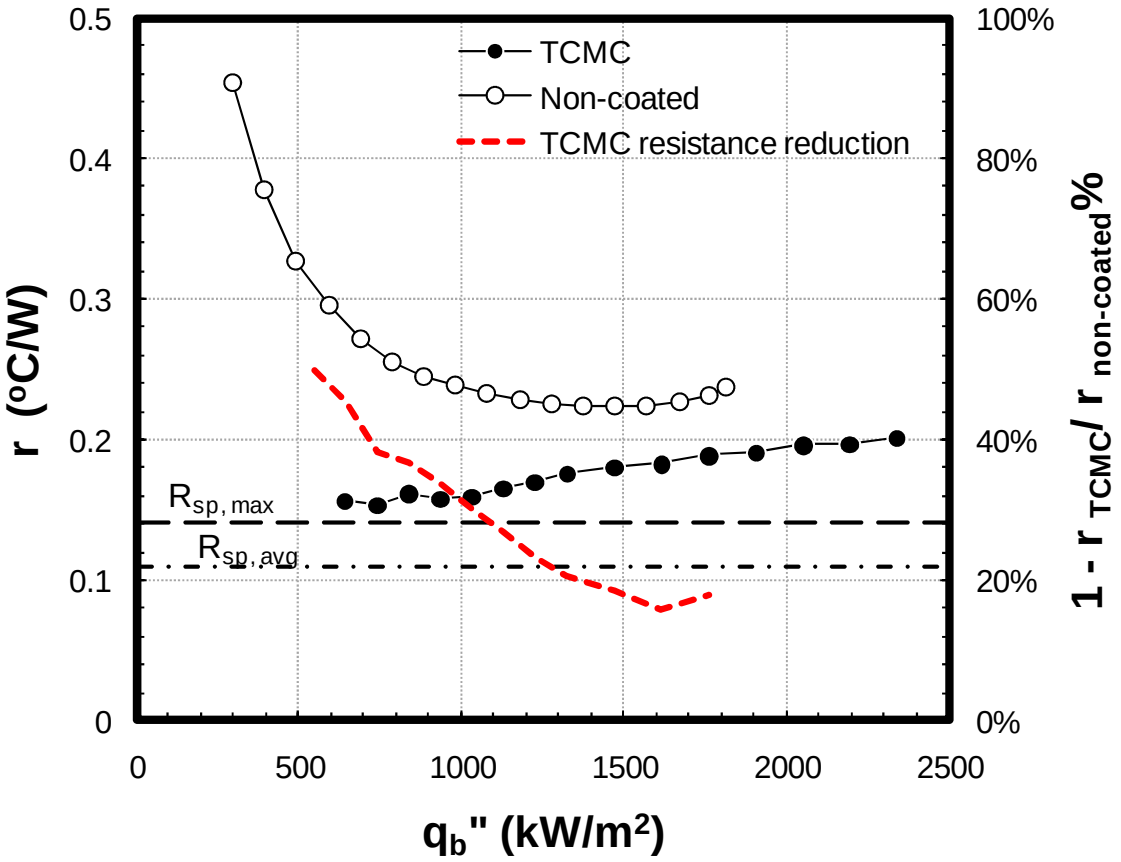

Figure 3.15. Thermal resistance of the coated and non-coated spreaders at 1 m/s

Other investigators have also used a combination of increased surface area and porous coatings to enhance FC-72 boiling performance. When comparing these previous results with those of the current study, the TCMC coated spreader is found to provide superior performance. For example, the total thermal resistance of the TCMC coated spreader can be as low as ~0.16℃/W (at q_b" between 500-1,000 kW/m^2). This is lower than the 0.20℃/W reported by El-Genk et al. [63] in pool boiling tests using porous graphite coated spreaders of similar dimensions or the 0.25℃/W calculated from Rainey [4] flow boiling data using microporous (ABM) coated finned (8 mm long) structures. Additionally, the 25 (8×1 mm) finned structures used by [4] provides the same surface area (9 cm^2) as does the current 30×30 mm spreader but has about 4× higher pressure drop, compared at the same velocity, due to the protruding fins.

3.3.4 Effect of Subcooling

The final sets of tests were done to investigate the effect of subcooling (non-degassed) on TCMC spreader performance. As was the case previously, the degree of subooling, for these tests, was $\Delta T_{sub} \approx 32K$ and the dissolved air content is estimate to be 0.0037 $moles_a / moles_f$. The flow boiling curves for the coated and non-coated spreader are provided in Fig. 3.16. For the non-coated case, the use of subcooled liquid decreases wall superheats and increases CHF. Most of this enhancement is from vapor condensation which significantly reduces vapor concentration and allows more liquid to surface contact. This effect is well demonstrated in Fig. 3.17, where the saturated spreader (left) is almost completely covered in vapor and most of the liquid to surface contact occurs at the leading edge while the downstream half is experience localized dryout especially in the hot central core. This is contrast to the cooler subcooled spreader (Fig. 3.17 right) where vapor condensation produces smaller bubble sizes which allow for more fluid to surface contact. The wedge shaped, non-boiling section at the leading edge of the subcooled heater is a result of higher velocities at the center of the channel (velocity profile) which increases incipience superheats [7].

For subcooled tests, the application of TCMC coating to the spreaders is found to have minimal effect. In fact, the subcooled, flow boiling curves at 0.5 m/s for the coated and non-coated (shown as a red line) spreaders are found to overlap one another indicating nearly identical results. Therefore, the only benefit that the coating could provide in this subcooled case is an increase in CHF. Even though this cannot be verified, due to heater limitations, the coating is observed to delay localized dryout at the spreader core. This is evident from Fig. 3.18 where the non-coated, subcooled spreader is observed to have a dry spot at its center while TCMC coating is shown to prevent this. This is likely a result of fluid wicking through the porous coating.

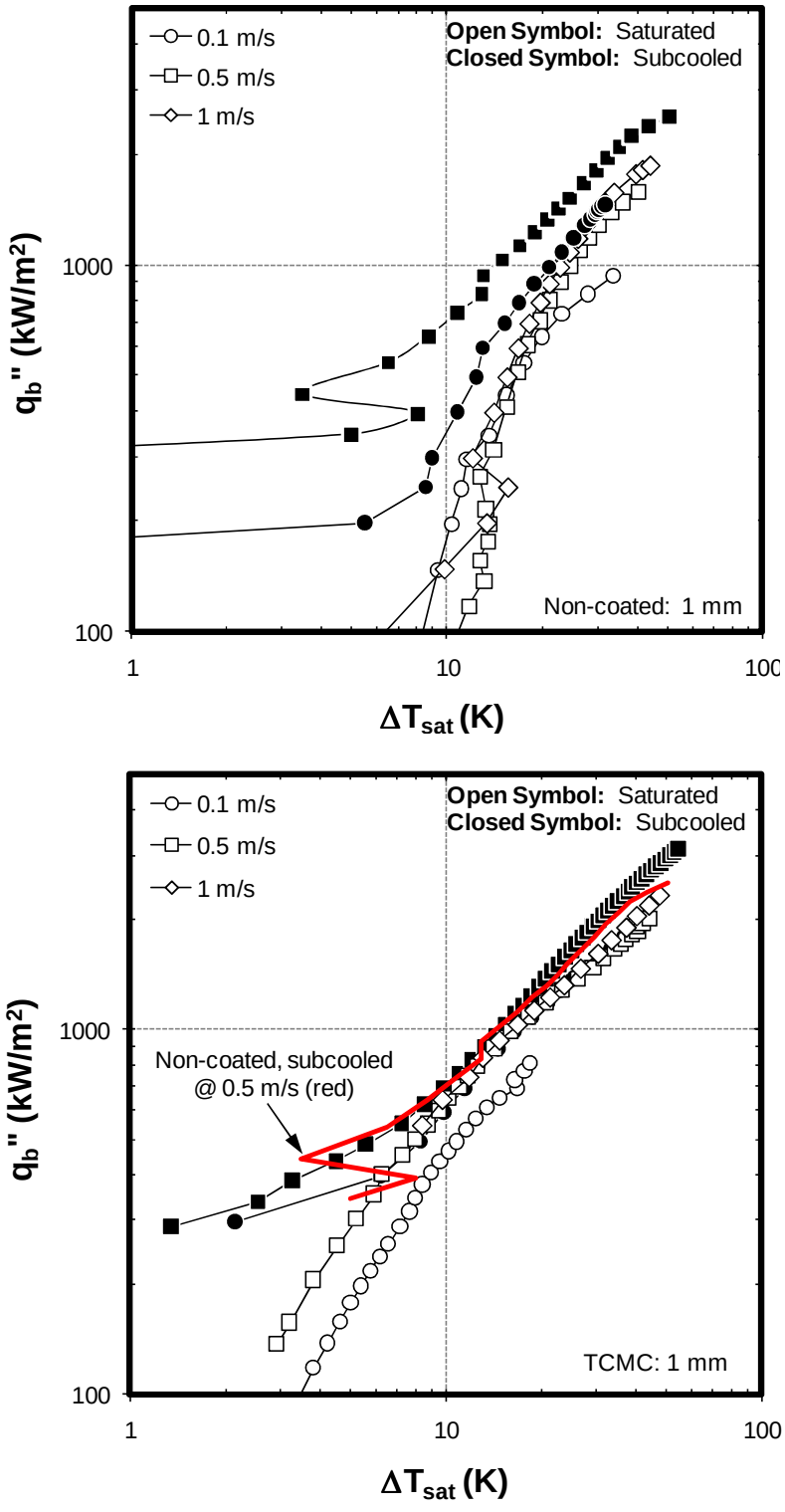

Figure 3.16. Saturated and subcooled flow boiling curves for the non-coated (top) and TCMC coated (bottom) spreader.

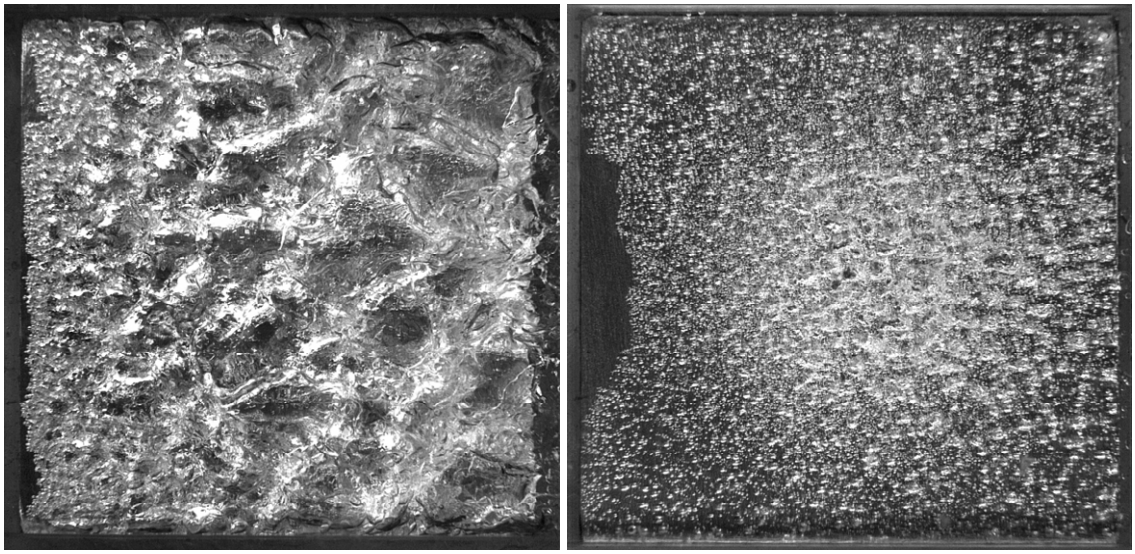

Figure 3.17. Flow boiling on saturated (left) and subcooled (right) non-coated spreaders both outputting 150 W (q_b"=1,500 kW/m^2). Velocity is 0.5 m/s for both cases.

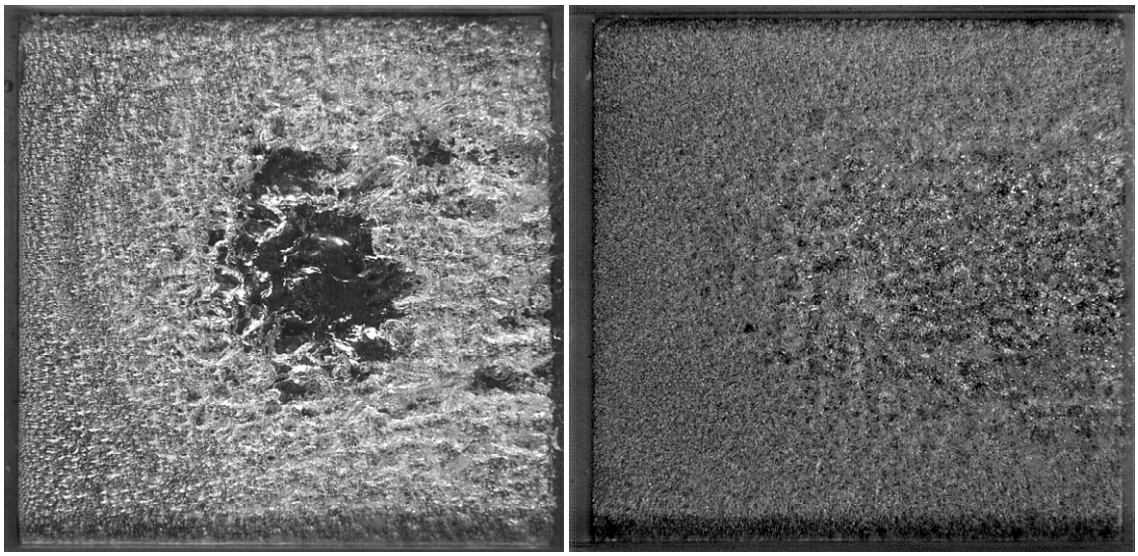

Figure 3.18. Subcooled flow boiling on non-coated (left) and TCMC coated (right) spreaders both outputting 250 W (q_b"=2,500 kW/m^2). Velocity is 0.5 m/s for both cases.

CHAPTER 4

SPRAY COOLING

This study will investigate using a thermally conductive microporous coating as a means to enhance spray cooling performance. The application of structured surfaces to spray cooling has received much less attention as compared to their application in other two-phase cooling schemes. Structured surfaces including finned structures [10, 29, 30, 32] and sandpaper roughened surfaces [28, 64] have been studied and each has demonstrated various degrees of spray cooling enhancement. However, to the author's knowledge, only one other spray cooling study has been carried out using microporous coatings [9] and thus much remains unknown about their effect on spray cooling. This current study will increase the current understanding on the effect of microporous coatings on spray cooling performance by conducting spray cooling tests using the 150 μm thick TCMC porous coating. The results from these tests and possible mechanisms behind any enhancements will be discussed in this chapter.

Tests were conducted using 10×10 mm copper heaters both with and without an attached heat spreader plate. Two different spray nozzles were tested at various flow rates and results compared. Due to the complexity in degassing the test section, tests were only conducted using non-degassed and subcooled FC-72 as the coolant fluid. A minimal number of experiments were also conducted using non-degassed, subcooled HFE-7000.

4.1 Nozzle Description

The spray nozzles used in this investigation were provided by the Parker Hannifin Corp. Two nozzles were tested and are designated as Nozzle 6 and Nozzle 20 which is the numbering scheme given to them by Parker Hannifin. Nozzle schematics and spray cone

images are shown in Fig. 4.1. Nozzle 6 is a pressure swirl nozzle producing a single, hollow cone spray. Hollow cone sprays generally create better atomization, as compared to full cone sprays, and hence are preferred in combustion applications [65]. Nozzle 20 is an array of 16 evenly spaced jets (plain orifice). At inlet pressures exceeding ~200 kPa (185 ml/min) the jets were found atomize upon exiting the nozzle and produce narrow spray cones (Fig. 4.1).

$$SMD = 4.52\left(\frac{\sigma\mu_l^2}{\rho_a\Delta P_l^2}\right)^{0.25}(t\cos\theta)^{0.25} + 0.39\left(\frac{\sigma\rho_l}{\rho_a\Delta P_l}\right)^{0.25}(t\cos\theta)^{0.75} \quad (4.1)$$

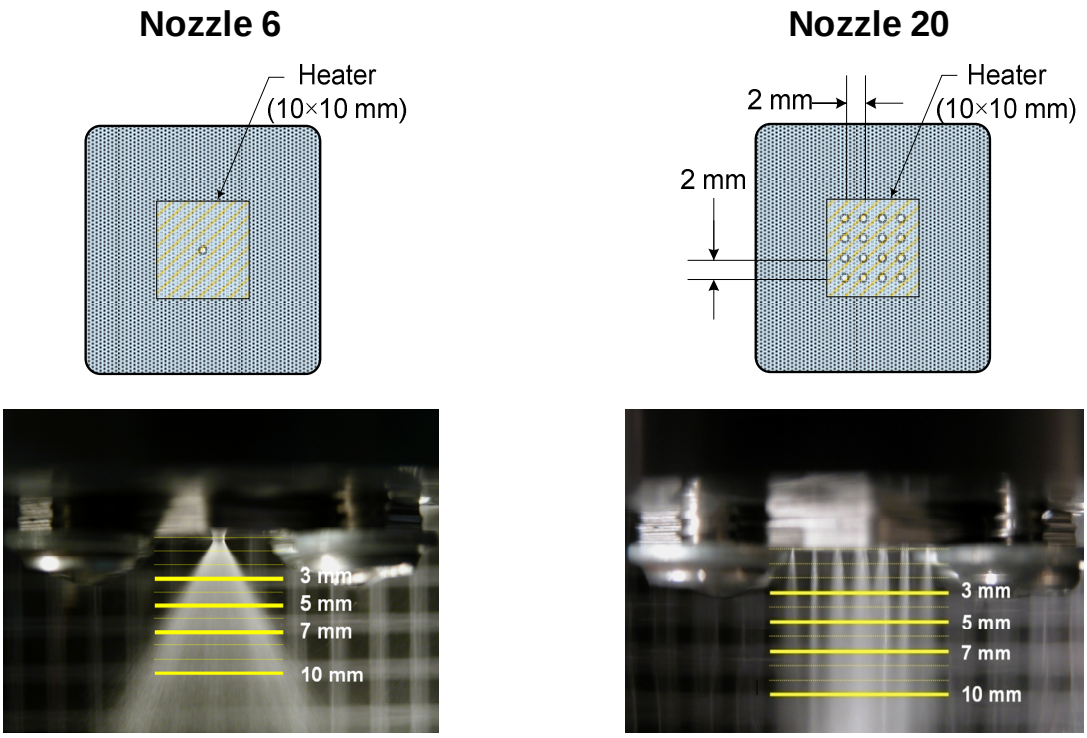

Figure 4.1. Single hollow cone (Nozzle 6) and 4×4 multi-jet (Nozzle 20) spray nozzles. Spray images shown were taken at a flow rate of 200 ml/min.

To estimate the droplet sizes produced by Nozzle 6, a correlation developed by Wang & Lefebvre [66] was used and is shown as eq. 4.1. This correlation predicts the Sauter Mean

Diameter (SMD) for hollow cone, pressure swirl spray nozzles considering both the hydrodynamic and aerodynamic forces involved in the liquid atomization process. The correlation considers the effects of spray cone angle (θ) and liquid film thickness (t) (prior to atomization) in addition to the liquid and vapor/air properties.

In these types of nozzles, the liquid initially exits the nozzle as a thin conical sheet which quickly atomizes. Equation 4.2 obtained from [65] was used to estimate the liquid film thickness (t), of the conical sheet, needed to solve eq. 4.1. To keep within the correlation constraints, the SMD was only calculated for the highest pressure tested (338 kPa). It should be noted that the viscosity and surface tension of FC-72 are lower than that of the fluids used to develop eq. 4.1 which could introduce error into this calculation. Droplet sizes were not calculated for Nozzle 20 since most of all the available SMD correlations for plain orifice nozzles were developed using inlet pressures which significantly exceeded those of the current experiment and used liquids with properties not matching those of the current 3M refrigerants tested [67, 68]. Relevant nozzle data is summarized in table 4.1. The pressure versus flow rate plots for both nozzles is provided in Fig. 4.2. Each nozzle has different pressure drop versus flow rate characteristics with Nozzle 6 having the lowest pressure drop.

$$t = 2.7\left(\frac{d_o \dot{m}_l \mu_l}{\mu_l \Delta P_l}\right)^{0.25} \tag{4.2}$$

Table 4.1. Measured spray cone angles and calculated SMD (Nozzle 6) using eq. 4.1 from [66].

Flow Rate (ml/min)	Nozzle 6			Nozzle 20		
	ΔP (kPa)	θ	SMD (μm)	ΔP (kPa)	θ	SMD (μm)
200	79	64°	-	235	10-15°	-
250				373	13-16°	-
300	186	68°	-			
400	338	70°	45			

For tests, the test heater is centered directly below the nozzle and its orientation with respect to the nozzle is shown in Fig. 4.1. Images of the spray cone(s) at 200 ml/min are also provided and the spray cone angles were measured from these images. To visualize how the spray impacts the heater at the different nozzle-to-heater distances, lines representing the heater were superimposed on these spray images. The line lengths were scaled to represent the approximate length of the heaters, taking into consideration the camera angle at which the image was taken. The line lengths were then scaled to represent the diagonally oriented heater. It is important to note that images do not have the same magnification and that the length scales drawn are approximate.

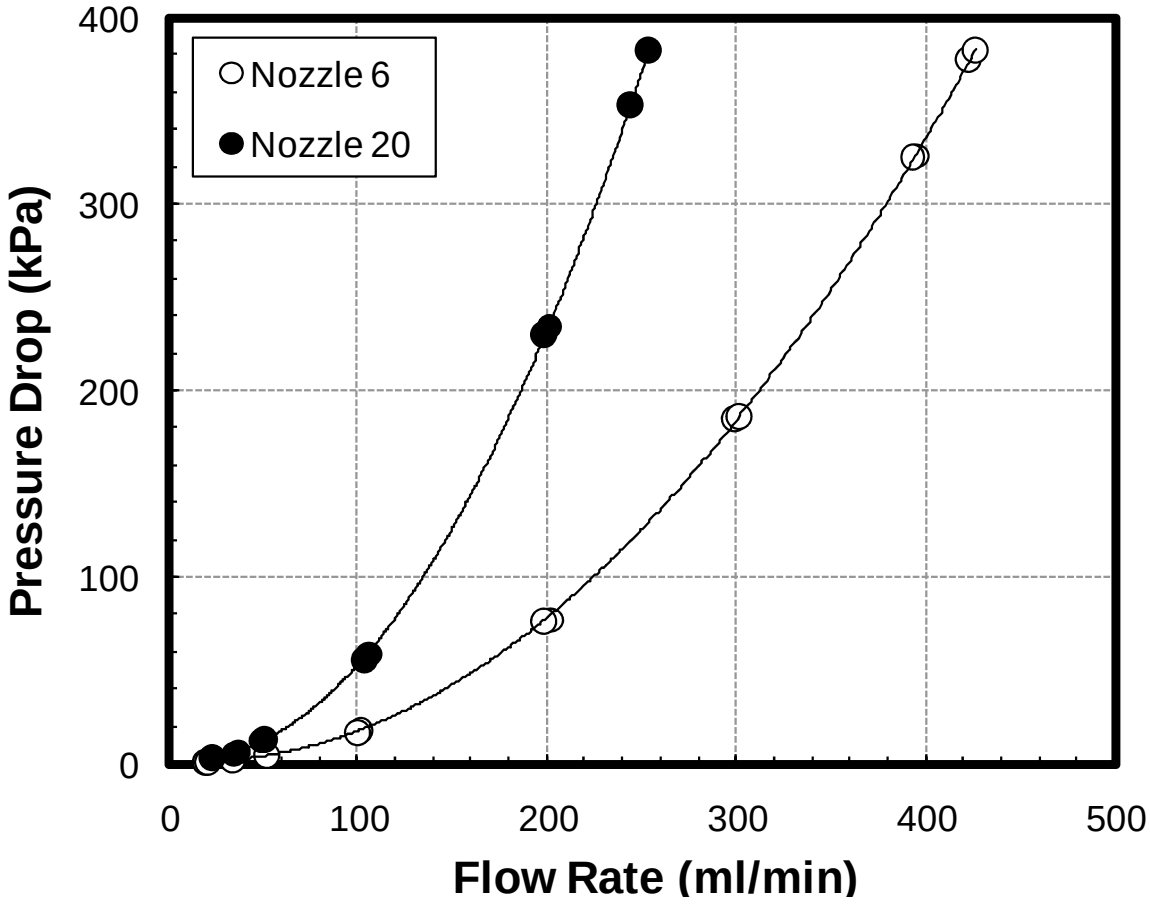

Figure 4.2. Pressure drop versus flow rate plot for Nozzles 6 & 20.

4.2 Parametric Effects

Prior to testing the microporous coated heater, a parametric study was conducted to determine the effect of nozzle-to-heater distance, flow rate, nozzle type on performance using non-coated heaters. Although an extensive study by Estes & Mudawar [50] reported the effect of nozzle-to-heater distance on CHF, their tests used single, full cone spray nozzles. However, the results from their study might not apply to the current study due to differences in spray patterns between full cones sprays and the currently used hollow cone spray and multi-jet sprays. Additionally, there is currently a lack of data on the use of hollow cone spray nozzles in spray cooling, especially their application to electronics cooling (i.e. small, square heaters). All this considered, it is necessary to conduct a parametric study to characterize and compare the performance of both nozzles (Nozzle 6 & 20) on a non-coated surface prior to investigating their effect on a microporous coated surface.

4.2.1 Effect of Nozzle-to-Heater Distance

As previously mentions, a detailed study on the effect of nozzle-to-heater distance on CHF has been reported by Mudawar & Estes [50] for full cone sprays. It was reported that the optimal nozzle-to-heater distance is at the point when perimeter of the spray cone just inscribes the heater. This optimal distance (H) can be calculated knowing the spray cone angle and the heaters size using eq. 4.3. However, unlike full cone sprays, hollow cones sprays concentrate their spray at the perimeter of the spray cone leaving the center void of any spray. This difference in spray distribution pattern between full and hollow spray cones could affect the nozzle-to-heaters distance behavior for hollow cone sprays. To investigate this, calculations were first done to determine H according to eq. 4.3 for Nozzle 6 at the various flow rates tested. Results are provided in table 4.2. Similar calculations were done for the multi-jet nozzle (Nozzle 20) using the distance from the center of the outermost nozzle orifice to the edge of the heater

as the length, L. The calculated distances for Nozzle 20 always exceeded the nozzle-to-heater distances tested and therefore are not shown.

$$H = \frac{{}^{L}/_{2}}{\tan\left({}^{\theta}/_{2}\right)} \tag{4.3}$$

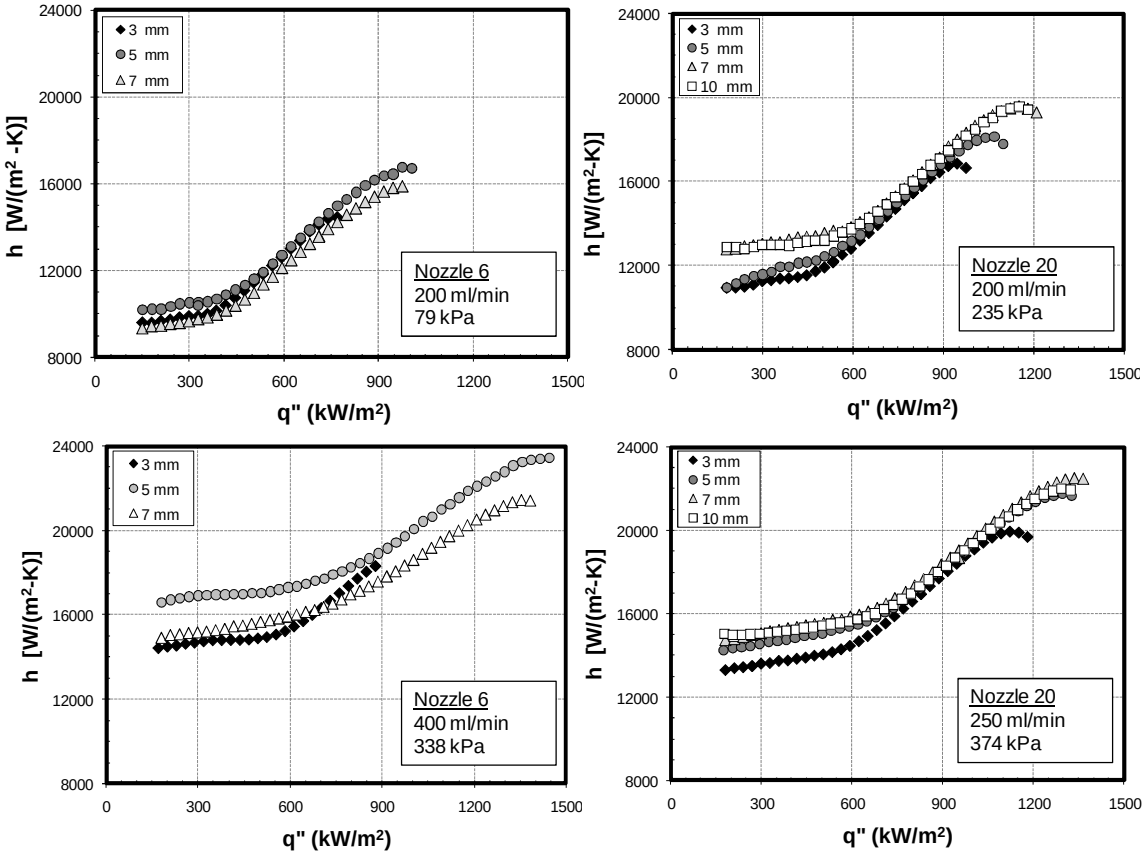

Figure 4.3. Heat transfer coefficients at various nozzle-to-heater distances for Nozzle 6 (left) and 20 (right).

Table 4.2. Nozzle-to-heater distances calculated using eq. 4.3 for Nozzle 6.

Flow Rate (ml/min)	H (mm)
200	8.0
300	7.4
400	7.1

Similar to pool and flow boiling behavior, spray boiling curves also demonstrate two distinct heat transfer regimes; single-phase dominant (low heat fluxes) and nucleate boiling dominant (high heat fluxes). These regimes are evident in Fig. 4.3 where the heat transfer coefficients (*h*-values) are plotted as a function of heat flux for both nozzles. In this figure, the onset of nucleate boiling regime is manifested by an increase in *h*-values leading to a change in slope for each plot. Unlike pool and flow boiling, evaporation contributes significantly to spray cooling heat transfer in both regimes and its contribution increases with increasing wall superheat. Additionally, the relatively high pumping powers required for atomization produce finely atomized droplets which are propelled towards the heater at relatively high velocities. This in turn provides spray cooling with a more effective forced convection mechanism as compared to flow boiling.

The effect of nozzle-to-heater distance on the heat transfer coefficient is demonstrated on Fig. 4.3. In this figure, the heat transfer coefficient is plotted versus heat flux for Nozzle 6 (left) and Nozzle 20 (right). Data shows that varying this distance has minimal effect on the heat transfer coefficient and this is the case for both nozzles. The exception being Nozzle 6 at 10 mm distance where significant heat transfer degradation was observed, however, this is due to spray cone exceeding the size of the heater resulting in lost spray (lower volume flux) and thus the results at this distance are not shown.

Even though nozzle-to-heater distance only has a minor influence on the heat transfer coefficients, there are distinct trends in performance. For example, in the case of Nozzle 6, the

highest heat transfer coefficient is consistently produced at 5 mm distance while the lowest heat transfer coefficients are found at either 3 or 7 mm and this is the case for all flow rates tested (200,300 & 400 ml/min). So for the single hollow cone spray nozzle (Nozzle 6) there appears to be an optimal distance to maximize heat transfer and this distance is less than that calculated in using eq. 4.3. There are two possible reasons for the heat transfer coefficient degradation at 7mm, as compared to 5 mm. First, the lack of direct spray at the center of the heater from hollow cone sprays creates a stagnant (relatively speaking) pool of liquid at the heater's center. This "stagnant" pool is inefficient in dissipating heat and its negative effects increase as spray cone widens (i.e. nozzle-to-heater distance increases). Second, since hollow cone spray nozzles concentrate their spray at the perimeter of the spray cone, it is possible that at distances close to those calculated using eq. 4.3, that a small portion of the spray actually falls beyond the measured spray cone angle and never strikes the heater surface and thus a decrease in heat transfer coefficient.

For nozzle 20, there does not appear to be any correlation between the heat transfer and nozzle-to-heater distance. For this nozzle the heat transfer coefficients are found to have some dependence on nozzle-to-heater distances (no more than ~17%) at lower heat fluxes but then merge in the nucleate boiling regime.

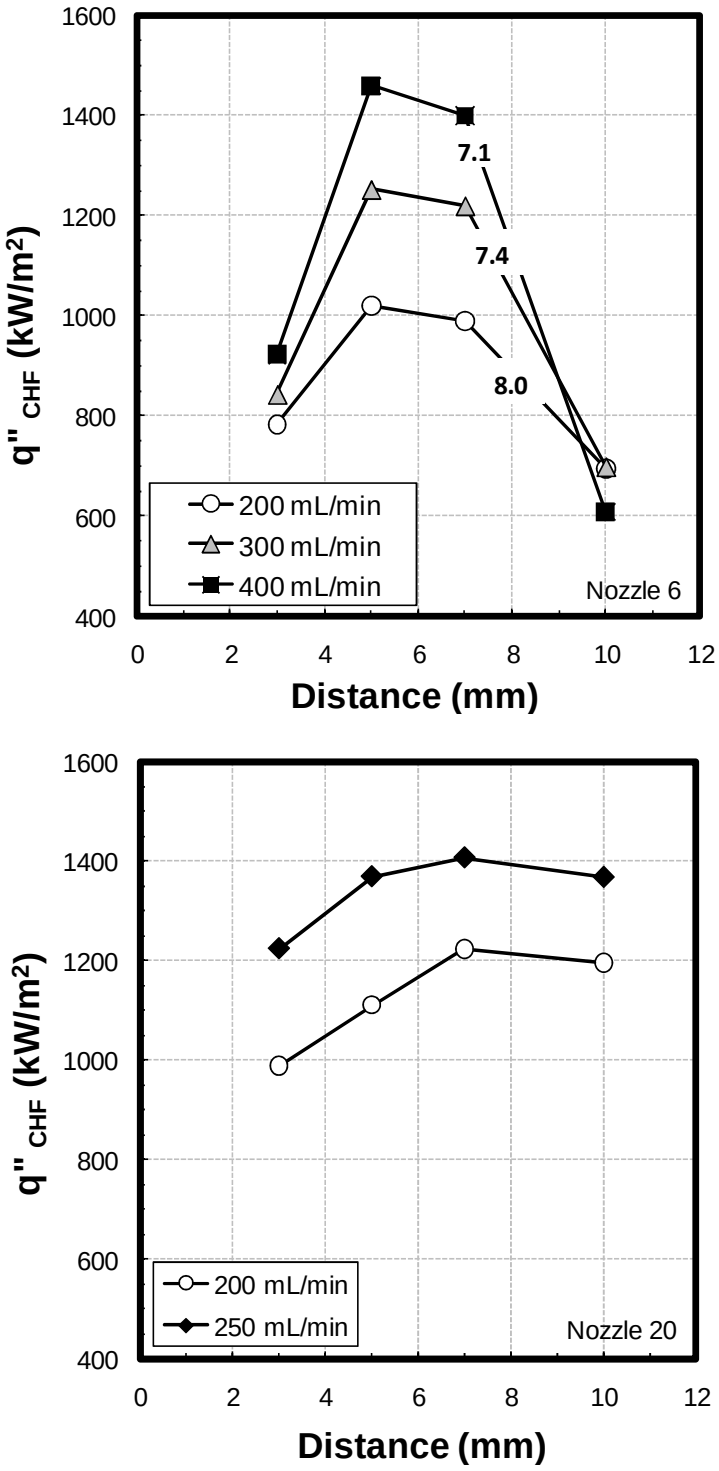

Figure 4.4. CHF values for Nozzles 6 (top) and 20 (bottom). The numbers displayed in the Nozzle 6 plot are those calculated using eq. 4.3.

In Fig. 4.4, CHF is plotted versus the nozzle-to-heater distance at various flow rates for both nozzles. From this figure, it is obvious that nozzle-to-heater distance has more of an influence on CHF for Nozzle 6 as compared to Nozzle 20. It should also be noted that CHF demonstrates more of a dependence on nozzle-to-heater distance, as compared to the heat transfer coefficient. This is especially true for Nozzle 6 where a change in the nozzle-to-heater distance from 3 to 5 mm results CHF increase of ~60%, at 400 ml/min. Of the two nozzles tested, the multi-jet nozzle consistently produced the highest CHF values (compared at the same flow rate). This might be attributed to the fact that this nozzle has more spray jets (16) uniformly distributed over the entire heater surface which helps to delay localized dryout conditions and in doing so extends the onset of CHF.

For Nozzle 6, there appears to be an optimal nozzle-to-heater distance to maximize CHF (Fig. 4.4). According to [50], the optimal nozzle-to-heater distance for full cone sprays is predicted using eq. 4.3 which, in this case, predicts optimal distances exceeding 7 mm (table 4.2). However, results show that the highest CHF is consistently produced at a distance of 5 mm (at 200-400 ml/min) and not at 7 mm. This indicates that the optimal nozzle-to-heater distance, to maximize CHF, is lower than that predicted by eq. 4.3 and thus the optimal distance for hollow cone sprays cannot be predicted using this equation. The likely reasons for this are the again attributed to hollow spray distribution of this nozzle and are the same ones previously explained when describing heat transfer coefficient results (i.e. stagnant pool of liquid at the center of the heater and overspray). Visual observations showed that at high heat fluxes, near CHF, localized dryout first occurs at the heater's center where there is no direct spray from the hollow cone spray nozzle.

4.2.2 Nozzle Performance Comparison

The spray boiling curves for each nozzle are plotted in Fig. 4.5. To best compare nozzle performance, the spray boiling curves shown, are those pertaining to the nozzle-to-heater distance which produced the highest heat transfer coefficients and CHF for each nozzle (i.e. Nozzle 6 @ 5mm & Nozzle 20 @ 7mm). The data shows that increasing flow rate increases both heat transfer and CHF, and this is the case for both nozzles. When comparing nozzle performance at 200 ml/min, it appears that the 4×4 multi-jet nozzle (Nozzle 20) has higher heat transfer and CHF than Nozzle 6. Moreover, Nozzle 20 at 250 ml/min is also found to have higher heat transfer and CHF than Nozzle 6 at 300 ml/min. This superior performance (at an equivalent flow rate) is also evident when comparing the heat transfer coefficients plots for Nozzles 6 & 20 at 200 ml/min in Fig. 4.3. However, it is important to note that the pressure drop for Nozzle 20 at 250 ml/min is about twice that of Nozzle 6 at 300 ml/min. The arrows shown at the end of the spray boiling curves, in this figure and all future figures, indicate the onset of CHF.

When comparing the performance of both nozzles at the same inlet pressure, Nozzle 6 demonstrates better performance. This is demonstrated in Fig. 4.3 where Nozzle 6 produces higher heat transfer coefficients at an inlet pressure of 338 kPa compared to Nozzle 20 at 374 kPa. The CHF, at these inlet pressures are similar with values of 1,460 kW/m^2 and 1,410 kW/m^2 for Nozzle 6 and 20, respectively (Fig. 4.4). Another observation that can be made from Fig. 4.5 is that at lower heat fluxes there is more distinction between the various spray boiling. However, at the higher heat fluxes, within the nucleate boiling regime, the various spray boiling curves begin to converge, showing less sensitivity to flow rate and nozzle type. This behavior better depicted in Fig. 4.6 which plots the heat transfer coefficients versus the heat flux for the two nozzles at all flow rates tested.

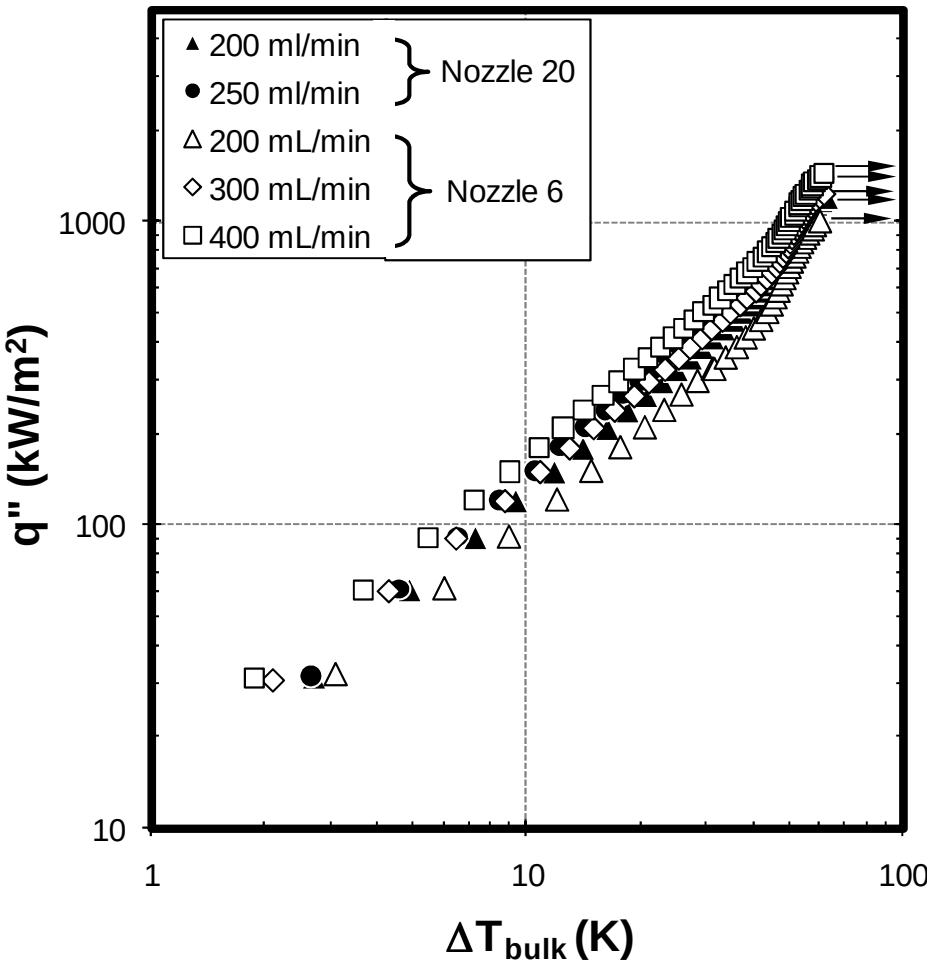

Figure 4.5. Spray boiling curves for both nozzles at various flow rates.

4.3 Effect of Extended Surface, Heat Spreaders

Additional tests were carried out using heat spreaders centered above the 10×10 mm heaters. As previously stated, the wall temperature given, for these heat spreader experiments are taken at the interface between the 10×10 mm heater and the heat spreader plate and the heat flux values were calculated using the area of the 10×10 mm heater and not the area of the heat spreader (see Section 2.1). Tests were conducted with three heat spreaders of different sizes and thicknesses (20×20×3, 30×30×1 & 30×30×3 mm). The same two nozzles used in previous tests were also used in these experiments. It should be noted that spray nozzles were

designed to cool a 10×10 mm area and therefore a significant portion of the heat spreader perimeter was not directly impacted by the spray.

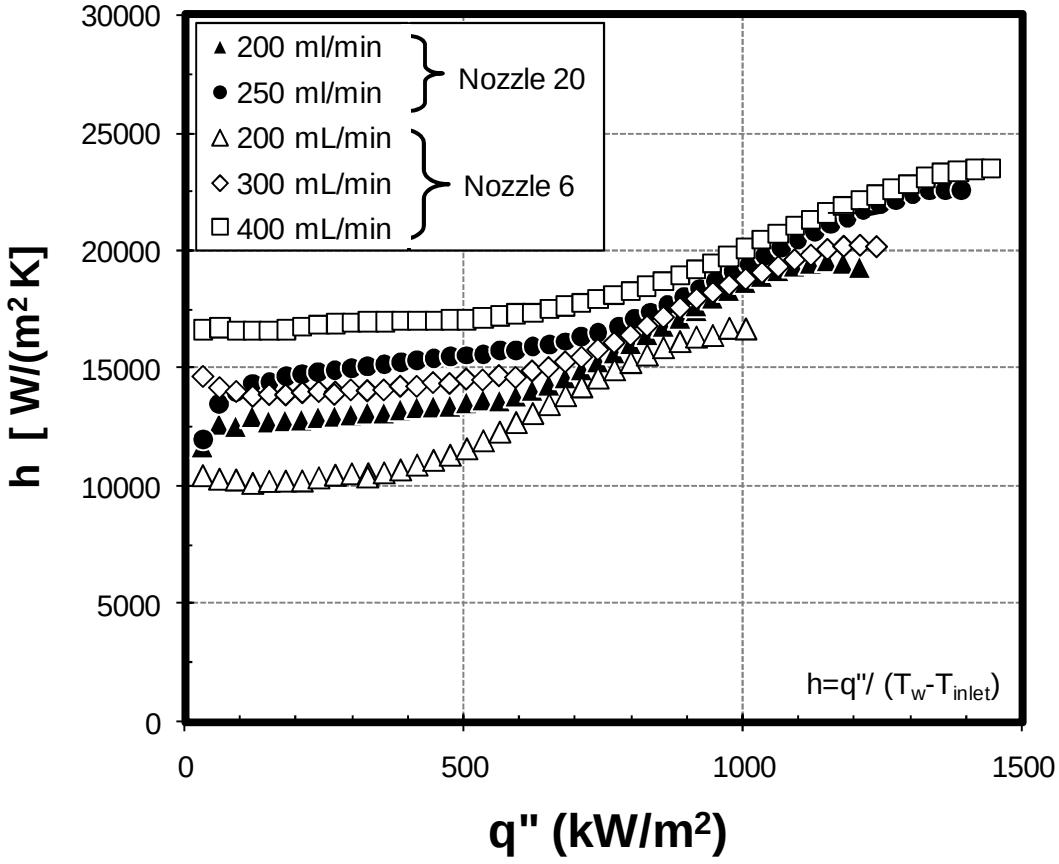

Figure 4.6. Heat transfer coefficients plotted versus heat flux for both nozzles at all flow rates tested.

The spray boiling curves for the three heat spreaders at 200 ml/min and 10 mm nozzle-to-heater distance are shown in Fig. 4.7. For reference, the spray boiling curve for the 10×10 mm heater (no heat spreader) at 200 ml/min and 5 mm nozzle-to-heater distance is also provided. Nozzle 6 was used in these tests; however, Nozzle 20 demonstrated similar results (results not shown). Results show a decrease in wall superheats and increase in CHF with all heat spreaders as compared to not using a heat spreader. Of the three tested, the largest heat

spreader (30×30×3 mm), showed the most enhancement. This heat spreader was found to increase CHF (based on chip area) by about 120% as compared to the non-heat spreader heater. The other two heat spreaders (20×20×3 & 30×30×1 mm) showed somewhat similar performance.

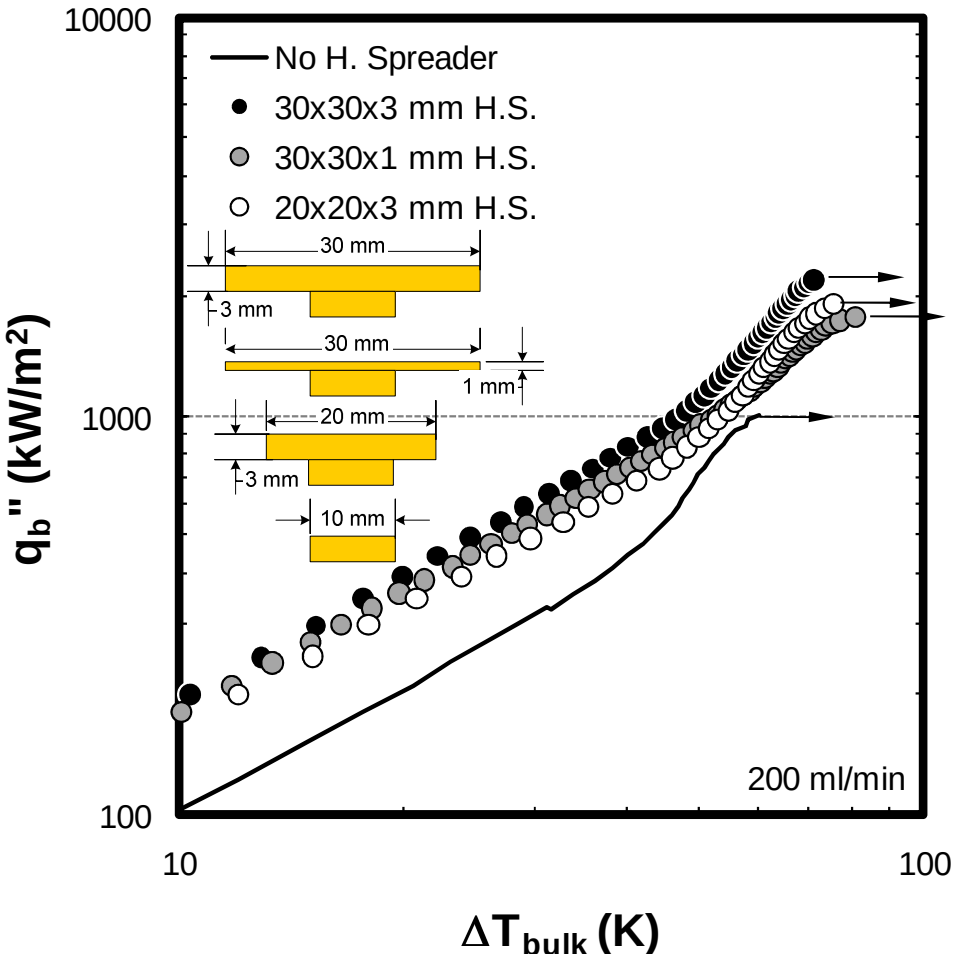

Figure 4.7. Spray boiling curves for using 10×10 mm heater with heat spreaders of various dimensions.

Spray cooling test using a 10×10 mm heater demonstrated that when compared at the same flow rate, Nozzle 20 outperformed Nozzle 6 by providing both higher *h*-values and CHF. However, spray cooling tests using heat spreader found little difference in performance between the two nozzles when compared at the same flow rate (Fig. 4.8). Therefore, the extended

surface of the heat spreader seems to nullify the advantages the multi-jet nozzle held over the single spray nozzle. This nozzle insensitivity is likely due to the fact that a large portion of the spreader is not directly impacted by the spray. This diminishes the effect of spray characteristics (i.e. full cone, hollow cone, multi-jet) on performance by limiting its area of influence to only the central core of the spreader. This then allows for significant boiling to occur at the perimeter of the spreader (Fig. 4.9). Nucleate boiling heat transfer then constitutes a higher percentage of the total heat transfer, making the spray cooling on spreader less sensitive to nozzle spray characteristics. Tests were done at 5 and 10 mm nozzle-to-heater distances using the heat spreaders. Results show that higher CHF is achieved at 10 mm for both nozzles (Fig. 4.8). In addition, changing the nozzle-to-heater distance (5 or 10 mm) showed no significant effect to the heat transfer coefficient.

As previously stated, the nozzles used in the heat spreader tests were designed to cool a 10×10 mm heated area and not the larger surface areas of the heat spreaders. The result is that only a small portion of the heater (the center) is directly impacted by the spray. The perimeter of the heat spreader area is cooled by a thin film of liquid which propagates outward from the spray core. Significant boiling is observes at to occur on this liquid film, at the heat spreader perimeter, at higher heat fluxes (Fig. 4.9). Near CHF, localized dryout is observed to begin at the heater perimeter, especially the corners of the heat spreader, and propagate inwards as heat fluxes approached CHF. The use of spray nozzles with a larger area of coverage might help to delay localized dryout and thus further increase CHF in heat spreaders.

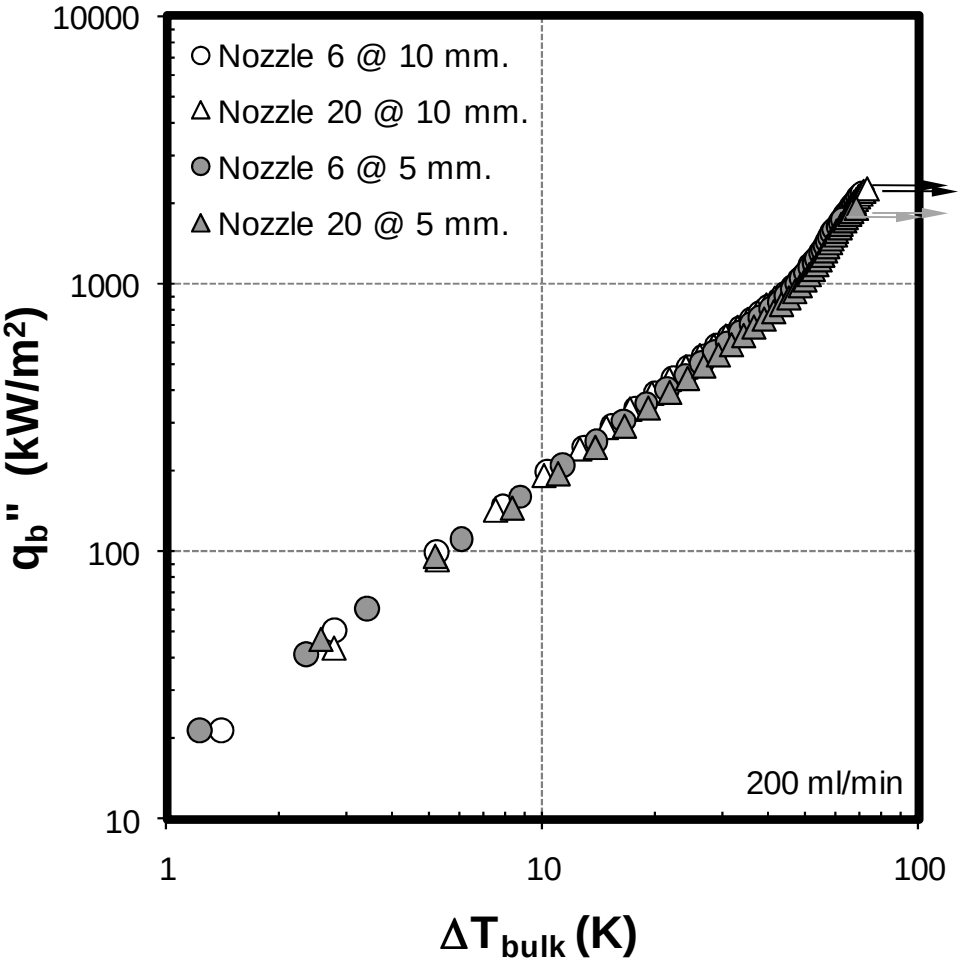

Figure 4.8. Spray boiling curves for Nozzles 6 & 20 at 200 ml/min using the 30×30×3 mm heat spreader heaters at 5 and 10 mm nozzle-to-heater distances.

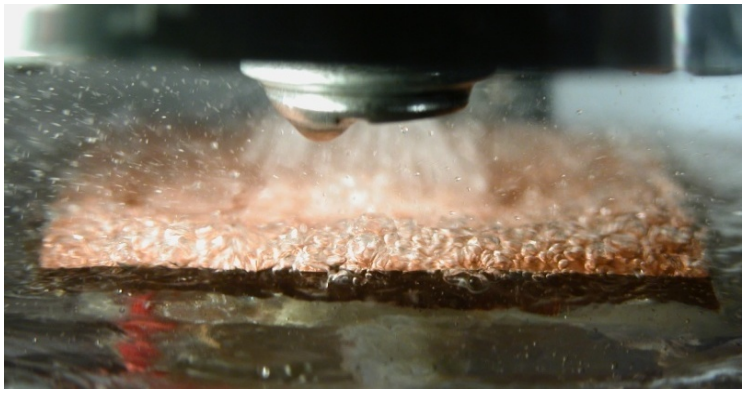

Figure 4.9. Image of spray cooling at 200 ml/min using the 30×30×3 mm heat spreader outputting 200 Watts. Vigorous boiling is observed at the perimeter of the heat spreader.

4.3.1 Effect of Subcooling

Tests were conducted to investigate the subcooling effect on spray cooling performance using the 30×30×3 mm heat spreader. Tests were conducted with nozzle inlet temperatures at 35℃ (ΔT_{sub}≈22℃) and 45℃ (ΔT_{sub}≈12℃) and compared to those previous completed at T_{inlet}=25℃. Fig. 4.10 displays the spray boiling curves, using Nozzle 6, for subcooling tests at 200 ml/min. The effect of increasing subcooling is observed to be similar to that of increasing the flow rate. That is, at lower heat fluxes there is a clear difference in performance between the three boiling curves, but once nucleate boiling begins, the three spray boiling curves begin to converge. As can be expected, the higher the degree of subcooling, the higher the CHF.

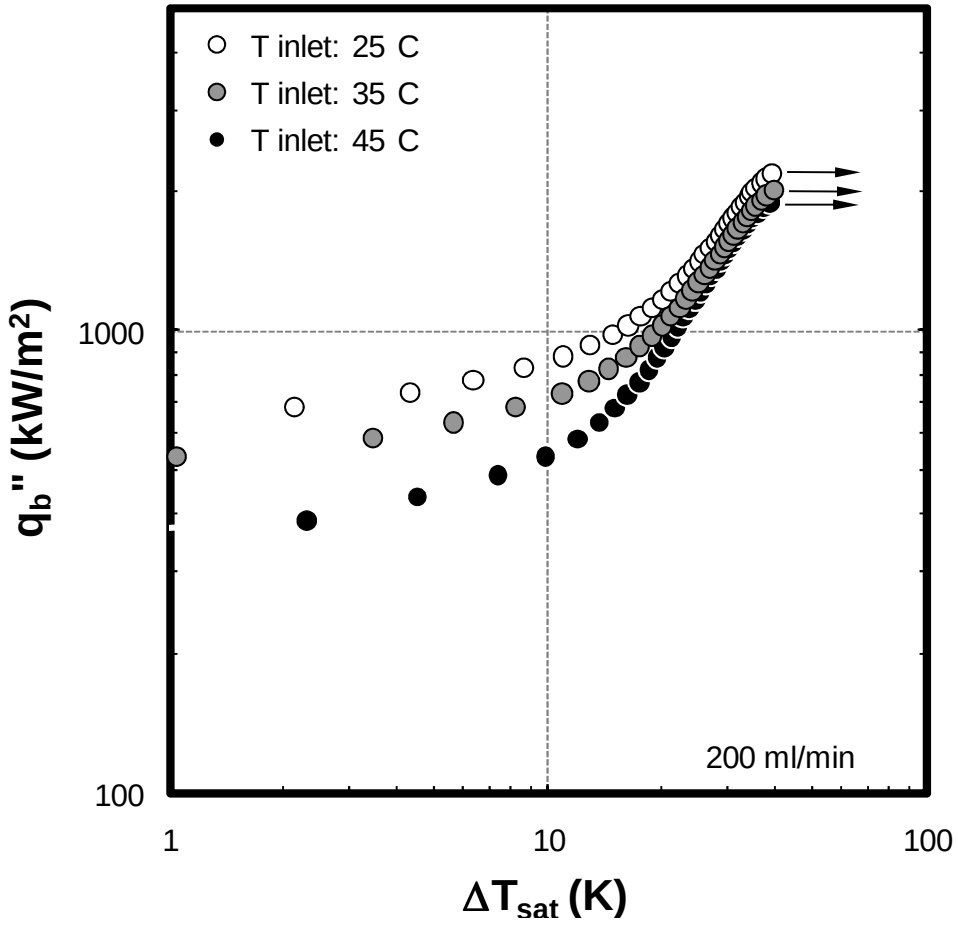

Figure 4.10. Spray boiling curves at nozzle inlet temperatures of 25, 35 & 45℃ using Nozzle 6.

4.4 Microporous Coating

The effect of using a thermally conductive microporous coating on spray cooling performance is reported in this section. Experiments were conducted using a 10×10 mm copper heater both with and without an attached heat spreader plate.

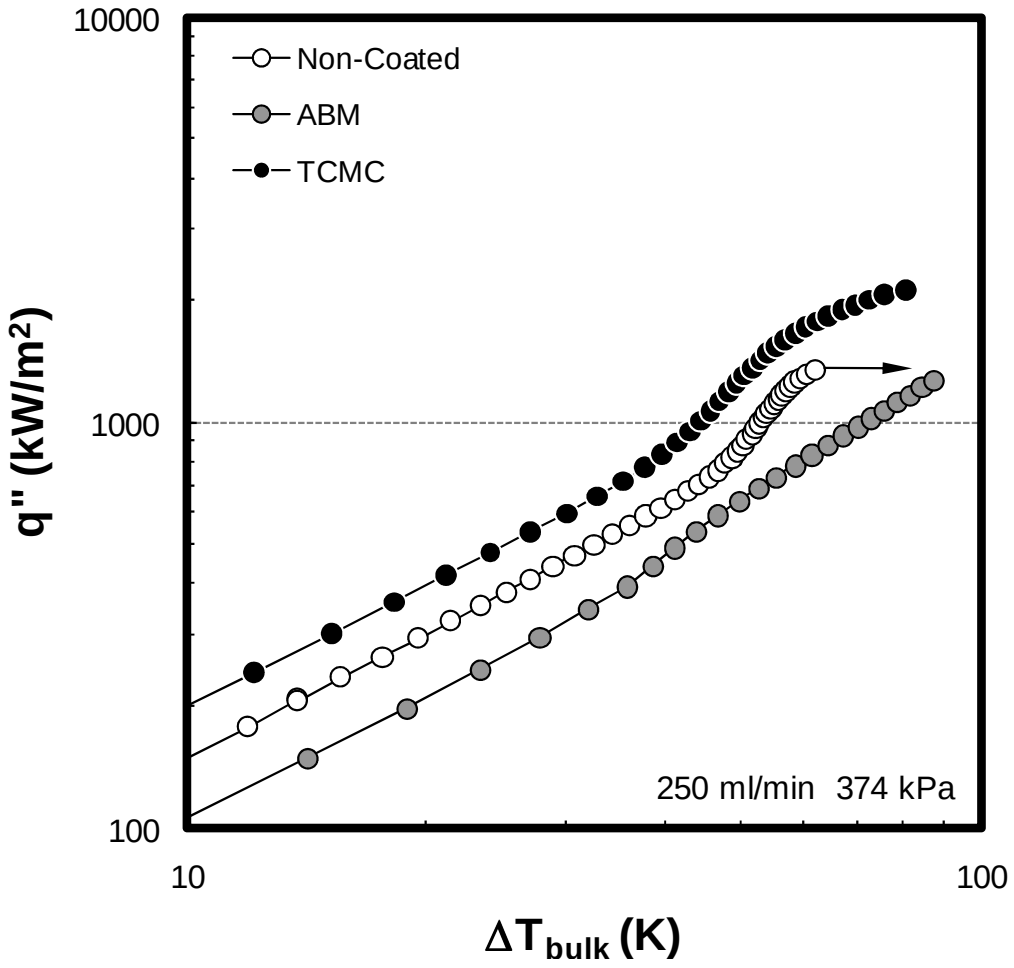

Figure 4.11. Spray boiling curves for TCMC, ABM and non-coated 10×10 mm heaters.

4.4.1 Microporous Coating on 10×10 mm heater

Tests were first carried out using the 10×10 mm heater with Nozzle 20. Three different surfaces were tested including a plain (non-coated), TCMC coated and ABM coated and results are provided in Fig. 4.11. The ABM coating is identical to that used by Kim et al. [9] in their spray cooling investigation in which they report spray cooling enhancement.

From Fig. 4.11, it is clear that the TCMC coated surface enhances both heat transfer coefficients and CHF as compared to the plain surface. On the other hand, the ABM coated surfaces is found to degrade performance which is contrary to the results reported by [9]. The main reason that the ABM coating degrades spray cooling performance, in this study, is its low thermal conductivity (estimated to be 1 $W\text{-}m^{-1}\ K^{-1}$ by [4]) which acts an added thermal resistance and has been shown to degrade flow boiling performance [4, 5] for this same reason. This is not an issue for the TCMC coated surface since it is created using metallic, highly thermally conductive materials. The main reasons the ABM coating performed well in previous Kim et al. [9] spray cooling tests, is that those tests were conducted at very low heat fluxes (< 30 kW/m^2) and flow rates (3 ml/min max.) which resulted in relatively low heat transfer coefficients (≤ 500 $W\text{-}m^{-2}\ K^{-1}$). The low heat transfer coefficients indicate that thermal resistance associated with evaporation and convection were greater than the thermal resistance of the ~50 μm thick ABM coating and thus, in their case, the coating was not the dominant resistance to heat flow.

The TCMC coating is observed to enhance heat transfer coefficients by about 45% in both the lower heat flux region (single-phase/evaporation dominant) and the higher heat flux region (nucleate boiling dominant) (Fig. 4.12). This increase in heat transfer results from the coating facilitating the phase-change mechanisms (i.e. evaporation and nucleation). The porous coating contains numerous cavities of varying micro-sizes which trap vapor/air pockets and increase the number of active nucleation sites. In addition, the wicking/capillary action created by the porous structure of the coating also helps in drawing the liquid to the surface, and in doing so, decreases the liquid film thickness. This decrease in film thickness might also

increases the total three-phase contact line length in much the same manner described by Stephan & Sodtke [32]. Both thinner liquid films and an increase in three-phase contact line length then result in higher evaporation. In the lower heat flux region, it is this increased evaporation which produces the increase in heat transfer. In the nucleate boiling regime, heat transfer enhancement results from both an increase in nucleation sites and evaporation.

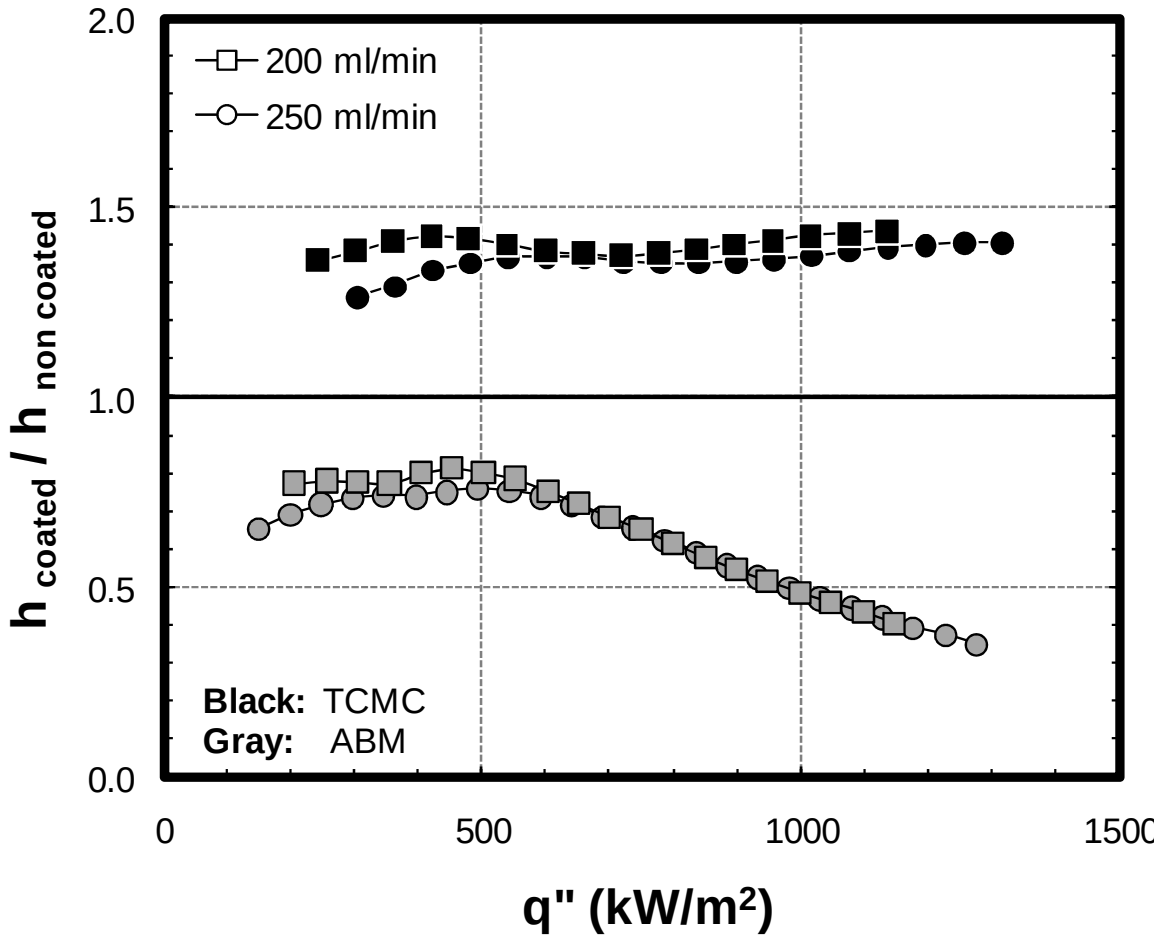

Figure 4.12. Heat transfer coefficient (h) ratios: h coated over h non-coated for Nozzle 20.

The unique flow characteristics of sprays might also present a possible scenario of spray cooling on porous structured surfaces. The vapor/air trapped or entrained by the spray (secondary nuclei) which has been was extensively studied by [49], could be forced into the

porous structure by the impinging droplets and in this manner, activate internal nucleation sites within the coating. This nuclei seeding process might be more effective in this porous situation than with a plain surface due to the significantly higher number of cavities (Fig 4.13). In a similar manner, the momentum of the impinging droplets could also penetrate into the porous coating and drive out vapor pockets which may be lingering within the coating (Fig. 4.13). This process of impinging droplets forcing out trapped vapor in combination with the passive fluid transport from the wicking effect of the coating both help to transport liquid to areas experiencing localized dryout which then delays CHF. These are some of the mechanisms that are believed to be responsible for the CHF enhancement produced by the TCMC coating. Due to heater temperature limitations it was not possible to achieve CHF for the coated heaters therefore, it was not possible to quantify the CHF enhancement produced by the TCMC coating. However, going by the last data point on the TCMC spray boiling curve, there it at least a 60% increase in CHF produced by the coating (Fig. 4.11).

The CHF increase by the microporous coating is in contrast to the decrease in CHF from sand paper roughened surfaces as reported by Tilton [64]. In their study the claim is made that the roughened surfaces increase nucleation sites which then increases vapor generation. This increased vapor generation then expels incoming droplets and decreases CHF for spray cooling. Since the TCMC coating is also expected to significantly increase nucleation, it is possible that the porous nature of the coating might provide preferential/additional paths for vapor to escape and thus decreases the vapor resistance to incoming droplets. This allows the coating to both increase heat transfer but not have a negative effect on CHF, as is the case with sand paper roughened surfaces.

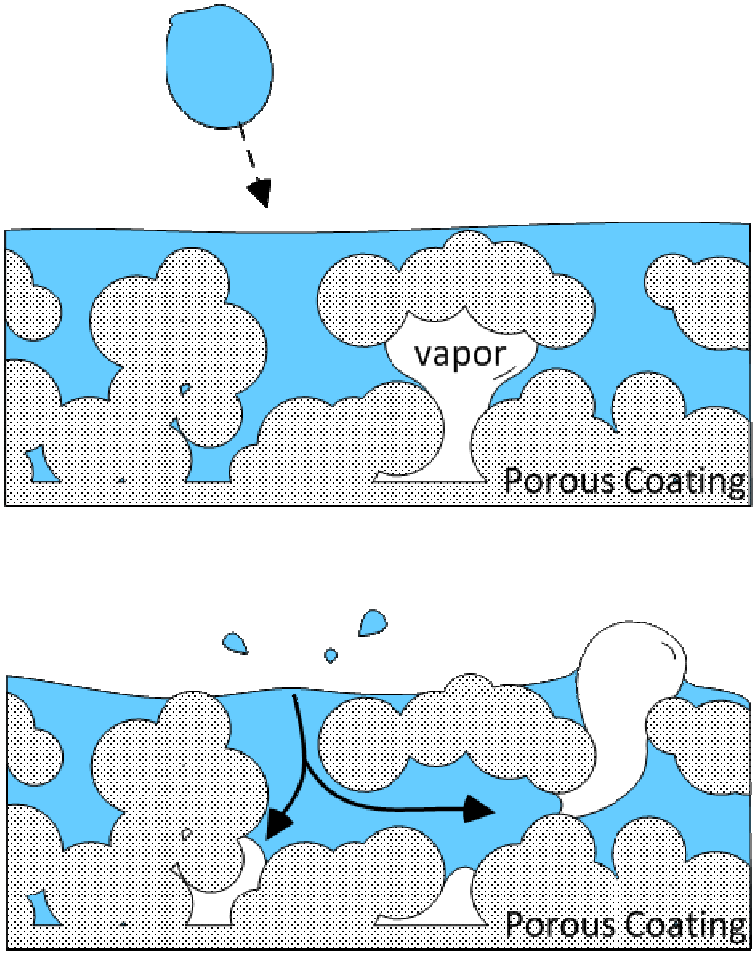

Figure 4.13. Depiction of an impinging droplet on a porous surface before (top) and after impact.

4.4.2 Microporous Coating on Extended Surfaces (Heat Spreaders)

Spray cooling tests were then conducted using the 30×30×3 mm heat spreaders in combination with the coatings in an effort to maximize enhancement. Experiments were conducted with a plain (reference), TCMC coated and ABM coated surfaces at various flow rates. The spray boiling curves for Nozzles 6 and 20 at 200 ml/min are provided in Fig. 4.14. Results show that the coating further increases the heat dissipation capabilities of heat spreaders by decreasing wall superheats throughout the entire spray boiling curve. In addition,

both nozzles provided nearly identical performance when compared at the same flow rate; again a result of the reduced influence of the direct spray to only the central core of the spreader. Unlike the previous 10×10 mm heater tests, the ABM coating had little effect on performance as compared to the non-coated heat spreader.

Since the temperatures at the top surface of the spreader are unknown, it is not possible to quantify the *h*-value enhancements. These coating enhancements are better represented by calculating the thermal resistance as defined as the difference between the temperature at the base of the spreader and the temperature of the bulk fluid divided by the total power dissipated. A plot of the thermal resistances for Nozzle 6 at 400 ml/min for both TCMC and non-coated spreaders are shown in Fig. 4.15. Thermal resistance values from the coating can be as low as 0.18 °C/W which is about a 33% decrease in resistance from that of the non-coated spreader. Once again, facilitation of phase change in both evaporation and nucleation by the coating is believed to be the reason for *h*-value enhancement.

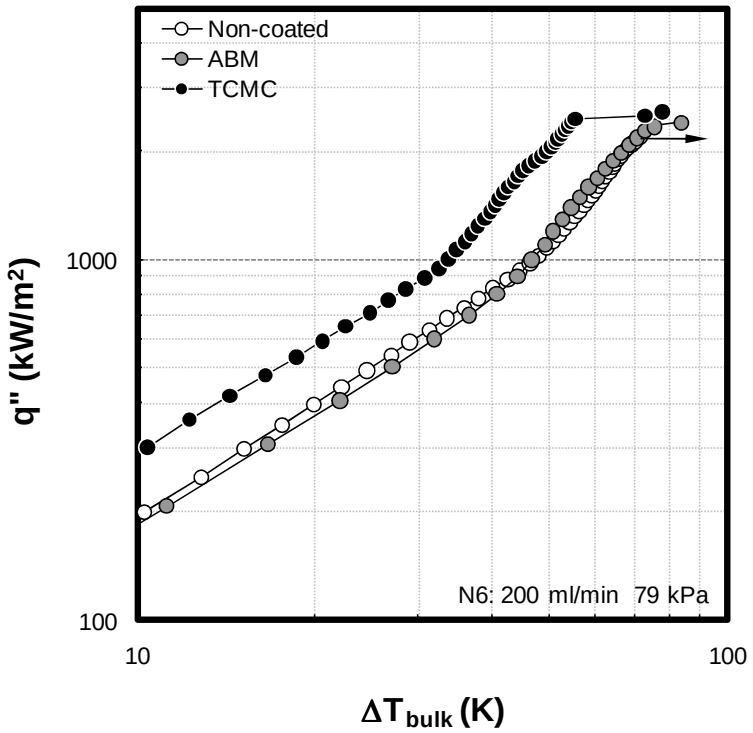

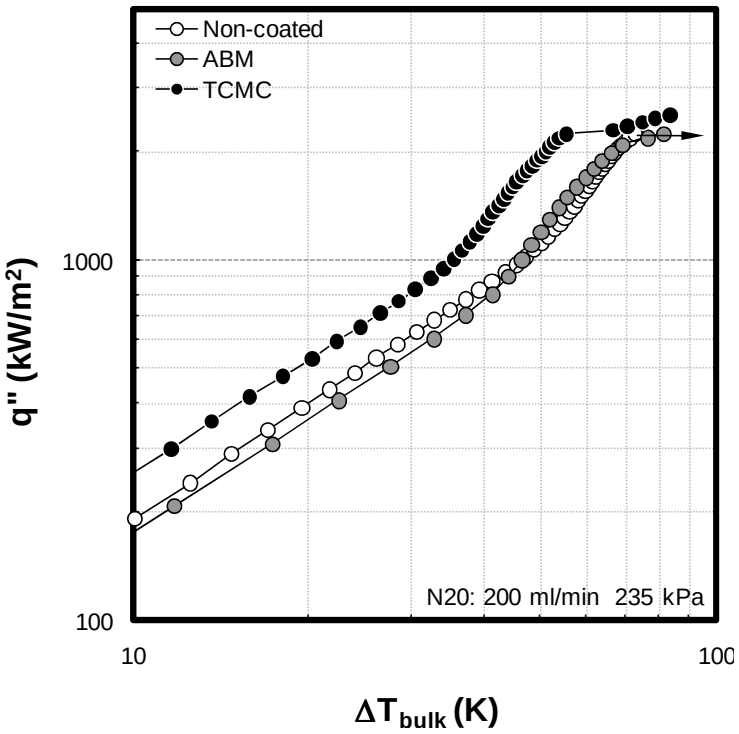

Figure 4.14. Spray boiling curves for TCMC, ABM and plain 30×30×3 mm heat spreaders for Nozzle 6 (top) and 20 (bottom) at 200 ml/min.

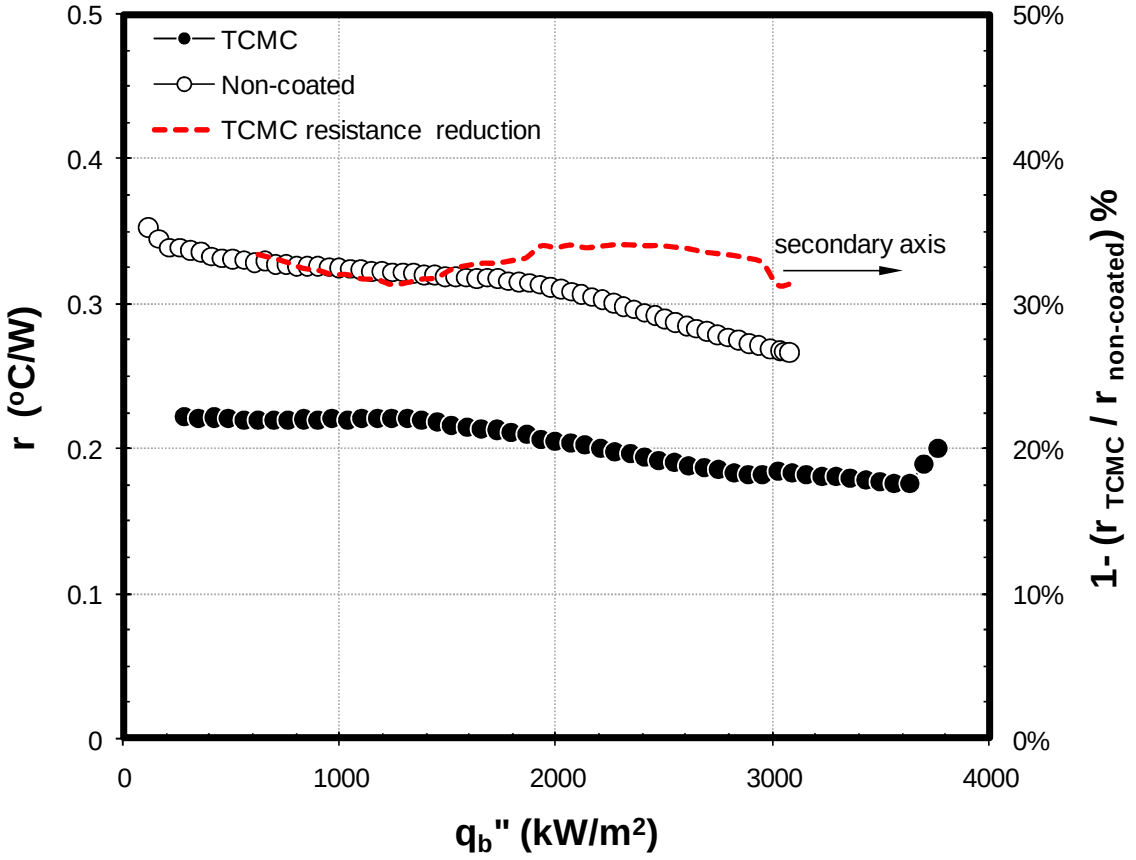

Figure 4.15. Thermal resistance for the coated and non-coated spreader at 400 ml/min.

Due to high heat dissipation of the heat spreaders and the temperature limitations on the heaters it was not always possible to achieve CHF. Therefore, it was not possible to fully investigate the effect of the coatings on CHF. However even with heater temperature limitations it was possible to observe some interesting behavior. For example, in all tested cases, at higher heat fluxes the spray boiling curves for the TCMC coated heat spreader were observed to change in slope (slope decreases) following a jump in temperature (Fig 4.14). The magnitude of theses temperature increases were less than $\Delta T<20℃$ and decreased with increasing flow rates (as low as $\Delta T<7℃$). In this study, CHF is said to occur when he ater shows a sudden increment in temperature and that jump in temperature exceeds the previous steady state value

by more than 20℃. Since the TCMC coated heater did not meet this criterion and since it was not possible to test to higher heat fluxes (due to heater limitations) then it is unclear whether this point/heat flux is CHF.

Even though the mechanisms which lead to CHF in pool boiling are different than those that lead to CHF in spray cooling, the end result for CHF in both cases is vapor blanketing a majority of the surface and a progression into the transition boiling regime (increasing temperature) or film boiling (increasing heat flux). Varies studies [69, 70] have documented the spray boiling curve from the nucleate boiling regime, to transition boiling and into the film boiling regime demonstrating that spray cooling behavior is identical to that of the classical pool boiling curve. Thus upon reaching CHF, surface temperatures are expected to dramatically increase (increasing heat flux) however, the TCMC coated heater does not seem to demonstrate this behavior; at least not in the heat flux range tested. Instead, at a heat flux (high heat flux) the spray boiling curves, for the TCMC coated surfaces are found to have a relatively minor temperature excursion after which they once again reach temperature equilibrium. This phenomenon was not observed with either the plain or ABM coated heat spreader.

So it seems that, for the heat spreader tests, the TCMC coating is delaying complete surface dryout and allows enough liquid to surface contact to produce a positive transition boiling slope. Positive slopes in the transition boiling regime have been observed for flow boiling at high mass fluxes using either water, Freon-113 or Freon-12 by [71-73]. In these cases, the traditionally large temperature excursions associated with CHF were not observed at high mass fluxes. Instead, transition boiling was observed for incrementing heat flux generated boiling curves up until the Liedenfrost condition was reached were no further liquid to surface contact was possible and film boiling initiated. These results are consistent with those observed in this study, with the exception that in this study, positive transition boiling slopes were recorded with spray cooling at relatively low flow rates (≤ 200 ml/min) using porous coatings.

This apparent absence of a CHF point then seems to stem from the coating. It is possible that the porous nature of the coating provides a structure to retain and transport fluid on the heated surface. Being that coating pore diameters can be on the order of the droplet diameters then the pores could, in a way, catch and contain the impinging droplets. In this way, the porous coating is retaining more liquid by containing fluid splatter within the coating pores and by absorbing/wicking droplets upon impact. This effect could be greater at higher heat fluxes, near CHF, when most of the thin liquid layer has evaporated allowing for some of the impinging droplets to directly impact the surface. This process of retaining fluid leaves less fluid to be expelled by rising vapor currents (at high heat fluxes) which are believed to be responsible for triggering CHF in spray and jet impingement cooling. Jet impingement experiments by Monde & Katto [74] have demonstrated that upon reaching CHF, all the liquid is "splashed out" immediately after impinging on the heated surface due to high vapor generation. A similar behavior was observed in spray cooling by Tilton [64] who showed that vapor generated at the heated surface can entrain and expel incoming droplets and trigger CHF.

There is also evidence that shows that porous coatings can affect the Leidenfrost temperature and this could be a reason for the observed behavior. A study by Avedisian & Koplik [75] using methanol droplets on heated surfaces found that ceramic (Al_2O_3) porous coatings significantly increased the Leidenfrost temperature and increasing the coating porosity further increased this temperature. At the highest porosity tested (40%) the Leidenfrost temperature was never achieved. Droplets dispensed on this surface (40% porosity) were observed to always remain in contact with the heated surface even at the highest temperatures tested. Therefore, by increasing the Leidenfrost temperature, the porous coatings allowed the droplet to remain in contact with the heated surface and thus increased heat transfer, as evidenced by the higher evaporation rates. In [75] there is no mention as to why the porous coatings increased the Leidenfrost temperature, however the capillary wicking effect of the coatings, which pulls the droplet towards the surface, is a likely reason. A similar effect could

be taking place with these spray cooling tests on porous coatings which are delaying/extending complete dryout.

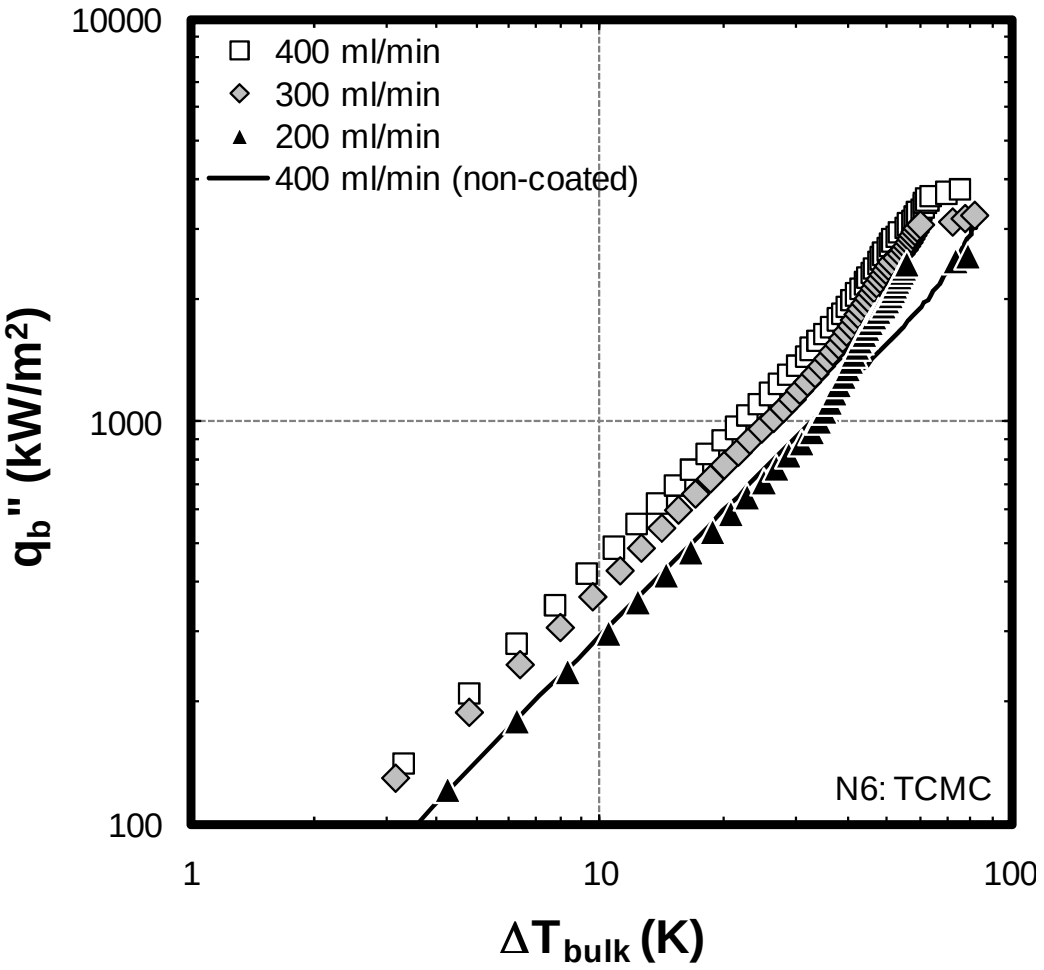

Figure 4.16. Spray boiling curves for TCMC coated spreaders at various flow rates.

The effect of increasing flow rate on TCMC spreader performance is shown in Fig. 4.16. The effects of forced convection heat transfer are more pronounced at lower heat fluxes where increasing flow rate is shown to increase heat transfer. At higher heat fluxes, within the nucleate boiling regime, cooling performance is less sensitive to flow rate as indicated by the near convergence of the spray boiling curves. The benefits of the coating are made clear plotting the

spray boiling curves for the non-coated spreader (solid black line) at 400 ml/min alongside those of TCMC coated spreader (Fig. 4.16). The performance of the TCMC spreader at 200 ml/min has about the same, if not better, performance as compared to the non-coated spreader at twice the flow rate and about 4.3× the pressure drop.

4.5 Spray Cooling using HFE-7000 Coolant

A limited number of experiments were conducted using non-degassed, subcooled HFE-7000 as the working fluid. To date, only a few spray cooling studies, including [76, 77], have been carried out using this dielectric fluid. HFE-7000 properties are provided in table 4.3 and compared to those of FC-72. Due to nozzle clogging issues with Nozzle 20, these tests were conducted using only Nozzle 6. The pressure drop vs. flow rates characteristics for HFE-7000 and FC-72 are plotted in Fig. 4.17. This figure demonstrates that HFE-7000 produces lower pressure drop as compared to FC-72, likely a result of its lower viscosity. The spray cone angle for HFE-7000 at 400 ml/min was similar to that produce with FC-72, ~69°.

Table 4.3. Properties of HFE-7000 and FC-72 evaluated at 25℃.

	Saturation Temp. (°C) @ 1 atm.	ρ (kg/m^3)	C_{pl} (kJ/(kg-K))	k (W/(m-K))	h_{lv} (kJ/kg)	ν ($m^2/s \times 10^{-6}$)	σ ($N/m \times 10^{-3}$)
FC-72	56.5	1,680	1.1	0.057	88	0.38	11.0
HFE-7000	34	1,400	1.3	0.075	142	0.30	12.4

Experiments using HFE-7000 were conducted using heaters with the 30×30×3 mm heat spreaders. The nozzle inlet temperatures were maintained at 25°C (ΔT_{sub}=9 K). Results for the non-coated and TCMC coated spreaders at flow rates of 200-400 ml/min are shown in Fig. 4.18. Due to the relatively low saturation temperature of HFE-7000, the spray boiling curves only experience a brief single-phase/evaporation period before transitioning into a nucleate boiling

dominant mode. Within the nucleate boiling regime, a change in flow rate shows no effect on heat transfer coefficients as observed by the convergence of the spray boiling curves. However, increasing flow rate is found to increase CHF. These results hold true for both the coated and non-coated spreaders.

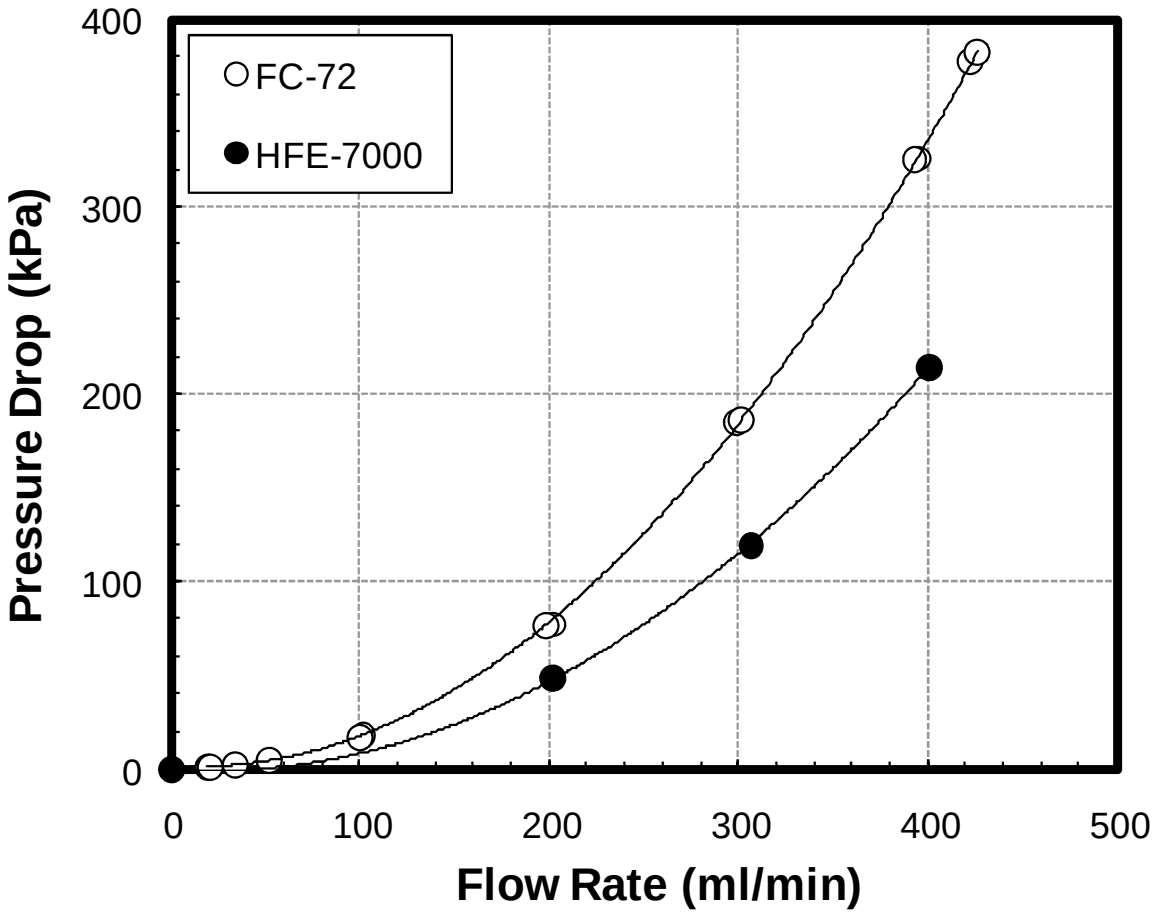

Figure 4.17. Pressure drop versus flow rate plot generated using Nozzle 6 with HFE-7000 and FC-72.

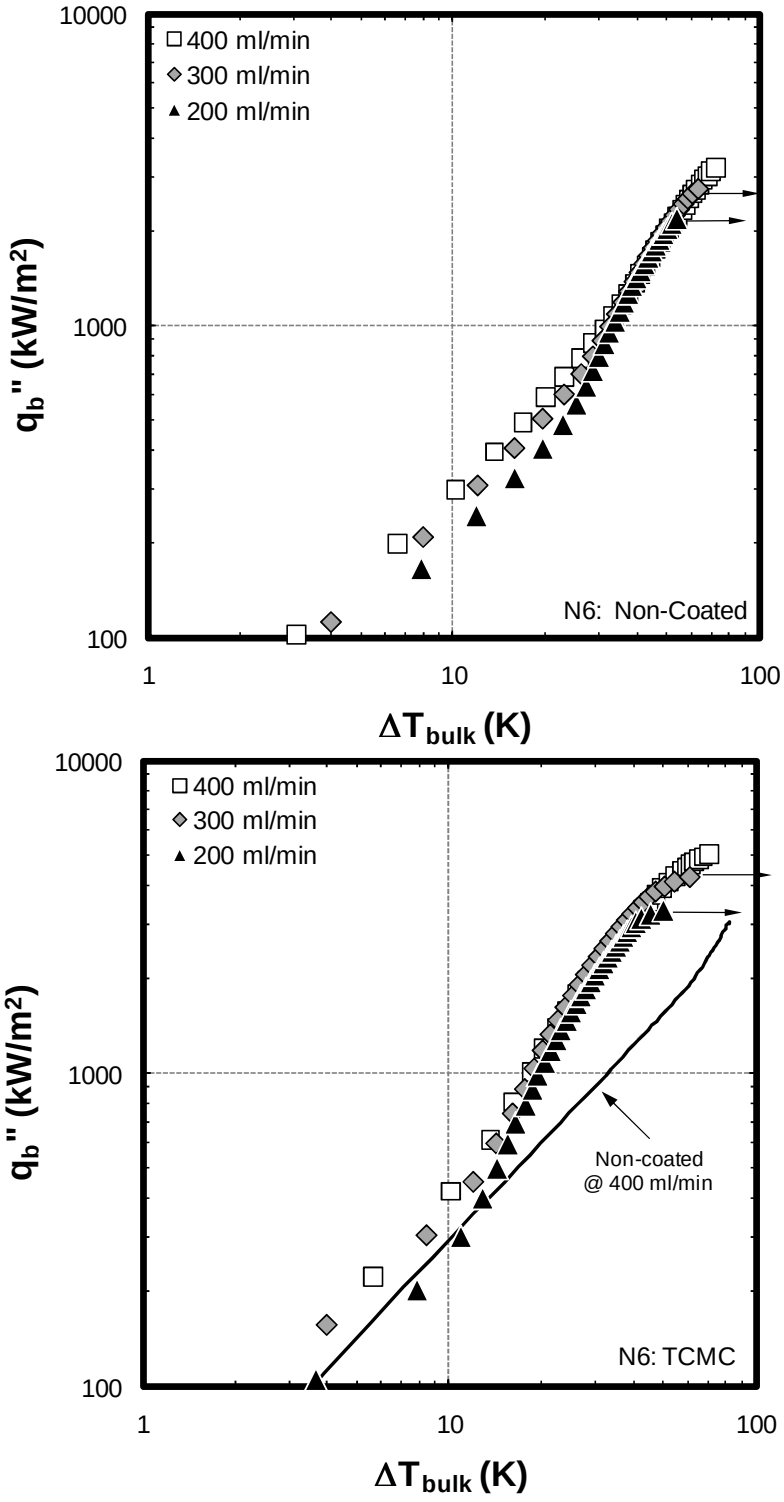

Figure 4.18. Spray boiling curves for HFE-7000 at various flow rates on a non-coated (top) and TCMC coated (bottom), 30×30×3 mm heat spreader.

TCMC coated spreader reduced the total thermal resistances (spreading resistance and convective boiling resistance) by about 42% throughout the entire boiling curve, producing values as low as about 0.13 °C/W. Additionally, the temperature excursion leading to a change in the spray boiling curve slope behavior which was observed in FC-72 experiments were not found to occur with HFE-7000 (Fig. 4.18). It is possible this occurrence could take place at higher flow rates and/or temperatures however, heater temperature limitations did not allow for such testing. As stated before, CHF is said to occur when the heater shows a sudden increment in temperature and that jump in temperature exceeds the previous steady state value by more than 20℃. This condition was met in HFE-7000 spray boiling curves at 200 & 300 ml/min for both coated and non coated surfaces allowing for a CHF comparison. Using these data sets, the coating provides about a 50% increase in CHF.

To compare the performance of HFE-7000 and FC-72 the spray boiling curves for both TCMC coated and non-coated spreaders at 400 ml/min are provided in Fig. 4.19. This figure shows similar heat transfer rates for both dielectric fluids within the single-phase/evaporation regime for both the coated and non-coated cases. This outcome is expected being that both fluids have about the same specific heat. At higher heat fluxes, HFE-7000 produces higher heat transfer rates, as evident by the lower wall superheats, as compared to FC-72 for both coated and uncoated cases. One reason for the superior performance by HFE-7000 is its higher latent heat of vaporization which is about 61% greater than that of FC-72. Moreover, the coating is found to be more effective at increasing *h*-values for HFE-7000. This is evident when comparing thermal resistances, where the TCMC coating reduces the total thermal resistance of the spreaders by about 42% and 33% for HFE-7000 and FC-72, respectively. It is possible that the micro-cavities of the coating are more optimized for HFE-7000. It is also possible that difference in the wetting between the fluids and the coating surface affect wicking behavior and thus affect performance.

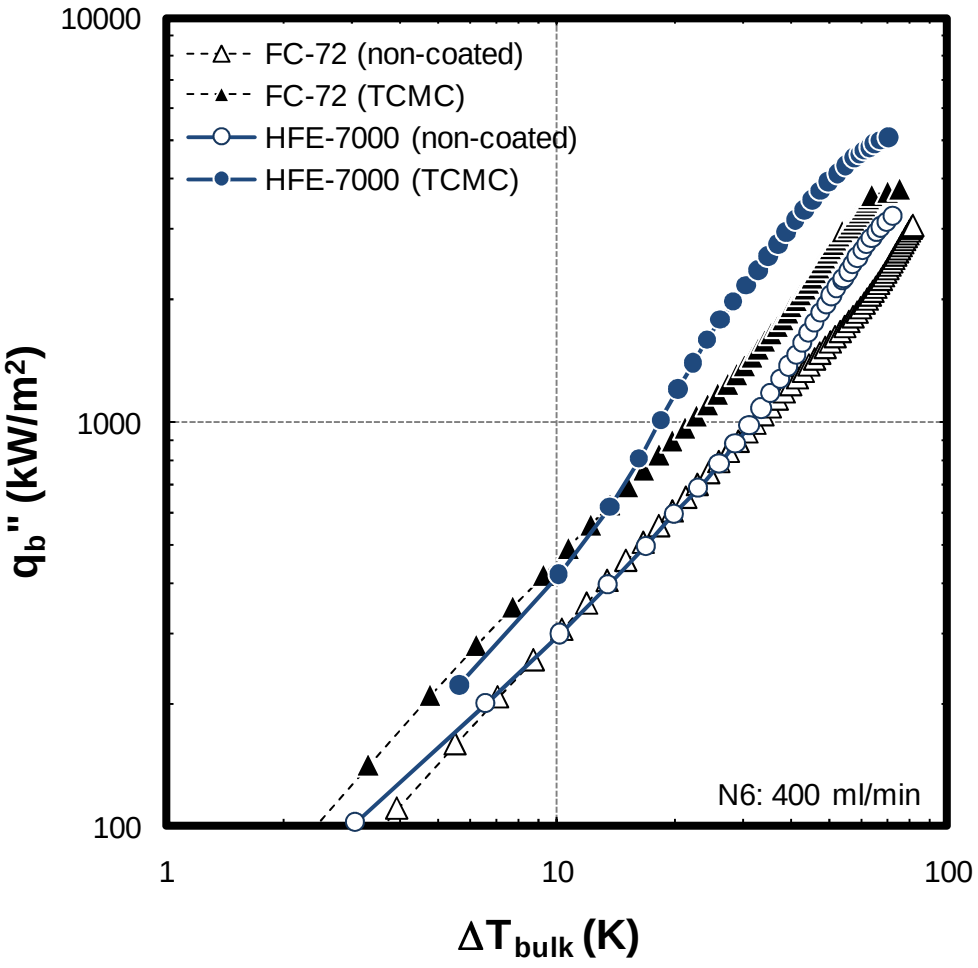

Figure 4.19. Spray boiling curves for TCMC and plain spreaders at 400 ml/min. HFE-7000 and FC-72 spray boiling curves shown.

CHAPTER 5

PERFORMANCE COMPARISON: FLOW BOILING AND SPRAY COOLING

The various methods of forced convection boiling including flow boiling, jet impingement and spray cooling are considered to be competing options for high power heat dissipation [78]. The cooling potential of each of these methods has been reported through extensive research activities undertaken at various laboratories. For example, heat flux dissipations of 6,430 [25], 11,270 [79] and 12,000 kW/m^2 [28] as have been reported using two-phase microchannel flow boiling, jet impingement and spray cooling, respectively. However, the use of different heat geometries/sizes, surface materials (i.e. silicon, copper) and surface conditions/roughness make it difficult to compare the results of one study from the other. In addition, each of these phase-change cooling methods has different pumping power requirements which should be considered when comparing their performance. Therefore, being that the flow boiling and spray cooling data sets, from this study, were generated using identical heaters allows for an accurate and fair comparison of their performance. Such a direct comparison between the two cooling schemes has yet to be reported making this evaluation useful for future reference. These performance comparison results will be the topic of this chapter.

There exist a few studies dedicated to comparing the performance of competing cooling techniques. One such study by Lee & Vafai [80] conducted an analytical analysis which predicted the single-phase cooling performance of jet impingement and microchannels using available correlations. They report that microchannels provide superior performance for smaller (< 0.07×0.07 m) target dimensions while jet impingement (multiple jets) provides better performance for larger target areas. An experimental study by Estes & Mudawar [81] compared the two-phase performance of jet impingement and spray cooling. They found that sprays produce higher single-phase *h*-values, CHF and produce more uniform surface temperatures as

compared to jets. Even though not discussed, their charts indicated that the nucleate boiling performance for each is comparable. Their comparisons were based on equal flow rates and thus the smaller nozzle orifices required for atomization, meant higher inlet pressures for spray cooling. For an additional, more general, review of current and past cooling techniques including the use of air cooling, refrigeration, hybrid systems, etc.., the reader is referred to [78, 82, 83].

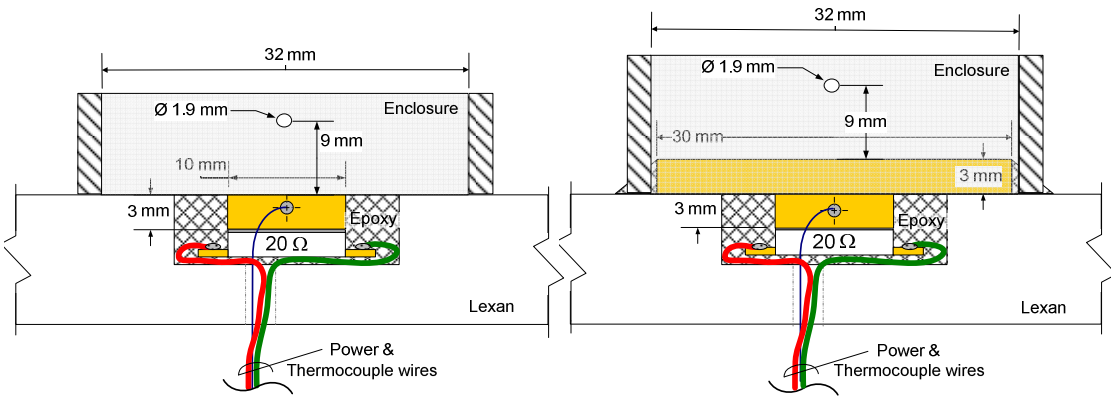

Figure 5.1. Schematic of enclosed heaters, 10×10 heater with (right) and without (left) a spreader.

In addition to comparing the performance of spray cooling and flow boiling, a limited number of additional experiments were conducted using both submerged sprays and jets. These submerged sprays and jets can be viewed as an intermediate between the generally considered superior performance of spray cooling to that of flow boiling. The results from these tests will then also be compared and analyzed with the previous data sets. The differences in performance between all data sets will then provide better insight into the mechanisms responsible for enhancing performance. The reason for testing submerged jets is that they require significantly lower inlet pressures, as compared to sprays, and therefore require less pumping power. This lower pumping power, by the submerged jets, is then more comparable to the lower pumping power requirements of flow boiling. One orifice plate nozzle with an orifice diameter of 1.59 mm (1/16”) was used to generate the jet and the nozzle-to-heater distance was

10 mm (L/d=6.3). The jet nozzle plate and the spray nozzle plates were of the same dimensions and thus were interchangeable within the test section.

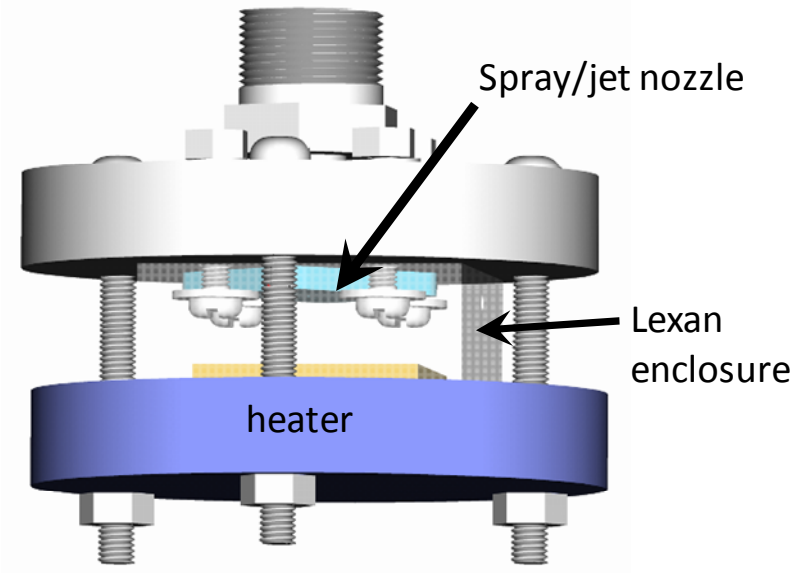

Figure 5.2. CAD model of the enclosed heater secured onto the nozzle support assembly.

The construction of the heaters used in the submerged spray/jet tests was identical to that of the previous flow and spray experiments with the only exception that a polycarbonate wall surrounded and enclosed the heater. Heater schematics for both enclosed 10×10 mm heaters with and without spreaders is show in Fig. 5.1. For these tests, the spray or jet nozzle was centered directly above the heater at 10 mm nozzle-to-heater distance (Fig. 5.2). As was the case for flow and spray cooling, subcooled (ΔT_{sub}≈32K: non-degassed) FC-72 was used as the coolant for these tests. Upon start-up, liquid exiting the nozzles would flood the heater. The liquid would exit the heater enclosure through two 1.9 mm diameter holes drilled into two sides of the polycarbonate enclosure. The spray or jet nozzles would then vigorously churn the fluid. An image of submerged sprays (Nozzle 20) at a flow rate of 200 ml/min, cooling a 30×30 spreader at 0 and 220 W (q_b"=2,200 kW/m^2) is shown in Fig. 5.3. Note the high gas, mostly air, content visible in the zero power image in this figure. Although the pressure within the enclosure

is not expected to be much higher than that of the Pyrex test section, the two 1.9 mm exit holes were restrictive enough to cause the fluid level, within the enclosure, to rise above the exit hole locations and completely flood the enclosure.

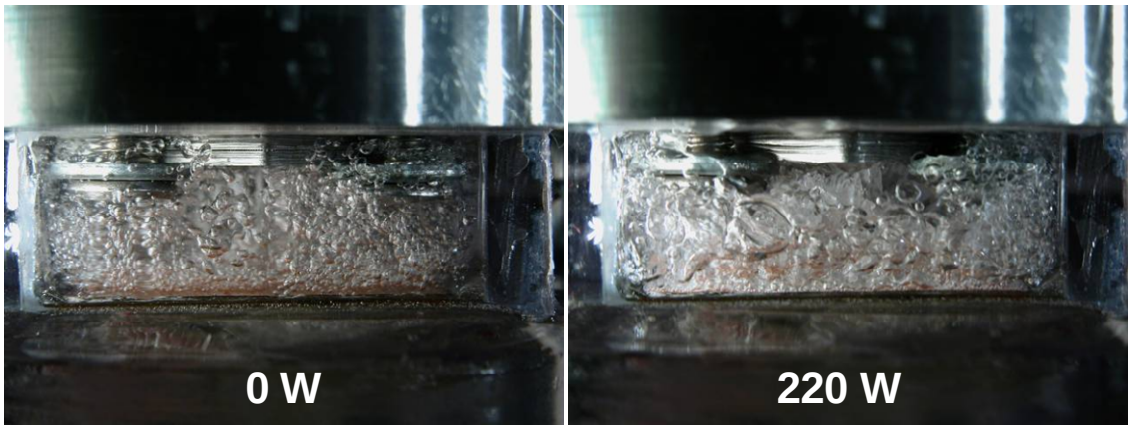

Figure 5.3. Enclose spreader outputting 0 and 220 W (q_b"=2,200 kW/m^2) cooled by a submerged spray (Nozzle 20) at a flow rate of 200 ml/min.

To provide a fair performance comparison between spray and flow, the pumping power requirements of each was calculated. In this manner, the higher pressure drop but lower flow rates of spray cooling could be compared the to much lower pressure drop but higher flow rates of flow boiling. The pumping power equation considers both differential pressure and flow rate to calculate the pumping power (Watts) (eq. 5.1). The differential pressure for spray cooling is the pressure drop across the nozzle (nozzle inlet pressure – test section pressure) and the differential pressure for flow boiling is the pressure drop across the heater (pressure upstream of heater – pressure downstream of heater). The flow rate used in flow boiling is the flow rate required to achieve the desired fluid velocity given the channel dimensions.

$$P_{pump} = Q \cdot \Delta P \tag{5.1}$$

It is worth mentioning that pressure drop in flow boiling is affected by channel dimensions with smaller channel cross sectional areas producing higher pressure drop but requiring lower flow rates. In these comparisons, the flow boiling tests conducted in the smaller, 1 mm channel were selected being that this smaller channel made better use of the available fluid as evident from its higher CHF (as compared to the 3 mm channel). This effect of channel size on pumping power makes the issue of flow boiling pumping power, a somewhat more subjective concept as compared to spray cooling pumping power.

5.1 Spray Cooling and Flow Boiling Comparison: 10×10 mm Heaters

The subcooled boiling curves for all cooling schemes are show in Fig. 5.4 for both coated and non-coated 10×10 mm heaters. To provide the best comparison, the highest velocity flow boiling curve is compared to that of the lowest flow rate spray boiling curve which provided the closest pumping power match possible. Higher pumping powers (i.e. higher fluid velocity) in flow boiling tests were not obtainable due to pumping limitations while lower pumping powers for spray cooling were not possible since there is a minimum differential pressure (flow rate) required to produce full atomization ($>\Delta P$=185 kPa for plain orifice nozzles according to [65]). In addition to the flow and spray boiling curves, the boiling curves for the submerged sprays (Nozzle 20) and submerged jets, both at 200 ml/min, are also provided. A summary of the flow rates, pressure drop values and the resulting pumping power, for all tests shown in Fig 5.4, is provided in table 5.1.

With reference to Fig. 5.4, there are a few performance trends which hold true for both the coated and non-coated heaters. For instance, at lower heat fluxes, spray cooling has the highest heat transfer while flow boiling has the lowest. This spray cooling advantage is due to the thin liquid film, over the heater, and finely atomized droplets produced by spray nozzles which facilitate evaporation and maximize convective heat transfer. The effect of these unique spray cooling characteristics (atomization and thin liquid films) can be seen when comparing

unconfined sprays to submerged sprays at the same pumping power. The flooded heaters in submerged sprays eliminate the beneficial effects of thin liquid films and atomized droplets resulting in a decrease in heat transfer at lower heat fluxes. This atomization/evaporation advantage held by spray cooling makes it unlikely that flow boiling could ever match the spray cooling performance (at lower heat fluxes) even if its pumping power were increased to match that of spray cooling. Yet, another interesting observation is found when comparing the performance of flow boiling to that of submerged jets. The submerged jets have lower pumping power requirements but still outperform flow boiling in the lower heat flux region. This is further evidence that the flow pattern, in the current flow boiling configuration where fluid flows smoothly across the flush mounted heater, does not provide sufficient turbulence and therefore, is not conducive to maximizing single phase heat transfer.

However at higher heat fluxes, once nucleation begins, the boiling curves pertaining to the various cooling schemes begin to approach one another. This clearly demonstrates that nucleate boiling heat transfer dictates the cooling performance at higher heat fluxes regardless of the cooling scheme used. But even within the nucleate boiling regime spray cooling still manages to slightly outperform all other cooling methods. Again, the beneficial effects of the thin liquid film and impinging, atomized droplets augment evaporation and forced convection resulting slightly better performance. This performance insensitivity within the nucleate boiling regimes is consistent the results of Estes & Mudawar [81] when comparing sprays and free jets. All previously mentioned performance trends hold true for both coated and non-coated heaters. It should be stressed that the pumping power requirements for flow boiling were an order of magnitude lower than those of spray cooling. Further converging between the spray and flow boiling curves is possible is flow boiling pumping powers are increased. It is also worth mentioning that the flow boiling curve, for the TCMC coated heater, is found to catch up with the spray boiling curve for the non-coated heater (Fig. 5.4).

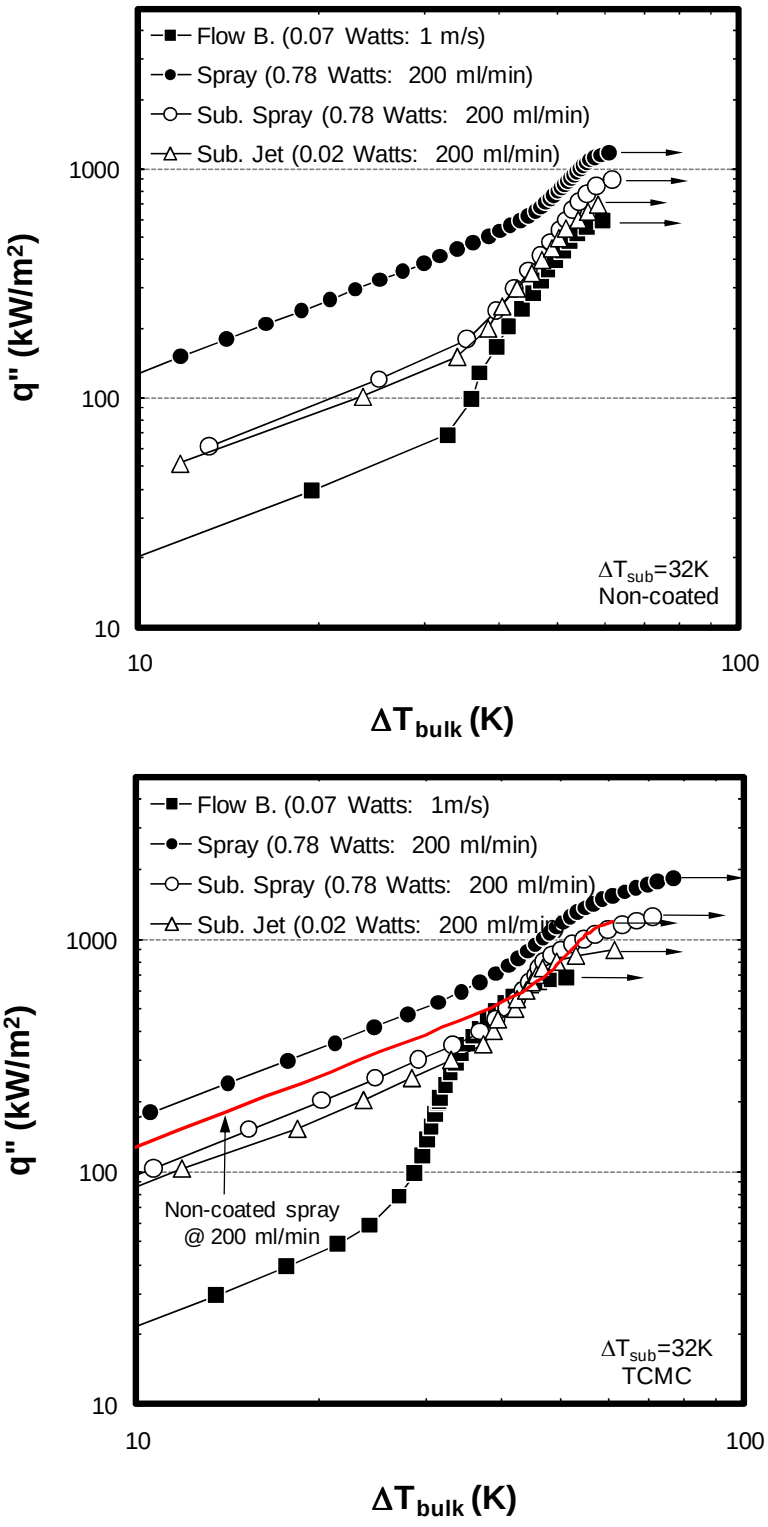

Figure 5.4. Boiling curves for flow, spray, submerged spray and submerged jet. Non-coated (top) and TCMC coated (bottom) 10×10 mm heater using subcooled FC-72 (ΔT_{sub}=32K).

Table 5.1 Measured flow rate and pressure drop as well as calculated pumping power for all boiling schemes.

	U (m/s)	Q $(m^3/s) \times 10^{-5}$	ΔP (kPa)	P_{pump} (W)
Flow *(1 mm channel)*	1	1.20	5.8	0.07
Spray *(Nozzle 20)*	-	0.33	235	0.78
Submerged Spray *(Nozzle 20)*	-	0.33	237	0.79
Submerged Jet	1.7	0.33	5.7	0.02

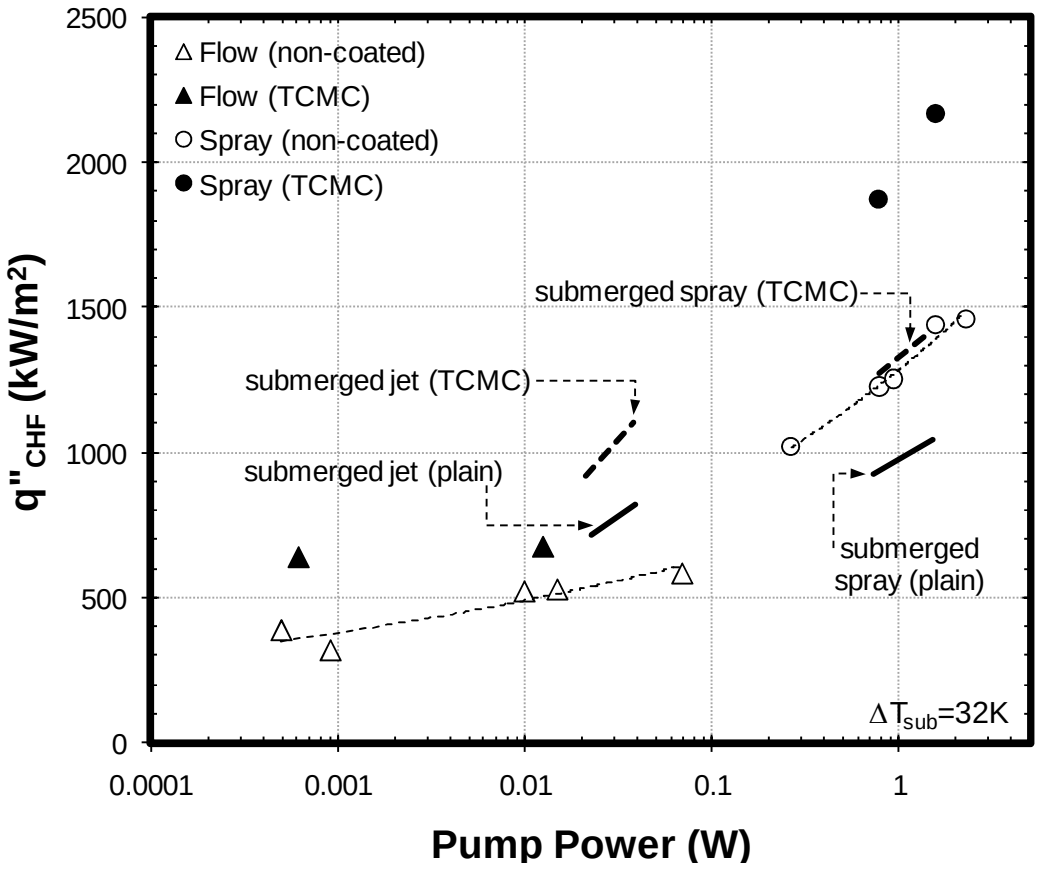

Figure 5.5. CHF values for all cooling schemes plotted versus pumping power requirements.

CHF values were then plotted versus pumping power for all cooling methods tested (Fig. 5.5). It is evident from this figure that spray cooling produces the highest CHF values at the expense of higher pumping power requirements which can be three orders of magnitude greater than those of flow boiling. It should be noted that the flow boiling flow velocities tested are

considered to be in the low velocity regime according to Mudawar & Maddox [56] who reported that CHF increases at a faster rate once fluid velocities are within the high velocity regime (~> 2 m/s).

The mechanisms believed to trigger CHF in flow boiling and spray cooling are not yet fully understood. This is especially true for spray cooling where the added complexity of the atomized sprays does not allow for sprays to be characterized by one dominant flow characteristic (i.e. velocity). Nonetheless, Tilton [64] proposed that CHF in spray cooling occurs when vapor generation from the surface is strong enough to expel incoming droplets thus preventing them from striking the surface. This droplet expulsion is also cited as a likely spray cooling, CHF trigger mechanism by [81]. For flow boiling, Haramura & Katto [84] proposed that CHF occurs when the heat flux is sufficient enough to evaporate the thin liquid sublayer (macrolayer), below the vapor blanket. This view is different than that of the more recent theory proposed by Mudawar et al. [57-59, 85, 86] who dismissed the idea of a continuous liquid layer over the heater. Instead that suggest at heat fluxes close to CHF, liquid to surface contact only occurs at the leading edge and as liquid/vapor interface waves ripple over the heater and intermittently make contact with the surface as the trough of this wave sweeps over the surface. CHF is then triggered when vapor generation is strong enough to push away incoming liquid waves severely restricting fluid to surface contact. Of the two mentioned theories, the latter, is more consistent with of the current study where a vapor boundary layer formed (high heat fluxes approaching CHF) at the leading edge of the heater and was observed to deflect most of the upstream liquid momentum up and away from the heater surface. Therefore, by deflecting the upstream liquid, the current flow configuration for flow boiling, is inherently inferior to the direct impacting spray pattern in spray cooling and therefore flow boiling will likely not achieve CHF values matching those of spray cooling even if tested at higher pumping powers (i.e. higher velocities). This is demonstrated if the CHF versus pumping power curve, for the non-coated heaters, is extended to higher pumping powers; indicating that its CHF values would still be below those of the non-coated spray. However, it is possible that increasing the flow boiling

pumping power for TCMC coated heaters could result in CHF values approaching those of spray cooling on plain heaters. Finally, as shown in Fig. 5.5, the addition of the TCMC coated increases CHF for all cooling schemes.

5.2 Spray Cooling and Flow Boiling Comparison: Heat spreaders

The subcooled boiling curves for spray cooling, submerged sprays and flow boiling for TCMC coated and non-coated spreaders is provided in Fig. 5.6. In general the same conclusions made when comparing the spray and flow using the smaller heater also apply when comparing spray and flow using spreaders. In summary, spray cooling provides superior performance in the lower heat flux regime. At higher heat fluxes nucleate boiling heat transfer becomes the dominant heat transfer mode for all cooling schemes, resulting in nearly identical performance between spray, submerged spray and flow boiling for the non-coated spreaders. With regard to the TCMC spreaders, the application of TCMC coating is found to be more beneficial for spray cooling (both free and submerged sprays) as evident by its slightly better performance, at higher heat fluxes, as compared to the flow boiling. The nucleation seeding effect from secondary nuclei in both free and subermerged sprays promote nucleation and thus could be the reason why TCMC coating enhances spray cooling more so than flow boiling.

Nevertheless, flow boiling on TCMC coated spreader is an effective means of heat dissipation and can be an effective alternative to spray cooling. For example, flow boiling curve for the TCMC spreader requiring only 0.03 watts of pumping power is found provide lower wall superheats (at higher heat fluxes) and higher CHF as compared to spray boiling with a non-coated, 10x10 mm (no-spreader) heater at 0.78 watts pumping power (Fig. 5.6). In addition to lower pumping power requirements, the current flow boiling configuration should not be susceptible to clogging issues, which can be an issue with sprays. However, maximum performance is achieved with spray cooling using the combination of TCMC coating on spreaders.

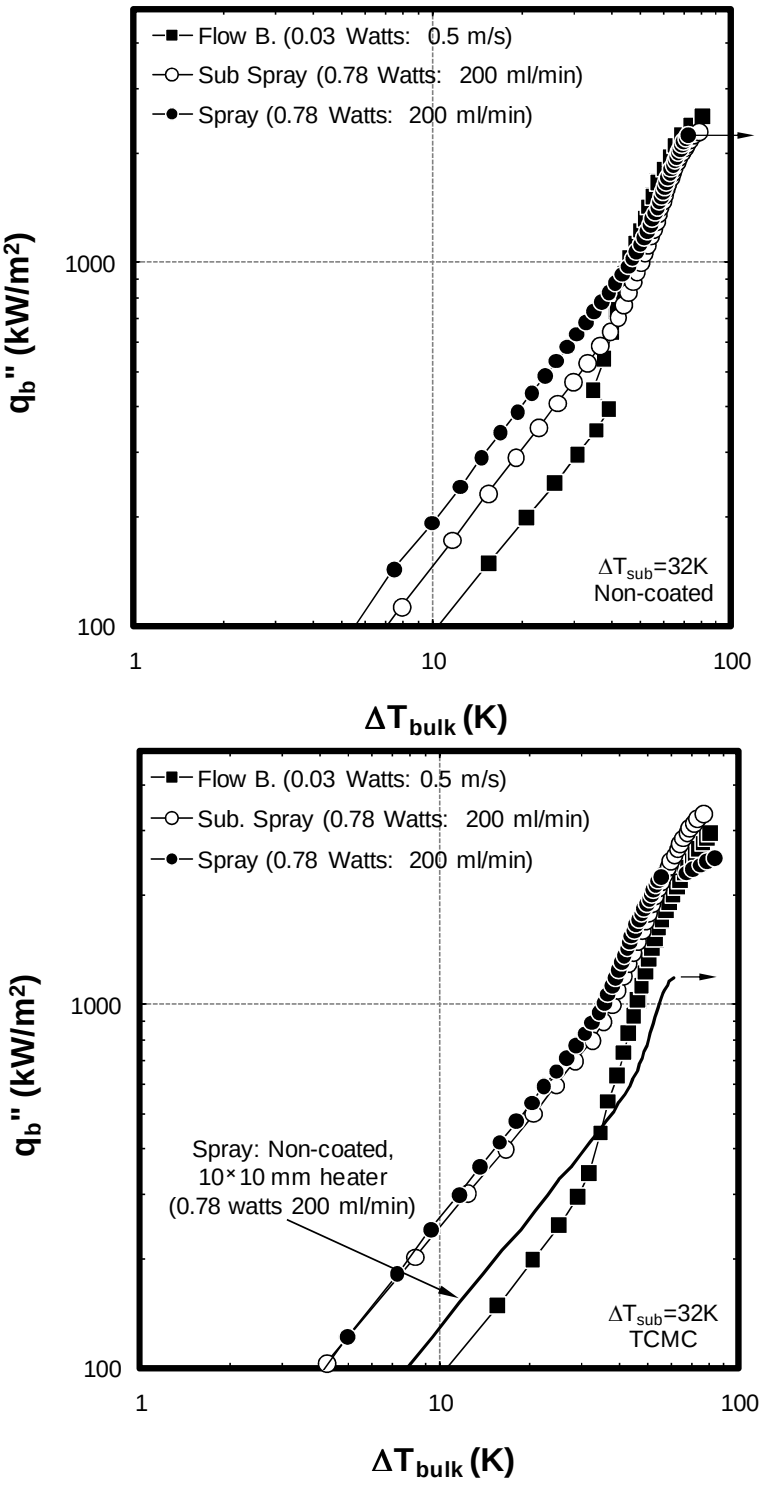

Figure 5.6. Boiling curves for flow, spray, submerged spray and submerged jet. Non-coated (top) and TCMC coated (bottom) 10×10 mm heater using subcooled FC-72 (ΔT_{sub}=32K).

In the case of spreaders, comparing CHF values between the various cooling schemes was not possible due to heater temperature limitations. Even though, the spray boiling curve in Fig. 5.6 is the only one marked with a CHF arrow, all other boiling curves (flow and submerged spray) were recorded to have a spike in temperature at the final heat flux recorded. However, those temperature spikes did not meet the current CHF criteria, due to heater limitations, and thus could not be defined as CHF.

CHAPTER 6

CONCLUSIONS

6.1 Conclusions of Chapter 3: Flow Boiling

1. The TCMC coating significantly enhances *h*-values by about 400% and produce values as high as ~42,000 W m^{-2} K^{-1}. These *h*-values are significantly high considering the generally poor thermal properties of FC-72. A combination of increase in the number of active nucleation sites and high thermally conductive nature of the coating are believed responsible for this enhancement.

2. At higher velocities (≥0.5 m/s), the flow boiling curves with the TCMC coated heaters are found to have two temperature excursions at high heat fluxes. The first temperature excursion is believed to be a result of localized dryout at the downstream end of the heater but complete dryout is prevented by fluid wicking through the coating. The second temperature excursion is followed by complete surface dryout and thus defined as CHF.

3. TCMC coating is found to outperform the previous developed aluminum and epoxy based, ABM coating by producing higher flow boiling *h*-values. ABM coating was reported to degrade performance [4, 5] at high velocities and subcoolings. This degradation was not observed for the TCMC coating at the velocities and degrees of subcooling tested.

4. Smaller channel heights (1 mm) did not affect heat transfer but did increase CHF for both coated and non-coated heaters at velocities ≥0.5 m/s. The smaller channel forces liquid closer to the heater surface which is more effective at “sweeping” vapor and thus

increasing CHF. This increase in CHF comes at the expense of a higher pressure drop (~4× higher).

5. The application of TCMC coating to heat spreaders reduces the total thermal resistance of the spreaders by 16-50% but is more effective at lower heat fluxes. Vapor production at the upstream side of the spreader deprives the downstream half of the spreader of liquid resulting in heat transfer degradation, for the spreaders, at higher heat fluxes. Therefore, at higher heat fluxes, the TCMC spreader only slightly outperforms the non-coated spreader but does increase CHF. Additionally, the application of TCMC coating does not provide any enhancement in subcooled case for the heat spreaders.

6.2 Conclusions of Chapter 4: Spray Cooling

1. Changing the nozzle-to-heater distance has more of an effect on spray cooling performance for the single hollow cone nozzle (Nozzle 6) than for the multi-jet nozzle (Nozzle 20) and affects CHF more so than heat transfer coefficients. In the case of the single hollow cone nozzle, there appears to be an optimal nozzle-to-heater distance to maximize both heat transfer and CHF and this distance appears to be less than the optimal distance to maximize CHF for full cone sprays. There are two possible causes for this, both of which are associated with the distribution of the spray in single hollow cone spray nozzles.

2. Experiments using a 10×10 mm heater demonstrated that when compared at the same flow rate, the multi-jet nozzle (Nozzle 20) is found to outperform the single spray nozzle (Nozzle 6) by producing both higher *h*-values and CHF values. At higher heat fluxes, within the nucleate boiling regime, the various spray boiling curves begin to converge showing less sensitivity to flow rate and nozzle type. In all cases, increasing flow rate increases CHF.

3. The use of heat spreaders in spray cooling decreases wall superheats and increases CHF. Furthermore, if the surface area of the spreaders is large in comparison to the spray impact area, as is the case in this study, then the effects of spray characteristics on spray cooling heat transfer are minimized resulting in essentially the same performance for Nozzles 6 & 20 when compared at the same flow rate.

4. TCMC coating enhances *h*-values throughout the entire spray boiling curve by facilitating phase change in both evaporation and nucleation. When applied to the 10×10 heaters it increases *h*-values by ~45% and when applied to the spreaders it decreases the overall thermal resistance by ~33%. Wicking from the porous coating is believed to draw the liquid towards the surface and thus decreases the film thickness and increase the three phase contact line length which promotes evaporation. Nucleate boiling is enhanced through the significant increase in the number of active nucleation sites from numerous micro-cavities on the coating.

5. The coating is found to increase CHF in the 10×10 heaters by at least 60% and when applied to the heat spreaders, the TCMC coating delays complete surface dryout and allows enough liquid to surface contact to produce a positive transition boiling slope. The coatings ability to retain and wick fluid is believed to be responsible for this effect. It is also possible that the coating could increase the Leidenfrost point which then could also contribute to this effect.

6. The TCMC coating was found to be more effective when used on spray cooling with HFE-7000. In this case, the coating reduced overall thermal resistances by ~42% and increased CHF by about 50%. Heat flux dissipations exceeding 5,000 kW/m^2 at wall temperatures below 100℃ were achieved without reac hing CHF.

6.3 Conclusions of Chapter 5: Performance Comparison: Flow Boiling and Spray Cooling

1. At low heat fluxes, the *h*-values of spray cooling are significantly higher than those produced by flow boiling. However, spray cooling does have pumping power requirements which are one order of magnitude higher that flow boiling. Nevertheless, the unique spray cooling characteristics of thin liquid films and atomized droplets, which enhance both evaporation and forced convection, makes it unlikely that flow boiling could ever match *h*-values even if its pumping powers were increased to match those of spray cooling. These observations hold true for both coated and non-coated heaters.

2. At high heat fluxes, the flow boiling and spray boiling curves begin to approach one another as both cooling scheme become more nucleate boiling heat transfer dependant. At these higher heat fluxes, further convergence between the two cooling schemes is possible, if flow boiling pumping power were increased to match those of spray cooling. These observations hold true for both coated and non-coated heaters.

3. Spray cooling consistently produces higher CHF values. The current flow boiling configuration, where the vapor deflects the incoming fluid, is inherently inferior to that of spray cooling. Therefore, even if flow boiling pumping powers were increased it is not likely that it could ever match spray cooling CHF values. This is evident in the CHF versus pumping power plot. These observations hold true for both coated and non-coated heaters.

4. When using non-coated heat spreaders, there is found to be no difference in performance between flow boiling and spray cooling at high heat fluxes. At low heat fluxes spray cooling does have higher heat transfer. When used in combination with spreaders, the TCMC coating is found to be more effective for spray cooling. Spray cooling on TCMC coated spreaders is therefore, found to outperform flow boiling on TCMC coated spreaders.

6.4 Recommendations for Future Work

1. Pumping limitations limited the fluid velocities in this study. Therefore, additional experiments should be conducted to investigate the effect of higher velocities (> 3 m/s) on TCMC flow boiling performance.

2. In some instances, heater temperature limits prevented CHF from being reached. Therefore, new high temperature heater should be designed to fully investigate the effect of the coating on CHF.

3. Spray cooling tests with TCMC coated spreaders should be repeated and extended to higher heat fluxes to investigate whether the positive transition boiling slopes, recorded in this study, continue on at higher heat fluxes.

4. Experiments should be conducted to characterize fluid wicking and wetting on TCMC coatings using dielectric fluids. However, care should be taken to either minimize or account for the effect of fluid evaporation since these fluids are highly volatile.

5. Since water is the most commonly used coolant, flow and spray cooling experiments should be conducted using water on TCMC coated surfaces.

APPENDIX A

UNCERTAINTY ANALYSIS

Calculated Heat Flux Uncertainty

A list of equipment elemental errors is provided in table A.1. The voltage precision errors shown were obtained from actual flow boiling test data with a heater outputting 20 watts.

Table A.1. List of equipment uncertainties classified as either bias or precision error.

	Elemental Errors	Bias	Precision
DAQ	Accuracy 300mV Range (% of reading + Volts)	±0.02%+8 μV	
	Accuracy 300V Range (% of reading + Volts)	±0.008%+700 μV	
	Age error (1 yr) (% of reading)	±0.01%	
Digital Calipers	Resolution (mm)		±0.01
	Accuracy (mm)	±0.04	
Shunt Resistor	Accuracy (% of reading)	0.10%	
voltage readings (Flow Boiling: experimental data)	V_{heater} Std. Deviation		58 μV (sample size: 6)
	V_{shunt} Std. Deviation		2 μV (sample size: 6)

Heat flux (q") was calculated using the equation,

$$q" = \frac{V_{heater}V_{shunt}}{R_{shunt}A_{heater}}$$

where V_{heater} is the voltage drop across the heater, V_{shunt}/R_{shunt} is the current through the heater and A_{heater} is the area of the heater.

The bias and precision errors were then each calculated through the equation below.

$$\omega = \left[\left(\frac{\partial q"}{\partial V_{heater}}\omega_{V_{heater}}\right)^2 + \left(\frac{\partial q"}{\partial V_{shunt}}\omega_{V_{shunt}}\right)^2 + \left(\frac{\partial q"}{\partial A_{heater}}\omega_{A_{heater}}\right)^2 + \left(\frac{\partial q"}{\partial R_{shunt}}\omega_{R_{shunt}}\right)^2\right]^{1/2}$$

For an actual test (flow boiling) with a heater output of 20 W, the total heat flux uncertainty was then calculated to be ~**5.14%**. Uncertainty of the shunt resistor (bias error) accounted for the majority of this error, about 5% of the total.

Calculated Flow Rate and Velocity Uncertainties

A list of all equipment, and their associated uncertainties, used to calculate flow rate and velocity measurements is provided in Table A.2.

The propagation of error equation applied to the flow rate (*Q*) equation (eq. 2.4).

$$\omega = \left[\left(\frac{\partial Q}{\partial f}\omega_f\right)^2 + \left(\frac{\partial Q}{\partial k}\omega_k\right)^2\right]^{1/2}$$

Dividing eq. 2.4 by the cross sectional area of the channel provides the fluid velocity. The propagation of error equation applied to the velocity (*U*) equation is then

$$\omega = \left[\left(\frac{\partial U}{\partial f}\omega_f\right)^2 + \left(\frac{\partial U}{\partial k}\omega_k\right)^2 + \left(\frac{\partial U}{\partial A_{channel}}\omega_{A_{channel}}\right)^2\right]^{1/2}$$

The above equations were used to sum the total bias and precision errors. In addition to the precision errors provided in Table A.2, precision errors associated with experimental scatter in both the frequency (*f*) output and *k* constant (calibration error) were used to calculate uncertainties. Standard deviation in frequency was 0.41 Hz (sample size=12) and was obtained from experimental data, for one test (flow boiling at 1.8 l/min). Calibration of the flow meter provided a calibration uncertainty in *k* of 183 pulses/litter (standard deviation: sample size=13).

Table A.2. List of equipment uncertainties classified as either bias or precision error.

	Elemental Errors	Bias	Precision
DAQ	Accuracy (frequency) ± count	±1	
	Resolution (frequency) ± count		±1
Flow Meter	Accuracy (% of reading)	±1%	
	Resolution (% of reading)		±0.1%
Digital Calipers	Resolution (mm)		±0.01
	Accuracy (mm)	±0.04	

Flow rate uncertainty was calculated to be **1.6%** at 1.8 l/min almost all of which was from flow meter error (accuracy, resolution and calibration). Velocity uncertainty was calculated to be **2%** at 0.5 m/s. Of the total error, the flow meter error contributed about 1.6% and the rest was from error associated with uncertainties in the measurement of the channel area.

APPENDIX B

FINITE ELEMENT MODEL

Heater FEM Analysis

Detailed heater FEM models were created to simulate actual conditions. The models included all components of the actual heaters (copper, epoxy, lexan, copper wires, thick film resistor, etc…). The heat transfer coefficients (*h*-values) and fluid/air temperatures, listed in Table B.1, were imposed on the heater FEM models and used to calculate the approximate heat lost through the heater insulation (sides & bottom). These conditions are intended to simulate flow boiling tests for a non-coated heater.

Table B.1. Imposed boundary conditions: heat transfer coefficients and fluid/air temperatures.

	h ($W/m^2 K$)	T_∞ (°C)
10×10 mm heater surface	10000	56
Top surface surrounding heater (lexan & epoxy)	2000	56
All other surfaces (i.e. sides & bottom)	10	22

Samples of the heater temperature solutions for both the 10×10 mm heater (outputting 20 W) and the 30×30×3 mm heat spreader (outputting 100 W) are provided in Fig. B.1.

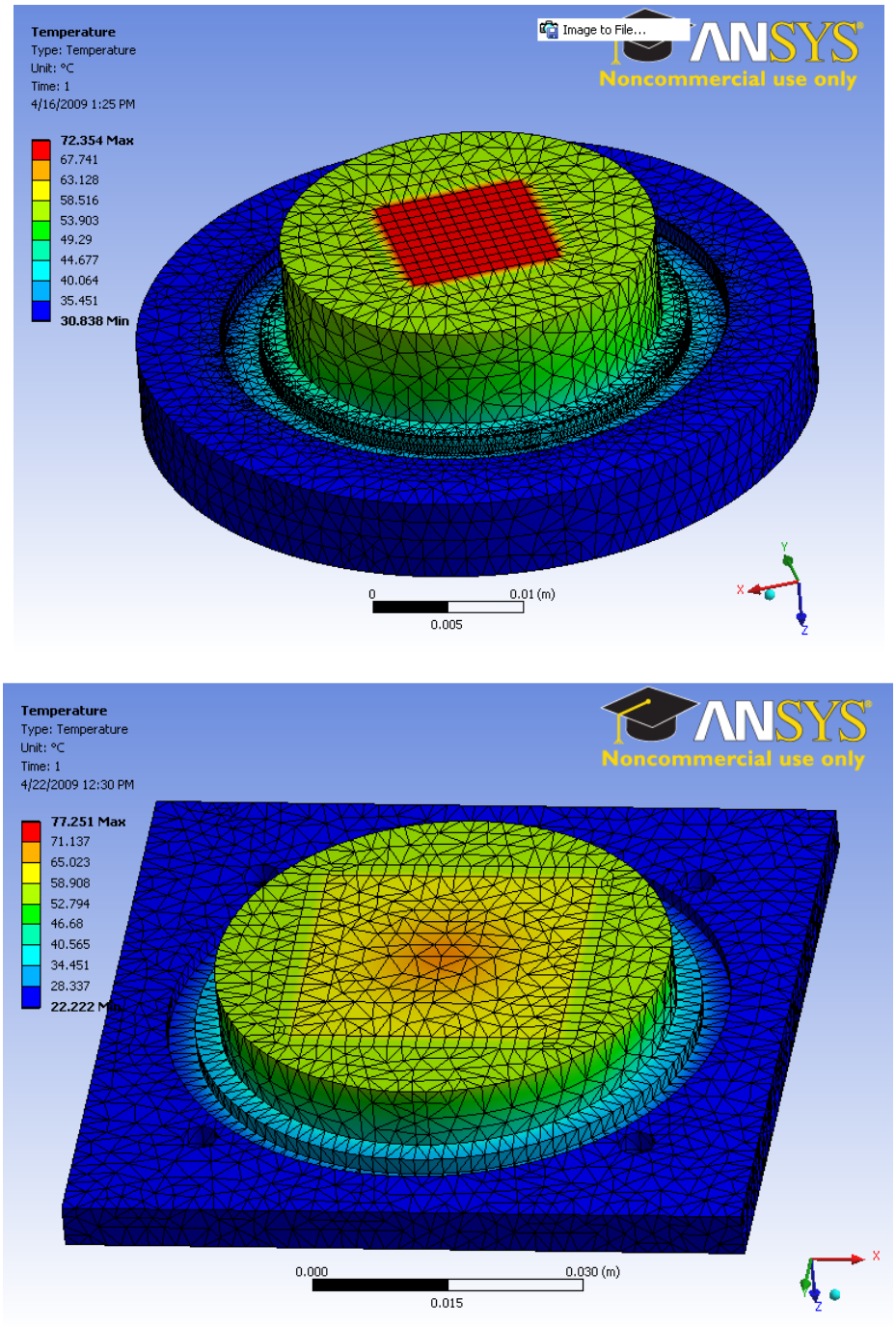

Figure B.1. FEM (ANSYS 11) temperature solutions for 10×10 mm heater (top) and 30×30×3 mm heat spreader (bottom).

REFERENCES

[1] O'Connor, J. P., and You, S. M., 1995, "A Painting Technique to Enhance Pool Boiling Heat Transfer in Saturated FC-72," Transactions of the ASME.Journal of Heat Transfer, **117**(2) pp. 387-393.

[2] Chang, J. Y., and You, S. M., 1997, "Boiling Heat Transfer Phenomena from Microporous and Porous Surfaces in Saturated FC-72," International Journal of Heat and Mass Transfer, **40**(18) pp. 4437-4447.

[3] Chang, J. Y., and You, S. M., 1997, "Enhanced Boiling Heat Transfer from Micro-Porous Surfaces: Effects of a Coating Composition and Method," International Journal of Heat and Mass Transfer, **40**(18) pp. 4449-4460.

[4] Rainey, K. N., 2001, "Pool and Flow Boiling Heat Transfer from Microporous Flat and Finned Surfaces in FC-72," .

[5] Ammerman, C. N., and You, S. M., 2001, "Enhancing Small-Channel Convective Boiling Performance using a Microporous Surface Coating," Transactions of the ASME.Journal of Heat Transfer, **123**(5) pp. 976-983.

[6] You, S. M., and Kim, J. H., 2006, "Thermally Conductive Microporous Coating," (US Patent Pending) .

[7] Carey, V.P., 1992, "Liquid-Vapor Phase Change Phenomena: An Introduction to the Thermophysics of Vaporization and Condensation Process in Heat Transfer Equipment," Taylor & Francis, Hebron, KY, .

[8] Bostanci, H., Saarloos, B. A., Rini, D. P., 2008, "Spray cooling with ammonia on micro-structured surfaces," 2008 11th Intersociety Conference on Thermal and Thermomechanical Phenomena in Electronic Systems (ITHERM '08), Anonymous IEEE, Orlando, FL, USA, .

[9] Kim, J. H., You, S. M., and Choi, S. U. S., 2004, "Evaporative Spray Cooling of Plain and Microporous Coated Surfaces," International Journal of Heat and Mass Transfer, **47**(14-16) pp. 3307-3315.

[10] Hsieh, C. C., and Yao, S. C., 2006, "Evaporative Heat Transfer Characteristics of a Water Spray on Micro-Structured Silicon Surfaces," International Journal of Heat and Mass Transfer, **49**(5-6) pp. 962-974.

[11] Marto, P. J., and Lepere, L. V. J., 1982, "Pool Boiling Heat Transfer from Enhanced Surfaces to Dielectric Fluids," Transactions of the ASME.Journal of Heat Transfer, **104**(2) pp. 292-299.

[12] Bergles, A. E., and Chyu, M. C., 1982, "Characteristics of Nucleate Pool Boiling from Porous Metallic Coatings," Transactions of the ASME.Journal of Heat Transfer, **104**(2) pp. 279-285.

[13] Nakayama, W., Daikoku, T., and Nakajima, T., 1982, "Effects of Pore Diameters and System Pressure on Saturated Pool Nucleate Boiling Heat Transfer from Porous Surfaces," Transactions of the ASME.Journal of Heat Transfer, **104**(2) pp. 286-291.

[14] Murthy, S., Joshi, Y., Gurrum, S., 2006, "Enhanced Boiling Heat Transfer Simulation from Structured Surfaces: Semi-Analytical Model," International Journal of Heat and Mass Transfer, **49**(11-12) pp. 1885-1895.

[15] Kim, J. H., Rainey, K. N., You, S. M., 2002, "Mechanism of Nucleate Boiling Heat Transfer Enhancement from Microporous Surfaces in Saturated FC-72," Transactions of the ASME.Journal of Heat Transfer, **124**(3) pp. 500-506.

[16] Chen Li, and Peterson, G. P., 2007, "Parametric Study of Pool Boiling on Horizontal Highly Conductive Microporous Coated Surfaces," Transactions of the ASME.Journal of Heat Transfer, **129**(11) pp. 1465-1475.

[17] Chen Li, and Peterson, G. P., 2008, "Experimental Studies on CHF of Pool Boiling on Horizontal Conductive Micro Porous Coated Surfaces," AIP Conference Proceedings, **969**pp. 12-20.

[18] Honda, H., and Wei, J. J., 2004, "Enhanced Boiling Heat Transfer from Electronic Components by use of Surface Microstructures," Experimental Thermal and Fluid Science, **28**(2-3) pp. 159-169.

[19] Maddox, D. E., and Mudawar, I., 1989, "Single and Two Phase Convective Heat Transfer from Smooth and Enhanced Microelectronic Heat Sources in a Rectangular Channel," J.Heat Transfer, **111**(4) pp. 1045-1052.

[20] Lie, Y. M., Ke, J. H., Chang, W. R., 2007, "Saturated Flow Boiling Heat Transfer and Associated Bubble Characteristics of FC-72 on a Heated Micro-Pin-Finned Silicon Chip," International Journal of Heat and Mass Transfer, **50**(19-20) pp. 3862-3876.

[21] Kandlikar, S. G., and Spiesman, P. H., 1998, "Effect of Surface Finish on Flow Boiling Heat Transfer," ASME Heat Transfer Division, Anonymous ASME, **1,** pp. 157-163.

[22] Rainey, K. N., Li, G., and You, S. M., 2001, "Flow Boiling Heat Transfer from Plain and Microporous Coated Surfaces in Subcooled FC-72," Transactions of the ASME.Journal of Heat Transfer, **123**(5) pp. 918-925.

[23] Sarwar, M. S., Jeong, Y. H., and Chang, S. H., 2007, "Subcooled Flow Boiling CHF Enhancement with Porous Surface Coatings," International Journal of Heat and Mass Transfer, **50**(17-18) pp. 3649-3657.

[24] Yildiz, S., 2008, "Effect of Porous Coating on Two-Phase Pressure Drop of Water during Up-Flow Boiling in Tubes," International Communications in Heat and Mass Transfer, **35**(3) pp. 326-337.

[25] Kuo, C. -., and Peles, Y., 2007, "Local Measurement of Flow Boiling in Structured Surface Microchannels," International Journal of Heat and Mass Transfer, **50**(23-24) pp. 4513-4526.

[26] Kuo, C. -., and Peles, Y., 2008, "Flow Boiling Instabilities in Microchannels and Means for Mitigation by Reentrant Cavities," Journal of Heat Transfer, **130**(7) pp. 1-10.

[27] Khanikar, V., Mudawar, I., and Fisher, T., 2008, "Flow Boiling in a Micro-Channel Coated with Carbon Nanotubes," Thermal and Thermomechanical Phenomena in Electronic Systems, 2008. ITHERM 2008. 11th Intersociety Conference on, pp. 960-969.

[28] Pais, M. R., Chow, L. C., and Mahefkey, E. F., 1992, "Surface Roughness and its Effects on the Heat Transfer Mechanism in Spray Cooling," Transactions of the ASME.Journal of Heat Transfer, **114**(1) pp. 211-219.

[29] Silk, E.A., Jungho Kim, Kiger, K., 2006, "2006 Proceedings. 10th Intersociety Conference on Thermal and Thermomechanical Phenomena in Electronics Systems (IEEE Cat. no. 06CH37733C),"IEEE, San Diego, CA, USA.

[30] Silk, E. A., 2008, "Investigation of Pore Size Effect on Spray Cooling Heat Transfer with Porous Tunnels," AIP Conference Proceedings, **969**pp. 112-122.

[31] Horacek, B., Kiger, K. T., and Kim, J., 2005, "Single Nozzle Spray Cooling Heat Transfer Mechanisms," International Journal of Heat and Mass Transfer, **48**(8) pp. 1425-1438.

[32] Stephan, P., and Sodtke, C., 2007, "Spray Cooling on Micro Structured Surfaces," International Journal of Heat and Mass Transfer, **50**(19-20) pp. 4089-4097.

[33] Willingham, T. C., and Mudawar, I., 1992, "Forced-Convection Boiling and Critical Heat Flux from a Linear Array of Discrete Heat Sources," International Journal of Heat and Mass Transfer, **35**(11) pp. 2879-2890.

[34] Gersey, C. O., and Mudawar, I., 1993, "Nucleate Boiling and Critical Heat Flux from Protruded Chip Arrays during Flow Boiling," Transactions of the ASME.Journal of Electronic Packaging, **115**(1) pp. 78-88.

[35] McAdams, W. H., Kennel, W. E., Minden, C. S., 1949, "Heat Transfer at High Rates to Water with Surface Boiling," Industrial and Engineering Chemistry, **41**(9) pp. 1945-1953.

[36] OConnor, J. P., You, S. M., and Chang, J. Y., 1996, "Gas-Saturated Pool Boiling Heat Transfer from Smooth and Microporous Surfaces in FC-72," Transactions of the ASME.Journal of Heat Transfer, **118**(3) pp. 662-667.

[37] Watwe, A. A., and Bar-Cohen, A., 1996, "Nucleate pool boiling and critical heat flux in gas-saturated dielectric coolants," 2nd European Thermal Sciences and 14th UIT Heat Transfer Conference, G. P. Celata, P. Di Marco and A. Mariani, eds. Edizioni ETS, pp. 1631-1638.

[38] Wu, P. S., and Simon, T. W., 1994, "Effects of dissolved gases on subcooled flow boiling from small heated regions with and without streamwise concave curvature," InterSociety

Conference on Thermal Phenomena in Electronic Systems. I-THERM IV. THEME: `Concurrent Engineering and Thermal Phenomena' IEEE K-16 on Heat Transfer in Electron. Equipment, Heat Transfer Div., ASME K-16 on Heat Transfer in Electron. Equipment, Heat Transfer Div., ASME, New York, NY, USA.

[39] Chen, T., and Garimella, S. V., 2006, "Effects of Dissolved Air on Subcooled Flow Boiling of a Dielectric Coolant in a Microchannel Heat Sink," Transactions of the ASME.Journal of Electronic Packaging, **128**(4) pp. 398-404.

[40] Willingham, T. C., and Mudawar, I., 1992, "Channel Height Effects on Forced-Convection Boiling and Critical Heat Flux from a Linear Array of Discrete Heat Sources," International Journal of Heat and Mass Transfer, **35**(8) pp. 1865-1880.

[41] Shunyu Su, Suyi Huang, and Xiaomo Wang, 2005, "Study of Boiling Incipience and Heat Transfer Enhancement in Forced Flow through Narrow Channels," International Journal of Multiphase Flow, **31**(2) pp. 253-260.

[42] Lie, Y. M., and Lin, T. F., 2005, "Saturated Flow Boiling Heat Transfer and Associated Bubble Characteristics of R-134a in a Narrow Annular Duct," International Journal of Heat and Mass Transfer, **48**(25) pp. 5602-5615.

[43] Bowers, M. B., and Mudawar, I., 1994, "High Flux Boiling in Low Flow Rate, Low Pressure Drop Mini-Channel and Micro-Channel Heat Sinks," International Journal of Heat and Mass Transfer, **37**(2) pp. 321-332.

[44] Ruey-Hung Chen, Chow, L. C., and Navedo, J. E., 2002, "Effects of Spray Characteristics on Critical Heat Flux in Subcooled Water Spray Cooling," International Journal of Heat and Mass Transfer, **45**(19) pp. 4033-4043.

[45] Estes, K. A., and Mudawar, I., 1995, "Correlation of Sauter Mean Diameter and Critical Heat Flux for Spray Cooling of Small Surfaces," International Journal of Heat and Mass Transfer, **38**(16) pp. 2985-2996.

[46] Rybicki, J. R., and Mudawar, I., 2006, "Single-Phase and Two-Phase Cooling Characteristics of Upward-Facing and Downward-Facing Sprays," International Journal of Heat and Mass Transfer, **49**(1-2) pp. 5-16.

[47] Cabrera, E., and Gonzalez, J. E., 2003, "Heat Flux Correlation for Spray Cooling in the Nucleate Boiling Regime," Experimental Heat Transfer, **16**(1) pp. 19-44.

[48] Liu, G. W., Morsi, Y. S., and Clayton, B. R., 2000, "Characterisation of the Spray Cooling Heat Transfer Involved in a High Pressure Die Casting Process," International Journal of Thermal Sciences, **39**(5) pp. 582-591.

[49] Rini, D. P., Ruey-Hung Chen, and Chow, L. C., 2002, "Bubble Behavior and Nucleate Boiling Heat Transfer in Saturated FC-72 Spray Cooling," Transactions of the ASME.Journal of Heat Transfer, **124**(1) pp. 63-72.

[50] Mudawar, I., and Estes, K. A., 1996, "Optimizing and Predicting CHF in Spray Cooling of a Square Surface," Transactions of the ASME.Journal of Heat Transfer, **118**(3) pp. 672-679.

[51] Lanchao Lin, and Ponnappan, R., 2004, "Critical Heat Flux of Multi-Nozzle Spray Cooling," Transactions of the ASME.Journal of Heat Transfer, **126**(3) pp. 482-485.

[52] Lin, L., and Ponnappan, R., 2003, "Heat Transfer Characteristics of Spray Cooling in a Closed Loop," International Journal of Heat and Mass Transfer, **46**(20) pp. 3737-3746.

[53] Pautsch, A. G., and Shedd, T. A., 2005, "Spray Impingement Cooling with Single- and Multiple-Nozzle Arrays. Part I: Heat Transfer Data using FC-72," International Journal of Heat and Mass Transfer, **48**(15) pp. 3167-3175.

[54] Wheeler, A.J., and Ganji, A.R., 1996, "Introduction to Engineering Experimentation," Prentice-Hall, New Jersey, pp. 417.

[55] Coleman, H.W., and Steele, G.W.J., 1989, "Experimental and uncertainty analysis for engineers," John Wiley & Sons, U.S.A., pp. 205.

[56] Mudawar, I., and Maddox, , 1989, "Critical Heat Flux in Subcooled Flow Boiling of Fluorocarbon Liquid on a Simulated Electronic Chip in a Vertical Rectangular Channel," International Journal of Heat and Mass Transfer, **32**(2) pp. 379-394.

[57] Galloway, J. E., and Mudawar, I., 1993, "CHF Mechanism in Flow Boiling from a Short Heated Wall. I. Examination of Near-Wall Conditions with the Aid of Photomicrography and High-Speed Video Imaging," International Journal of Heat and Mass Transfer, **36**(10) pp. 2511-2525.

[58] Galloway, J. E., and Mudawar, I., 1993, "CHF Mechanism in Flow Boiling from a Short Heated Wall. II. Theoretical CHF Model," International Journal of Heat and Mass Transfer, **36**(10) pp. 2527-2540.

[59] Gersey, C. O., and Mudawar, I., 1995, "Effects of Heater Length and Orientation on the Trigger Mechanism for Near-Saturated Flow Boiling Critical Heat Flux. I. Photographic Study and Statistical Characterization of the Near-Wall Interfacial Features," International Journal of Heat and Mass Transfer, **38**(4) pp. 629-641.

[60] Rainey, K. N., You, S. M., and Lee, S., 2003, "Effect of Pressure, Subcooling, and Dissolved Gas on Pool Boiling Heat Transfer from Microporous, Square Pin-Finned Surfaces in FC-72," International Journal of Heat and Mass Transfer, **46**(1) pp. 23-35.

[61] Rainey, K. N., You, S. M., and Lee, S., 2003, "Effect of Pressure, Subcooling, and Dissolved Gas on Pool Boiling Heat Transfer from Microporous, Square Pin-Finned Surfaces in FC-72," International Journal of Heat and Mass Transfer, **46**(1) pp. 23-35.

[62] Song, S., Lee, S., and Au, V., 1994, "Closed-form equation for thermal constriction/spreading resistances with variable resistance boundary condition," Proceedings of the 1994 International Electronics Packaging Conference, Anonymous Int. Electron. Packaging Soc Int. Electron. Packaging Soc Int. Electron. Packaging Soc, Atlanta, GA, USA.

[63] El-Genk, M., Saber, H. H., and Parker, J. L., 2007, "Efficient Spreaders for Cooling High-Power Computer Chips," Applied Thermal Engineering, **27**(5) pp. 1072-1088.

[64] Tilton, D. E., 1989, "Spray Cooling," .

[65] Lefebvre, A.H., 1989, "Atomization and Sprays," Hemisphere Publishing Corporation, United States, pp. 420.

[66] Wang, X. F., and Lefebvre, A. H., 1987, "Mean Drop Sizes from Pressure-Swirl Nozzles," **3**pp. 11-18.

[67] Hiroyasu, H., Arai, M., and Tabata, M., 1989, "Empirical Equations for the Sauter Mean Diameter of a Diesel Spray," International Congress and Exposition, SAE, Detroit, MI, pp. 97-106.

[68] Elkotb, M. M., 1982, "Fuel Atomization for Spray Modelling," Progress in Energy and Combustion Science, **8**(1) pp. 61-91.

[69] Mudawar, I., and Valentine, W., 1989, "Determination of the Local Quench Curve for Spray-Cooled Metallic Surfaces," Journal of Heat Treating, **7**(2) pp. 107-121.

[70] Klinzing, W., Rozzi, J., and Mudawar, I., 1992, "Film and Transition Boiling Correlations for Quenching of Hot Surfaces with Water Sprays," Journal of Heat Treating, **9**(2) pp. 91-103.

[71] Groeneveld, D. C., 1986, "The Onset of Dry Sheath Condition- a New Definition of Dryout," Nuclear Engineering and Design, **92**(2) pp. 135-140.

[72] Roday, A. P., Borca-Tasciuc, T., and Jensen, M. K., 2008, "The Critical Heat Flux Condition with Water in a Uniformly Heated Microtube," J.Heat Transfer, **130**(1) pp. 012901.

[73] Fukayama, Y., and Hirata, M., 1982, "Boiling heat transfer characteristics with high mass flux and disappearance of CHF following to DNB," Anonymous Proc. of 7th international heat transfer conference, Munchen, Germany, **4,** pp. 273-278.

[74] Monde, M., and Katto, Y., 1978, "Burnout in a High Heat-Flux Boiling System with an Impinging Jet," International Journal of Heat and Mass Transfer, **21**(3) pp. 295-305.

[75] Avedisian, C. T., and Koplik, J., 1987, "Leidenfrost Boiling of Methanol Droplets on Hot porous/ceramic Surfaces," International Journal of Heat and Mass Transfer, **30**(2) pp. 379-393.

[76] Bonner,R.W.,,III, Wadell, R. P., and Popov, G., 2008, "Local heat transfer coefficient measurements of flat angled sprays using thermal test vehicle," SEMI-THERM '08. 2008 24th Annual IEEE Semiconductor Thermal Measurement and Management Symposium, IEEE, Piscataway, NJ, USA.

[77] Kreitzer, P. J., and Kuhlman, J. M., 2008, "Visualization of Electrohydrodynamic Effects and Time Scale Analysis for Impinging Spray Droplets of HFE-7000," AIP Conference Proceedings, **969**pp. 86-93.

[78] Mudawar, I., 2001, "Assessment of High-Heat-Flux Thermal Management Schemes," Components and Packaging Technologies, IEEE Transactions on [See also Components, Packaging and Manufacturing Technology, Part A: Packaging Technologies, IEEE Transactions on], **24**(2) pp. 122-141.

[79] Sung, M. K., and Mudawar, I., 2009, "Single-Phase and Two-Phase Hybrid Cooling Schemes for High-Heat-Flux Thermal Management of Defense Electronics," Journal of Electronic Packaging, **131**(2) pp. 021013.

[80] Lee, D. -., and Vafai, K., 1999, "Comparative Analysis of Jet Impingement and Microchannel Cooling for High Heat Flux Applications," International Journal of Heat and Mass Transfer, **42**(9) pp. 1555-1568.

[81] Estes, K. A., and Mudawar, I., 1995, "Comparison of Two-Phase Electronic Cooling using Free Jets and Sprays," Transactions of the ASME.Journal of Electronic Packaging, **117**(4) pp. 323-332.

[82] Chu, R. C., Simons, R. E., Ellsworth, M. J., 2004, "Review of Cooling Technologies for Computer Products," IEEE Transactions on Device and Materials Reliability, **4**(4) pp. 568-585.

[83] Chu, R. C., 2004, "The Challenges of Electronic Cooling: Past, Current and Future," Journal of Electronic Packaging, **126**(4) pp. 491-500.

[84] Haramura, Y., and Katto, Y., 1983, "A New Hydrodynamic Model of Critical Heat Flux, Applicable Widely to both Pool and Forced Convection Boiling on Submerged Bodies in Saturated Liquids," International Journal of Heat and Mass Transfer, **26**(3) pp. 389-399.

[85] Gersey, C. O., and Mudawar, I., 1995, "Effects of Heater Length and Orientation on the Trigger Mechanism for Near-Saturated Flow Boiling Critical Heat Flux. II. Critical Heat Flux Model," International Journal of Heat and Mass Transfer, **38**(4) pp. 643-654.

[86] Mudawar, I., Hui Zhang, and Hasan, M. M., 2007, "CHF Model for Subcooled Flow Boiling in Earth Gravity and Microgravity," International Journal of Heat and Mass Transfer, **50**(19-20) pp. 4039-4051.

BIOGRAPHICAL INFORMATION

Gilberto Moreno, Jr. received his B.S. in Mechanical Engineering from the University of Texas at El Paso. After graduation, he worked at Lockheed Martin Missiles Fire Control in Grand Prairie, TX as a Facilities Mechanical Design Engineer. After 2 ½ years of working with the company he took an educational leave of absence from work to pursue a Master's Degree. He obtained a M.S. in Mechanical Engineering from the University of Texas at Arlington in December 2005.